



University  
of Glasgow

Al shalwi, Matar (2012) *The preparation of molybdenum carbonitrides by single source routes and a study of their lattice reactivity*. MSc(R) thesis.

<http://theses.gla.ac.uk/3346/>

Copyright and moral rights for this thesis are retained by the author

A copy can be downloaded for personal non-commercial research or study, without prior permission or charge

This thesis cannot be reproduced or quoted extensively from without first obtaining permission in writing from the Author

The content must not be changed in any way or sold commercially in any format or medium without the formal permission of the Author

When referring to this work, full bibliographic details including the author, title, awarding institution and date of the thesis must be given

**The preparation of molybdenum carbonitrides by  
single source routes and a study of their lattice  
reactivity**



**UNIVERSITY  
OF  
GLASGOW**

**Matar Al shalwi**

**Thesis Presented to the University of Glasgow for the  
Degree of MSc**

**School of Chemistry**

**2012**

## Abstract

Thermal decomposition of hexamethylenetetramine molybdate and ethylenediammonium molybdate were studied using a temperature programmed reaction procedure under different reaction atmospheres. The obtained materials were characterised by X-ray diffraction (XRD), surface area measurement (BET), scanning electron microscopy (SEM), elemental analysis (CHN), thermogravimetric analysis (TGA) and X-ray photoelectron spectroscopy (XPS). The results indicated that the decomposition of both precursors under  $H_2/N_2$  in a ratio of 3:1 or 1:3 leads to production of molybdenum carbide, and also a mixture of molybdenum metal and molybdenum carbide is obtained from the thermal decomposition of both precursors under 1:3 Ar/ $H_2$ . In contrast, the decomposition of hexamethylenetetramine molybdate under  $N_2$  or Ar leads to production of  $\gamma$ - $Mo_2N$ , whereas impure phases were obtained from the decomposition of ethylenediammonium molybdate where molybdenum carbide, molybdenum metal and molybdenum oxide were obtained under an Ar atmosphere while gamma molybdenum nitride, molybdenum carbide and molybdenum oxide were obtained under a  $N_2$  atmosphere. In order to characterise the reactivity of the lattice carbon and nitrogen species within the obtained materials various techniques have been applied. The results have indicated that nitrogen is much more reactive than carbon and the nature of its reactivity is influenced by composition. The difference in reactivity observed indicates that molybdenum carbonitrides are not suitable candidates as reagents for which the simultaneous loss of nitrogen and carbon from the lattice would be desirable.

# Contents

Abstract.....	I
Contents.....	II
List of Figures.....	VII
List of Tables.....	XIII
Publication.....	XIV
Acknowledgements.....	XV
Author's Declaration.....	XVI
1 Introduction .....	1
1.1 General Introduction.....	1
1.2 Crystal Structure and Composition.....	2
1.3 Physical and Electronic Properties.....	5
1.4 Catalytic Applications.....	6
1.5 Lattice Reactivity.....	8
1.6 Preparation.....	10
1.7 Aim.....	15
2. Experimental.....	16
2.1 Introduction.....	16
2.2 Preparation of precursors.....	16
2.2.1 Preparation of ethylenediammonium molybdate.....	16
2.2.2 Preparation of hexamethylenetetramine molybdate.....	16
2.3 Reactor design.....	17
2.3.1 Decomposition of precursors.....	17
2.3.2 Lattice nitrogen reactivity studies.....	20
2.3.3 Stability studies.....	21
2.4 Characterisation methods.....	23
2.4.1 Powder X-ray diffraction (XRD) .....	23
2.4.2 Surface Area Determination.....	23
2.4.3 Thermogravimetric Analysis.....	24

2.4.4	Determination of Carbon, Hydrogen and Nitrogen Content.....	24
2.4.5	Scanning Electron Microscopy (SEM) .....	24
2.4.6	Thermal volatilisation analysis (TVA).....	25
2.4.7	X-ray photoelectron spectroscopy (XPS).....	26
3.	Chapter 3: Hexamethylenetetramine molybdate single source route .....	27
3.1	Investigation of hexamethylenetetramine molybdate .....	28
3.1.1	Decomposition of precursor I under an argon atmosphere at 800 °C.....	31
3.1.1.1	XRD patterns.....	31
3.1.1.2	C H N analysis.....	32
3.1.1.3	BET surface area measurements.....	32
3.1.1.4	SEM images.....	33
3.1.1.5	Summary.....	34
3.1.2	Decomposition under an argon atmosphere at 700 °C.....	35
3.1.2.1	XRD patterns.....	35
3.1.2.2	C H N analysis.....	36
3.1.2.3	BET surface area measurements.....	36
3.1.2.4	SEM images.....	37
3.1.2.5	Summary.....	38
3.1.3	Decomposition under an argon atmosphere at 700°C using different ramp rate.....	39
3.1.3.1	XRD patterns.....	39
3.1.3.2	C H N analysis.....	40
3.1.3.3	BET surface area measurement.....	40
3.1.3.4	SEM images.....	41
3.1.3.5	Summary.....	41
3.1.4	Decomposition under different reaction atmospheres at 700°C.....	42
3.1.4.1	XRD patterns.....	42
3.1.4.2	C H N analysis.....	43
3.1.4.3	BET surface area measurements.....	43
3.1.4.4	SEM images.....	44

3.1.4.5	Summary.....	45
3.2	Investigation of various precursors.....	47
3.2.1	Molybdenum trioxide ( $\text{MoO}_3$ ) .....	47
3.2.1.1	XRD patterns.....	47
3.2.1.2	C H N analysis.....	49
3.2.1.3	SEM images.....	50
3.2.1.4	Summary.....	51
3.2.2	Ammonium heptamolybdate (AHM).....	52
3.2.2.1	XRD patterns.....	52
3.2.2.2	C H N analysis .....	53
3.2.2.3	SEM images.....	54
3.2.2.4	Summary.....	54
3.2.3	Molybdic acid ( $\text{H}_2\text{MoO}_4$ ).....	55
3.2.3.1	XRD patterns.....	55
3.2.3.2	C H N analysis.....	56
3.2.3.3	SEM images.....	57
3.2.3.4	Summary.....	57
3.3	Conclusion.....	58
4.	Chapter 4: Ethylenediammonium-molybdate single source route.....	59
4.1	Investigation of ethylenediammonium-molybdate.....	59
4.1.1	Investigation of precursor E under an argon atmosphere at $800\text{ }^\circ\text{C}$ .....	63
4.1.1.1	XRD patterns.....	63
4.1.1.2	C H N analysis.....	64
4.1.1.3	BET surface area measurements.....	64
4.1.1.4	SEM images.....	65
4.1.1.5	Summary.....	66
4.1.2	Decomposition under an argon atmosphere at $700\text{ }^\circ\text{C}$ .....	67
4.1.2.1	XRD patterns.....	67
4.1.2.2	C H N analysis.....	68
4.1.2.3	BET surface area measurements.....	68

4.1.2.4	SEM images.....	69
4.1.2.5	Summary.....	70
4.1.3	Investigation of mixed precursor preparing by using mechanical mixture of MoO <sub>3</sub> with precursor E under an argon atmosphere at 700 °C.....	71
4.1.3.1	XRD patterns.....	71
4.1.3.2	C H N analysis.....	72
4.1.3.3	BET surface area measurements.....	72
4.1.3.4	SEM images.....	73
4.1.3.5	Summary.....	73
4.1.4	Decomposition under different reaction atmospheres at 700°C.....	74
4.1.4.1	XRD patterns.....	74
4.1.4.2	C H N analysis.....	75
4.1.4.3	BET surface area measurements.....	75
4.1.4.4	SEM image.....	76
4.1.3.5	Summary.....	77
4.2	Conclusion.....	79
5.	Chapter 5: Lattice Nitrogen Reactivity and Stability Studies.....	80
5.1	TPR Studies of Lattice Nitrogen Reactivity.....	80
5.1.1	Reaction Data.....	81
5.1.2	XRD Patterns.....	82
5.1.3	C H N Analysis.....	84
5.1.4	Summary.....	84
5.2	Thermal Stability Studies.....	85
5.2.1	Ar/H <sub>2</sub> 1:3 feed gas reactions.....	85
5.2.1.1	XRD patterns.....	85
5.2.1.2	C H N analysis.....	87
5.2.2	Ar-only feed gas reactions.....	88
5.2.2.1	XRD patterns.....	88
5.2.2.2	C H N analysis.....	90
5.2.3	Summary.....	90

5.3	Thermal Volatilisation Analysis (TVA).....	91
5.3.1	TVA of sample I-21.....	91
5.3.1.1	Non-Condensable products analysis.....	92
5.3.1.2	Condensable products analysis.....	93
5.3.1.3	Summary.....	96
5.3.2	TVA of sample I-26.....	97
5.3.2.1	Non-condensable product analysis.....	97
5.3.2.2	Condensable products analysis.....	98
5.3.2.3	Summary.....	100
5.3.3	TVA of sample E-23.....	100
5.3.3.1	Non-condensable product analysis.....	101
5.3.3.2	Condensable products analysis.....	102
5.3.3.3	Summary.....	105
5.3.4	C H N analysis.....	105
5.3.5	Summary.....	106
5.4	Thermogravimetric Analysis (TGA).....	107
5.4.1	TGA profile.....	107
5.4.2	Mass spectrometry results.....	108
5.4.3	C H N results.....	110
5.4.4	Summary.....	110
5.5	Conclusion.....	111
6.	Chapter 6: Conclusion.....	112
	References.....	113

## List of Figures

Figure 1.1	Crystal structure of common binary molybdenum nitrides and carbides.....	3
Figure 1.2	Schematic diagram showing the Mars-van-Krevelen mechanism in oxidation catalysis .....	8
Figure 1.3	Schematic diagram showing the conversion pathways during ammonolysis of MoO <sub>3</sub> . The low, medium and high surface area catalysts are represented by LSA,MSA and HAS, respectively .....	12
Figure 2.1	Reactor for thermal decomposition preparation.....	18
Figure 2.2	Apparatus employed for studies of the reactivity of lattice nitrogen...	20
Figure 2.3	Temperature profile of lattice nitrogen reactivity studies.....	21
Figure 2.4	Temperature profile of stability studies under Ar.....	22
Figure 2.5	Temperature profile of stability studies under 1:3 Ar /H <sub>2</sub> .....	22
Figure 2.6	Schematic diagram of the TVA apparatus.....	25
Figure 3.1	XRD pattern of precursor I .....	28
Figure 3.2	TGA-DSC profile of precursor I under argon atmosphere.....	29
Figure 3.3	<i>In-situ</i> XRD patterns at room temperature, 500 °C, 600 °C, 700 °C and 800 °C.....	30
Figure 3.4	XRD patterns of samples I-4 and I-6.....	31
Figure 3.5	SEM images of A) precursor I, B) sample I-4, C) sample I-7 <i>in-situ</i> and D) sample I- 6. ....	33
Figure 3.6	XRD patterns of samples I-12, I- 10, I-14 and I-21.....	35
Figure 3.7	SEM images of A) sample I-12, B) sample I-10, C) sample I-14 and D) sample I-21.....	37
Figure 3.8	XRD patterns of samples I-16 and I-17.....	39
Figure 3.9	SEM images of A) sample I-17 and B) sample I-16. ....	41

Figure 3.10	XRD patterns of samples I-28, I-22, I-24 and I-26.....	42
Figure 3.11	SEM images of A) sample I- 28, B) sample I-22, C) sample I-24 and D) sample I-26.....	44
Figure 3.12	Schematic diagram shows resulting materials from thermal decomposition of hexamethylenetetramine molybdate under different atmospheres.....	46
Figure 3.13	XRD pattern of MoO <sub>3</sub> . The pattern is consistent with that expected for the MoO <sub>3</sub> phase.....	47
Figure 3.14	XRD pattern of samples M-1 and M-2 prepared at 700 °C.....	48
Figure 3.15	XRD pattern of sample M-3, M-4, M-5 and M-6 prepared under H <sub>2</sub> /N <sub>2</sub> 3:1.....	48
Figure 3.16	SEM images of A) sample M-1 and B) sample M-2.....	50
Figure 3.17	SEM images of A) sample M-3, B) sample M-4, sample M-5 and sample M-6.....	51
Figure 3.18	XRD pattern of AHM. The pattern is consistent with that expected for the AHM phase.....	52
Figure 3.19	XRD patterns of samples A-1, A-2 and A-3 .....	53
Figure 3.20	SEM images of A) pure AHM, B) sample A-1, C) sample A-2 and D) sample A-3.....	54
Figure 3.21	XRD pattern of pure H <sub>2</sub> MoO <sub>4</sub> . The pattern is consistent with that expected for the H <sub>2</sub> MoO <sub>4</sub> phase.....	55
Figure 3.22	XRD patterns of samples H-1 and H-2.....	56
Figure 3.23	SEM images of A) pure H <sub>2</sub> MoO <sub>4</sub> , B) sample H-1 and C) Sample H-2.....	57
Figure 4.1	XRD pattern of precursor E.....	60
Figure 4.2	TGA-DSC profile of precursor E conducted under an argon atmosphere.....	61
Figure 4.3	<i>In-situ</i> XRD patterns at room temperature, 500 °C, 600 °C, 700 °C and 800 °C.....	62

## VIII

Figure 4.4	XRD patterns of samples E-5 and E-9.....	63
Figure 4.5	SEM images of A) precursor E, B) sample E-5, C) sample E-8 <i>in-situ</i> and D) sample E-9.....	65
Figure 4.6	XRD patterns of samples E-13, E-11 and E-15.....	67
Figure 4.7	SEM images of A) sample E- 13 B) sample E- 11 and C) sample E- 15;all images correspond to the same magnification.....	69
Figure 4.8	XRD patterns of samples E-18 and E-19.....	71
Figure 4.9	SEM images of A) sample E- 18 and B) sample E- 19;all images correspond to the same magnification.....	73
Figure 4.10	XRD patterns of samples E-29, E-23, E-25 and E-27.....	74
Figure 4.11	SEM images of A) sample E- 29, B) sample E- 23, C) sample E-25 and D) sample E- 27.....	76
Figure 4.12	Schematic diagram shows the resulting materials from thermal decomposition of ethylenediammonium molybdate under different atmospheres.....	78
Figure 5.1	Conductivity versus time plots for temperature programmed reactions of samples I-21, I-22 and E-23 under Ar/H <sub>2</sub> 1:3.....	81
Figure 5.2	XRD patterns showing the differences before and after reaction for sample I- 21.....	82
Figure 5.3	XRD patterns showing the differences before and after reaction for sample I- 22.....	82
Figure 5.4	XRD patterns showing differences before and after reaction for sample E- 23.....	83
Figure 5.5	XRD patterns showing differences before and after reaction for sample I-22 under Ar/H <sub>2</sub> 1:3.....	85
Figure 5.6	XRD patterns showing the differences between before and after reaction for sample E-23 under Ar/H <sub>2</sub> 1:3.....	86

Figure 5.7	XRD patterns showing the differences before and after reaction for sample I-22 under an Ar-only atmosphere.....	88
Figure 5.8	XRD patterns showing the differences between before and after reaction for sample E-23 under an Ar atmosphere.....	89
Figure 5.9	TVA plot of the degradation of sample I-21 showing non-condensable volatile product in the liquid N <sub>2</sub> trap.....	92
Figure 5.10	The mass spectrum for the N <sub>2</sub> , H <sub>2</sub> and H <sub>2</sub> O evolved from sample I-21 in TVA.....	93
Figure 5.11	Sub-ambient thermal volatilisation analysis of volatiles and components evolved by heating the liquid N <sub>2</sub> trap.....	94
Figure 5.12	The mass spectrum for the CO <sub>2</sub> evolved from sample I-21 in TVA...	95
Figure 5.13	The mass spectrum for the NH <sub>3</sub> evolved from sample I-21 in TVA...	95
Figure 5.14	The mass spectrum for water evolved from sample I-21 in TVA.....	96
Figure 5.15	TVA plot of the degradation of sample I-26 showing non-condensable volatile product in the liquid N <sub>2</sub> trap.....	97
Figure 5.16	The mass spectrum for the nitrogen evolved from sample I-26 in TVA.....	98
Figure 5.17	Sub-ambient thermal volatilisation analysis of volatiles and components evolved by heating the liquid N <sub>2</sub> trap.....	98
Figure 5.18	The mass spectrum for the carbon dioxide evolved from sample I-26 in TVA.....	99
Figure 5.19	The mass spectrum for the water evolved from sample I-26 in TVA.....	99
Figure 5.20	TVA plot of the degradation of sample E-23 showing non-condensable volatile product in the liquid N <sub>2</sub> trap.....	101
Figure 5.21	The mass spectrum for the nitrogen evolved from sample E-23 in TVA.....	102
Figure 5.22	Sub-ambient thermal volatilisation analysis of volatiles and components evolved by heating the liquid N <sub>2</sub> trap .....	102
Figure 5.23	The mass spectrum for the CO <sub>2</sub> evolved from sample E-23 in TVA...	103

Figure 5.24	The mass spectrum for the $\text{NH}_3$ evolved from sample E-23 in TVA..	104
Figure 5.25	The mass spectrum for the water evolved from sample E-23 in TVA.....	104
Figure 5.26	TGA profile of sample E-23-A under Ar/ $\text{H}_2$ 1:3.....	107
Figure 5.27	The mass spectrum for $\text{NH}_3$ evolved from sample E-23-A in TGA...	108
Figure 5.28	The mass spectrum for $\text{H}_2\text{O}$ evolved from sample E-23-A in TGA...	108
Figure 5.29	The mass spectrum for CO evolved from sample E-23-A in TGA.....	109

## List of Tables

Table 1.1	General methods of synthesis molybdenum carbide and nitride.....	10
Table 2.1	Conditions used for the decomposition of hexamethylentetramine molybdate.....	18
Table 2.2	Conditions used for the decomposition of different precursors.....	19
Table 2.3	Conditions used for the decomposition of ethylenediammonium molybdate.....	19
Table 3.1	Carbon and nitrogen content of sample I-4, I-6 and I-7 in-situ.....	32
Table 3.2	BET surface area of samples I- 4, I- 6 and I- 7.....	32
Table 3.3	Carbon and nitrogen content of samples I-12, I-10, I-14 and I-21.....	36
Table 3.4	BET surface area of samples I-12, I-10, I-14 and I-21.....	36
Table 3.5	Carbon and nitrogen content of samples I-17 and I-16 .....	40
Table 3.6	BET surface area of samples I-17 and I-16.....	40
Table 3.7	Carbon and nitrogen content of sample I-28, I-22, I-24 and I-26.....	43
Table 3.8	BET surface area of samples I-28, I-22, I-24 and I-26.....	43
Table 3.9	Carbon and nitrogen content of samples M-1, M-2, M-3, M-4, M-5 and M-6.....	49
Table 3.10	Carbon and nitrogen content of samples A-1, A-2 and A-3.....	53
Table 3.11	Carbon and nitrogen content of samples H-1 and H-2.....	56
Table 4.1	Carbon and nitrogen content of samples E-5, E-9 and E-8 <i>in-situ</i> .....	64
Table 4.2	BET surface area of samples E-5, E-9 and E-8 <i>in-situ</i> .....	64
Table 4.3	Carbon and nitrogen content of samples E- 13, E- 11 and E- 15.....	68
Table 4.4	BET surface area of samples E- 13, E- 11 and E- 15.....	68
Table 4.5	Carbon and nitrogen content of samples E-18 and E-19.....	72
Table 4.6	BET surface area of samples E-18 and E-19.....	72
Table 4.7	Carbon and nitrogen content of samples E-29, E-23, E-25 and E- 27.....	75
Table 4.8	BET surface area of samples E-29, E-23, E-25 and E-27.....	76

Table 5.1	Carbon and nitrogen content pre- and post- reaction and assumed stoichiometry of samples I-21, I-22 and E-23 in lattice reactivity study.....	84
Table 5.2	Carbon and nitrogen content pre-and post -reaction and assumed stoichiometry of samples I-22 and E-23 in the stability study in Ar/H <sub>2</sub> 1:3.....	87
Table 5.3	Carbon and nitrogen content pre- and post-reaction and assumed stoichiometry of samples I-22 and E-23 in the stability study in Ar-only.....	90
Table 5.4	Carbon and nitrogen content of samples I-21, I-26 and E-23 in pre-reaction and post- reaction in TVA and assumed stoichiometry .....	105
Table 5.5	Carbon and nitrogen content of samples E-23-A and E-23-B in pre-reaction and post- reaction in TGA and assumed stoichiometry .....	110

## **Publication**

M. AlShalwi, J. S. J. Hargreaves, J. J. Liggat and D. Todd, “Upon the reactivity of lattice carbon and nitrogen species in molybdenum (oxy) carbonitrides prepared using single-source routes”(2011), Materials Research Bulletin, Accepted for publication.

## Acknowledgements

I wish to express my sincere gratitude to my supervisor **Dr. Justin Hargreaves** for all of the help, knowledge, support and enthusiasm that he has been given to me during my MSc study.

I would like to thank **Dr. John Liggat** and **Miss Debbie Todd** from the Department of Pure and Applied Chemistry, University of Strathclyde, for their kind assistance in performing the TVA studies. I would like also to thank **Dr. David Morgan** from Cardiff University for kindly conducting the XPS analysis.

I am also very grateful to **Prof. Saud Al-Resayes**, **Prof. Abdulaziz Al-Suhybany** and **Prof. Abdullah Al-Mayouf** from King Saud University, Chemistry Department for their encouragement and also allowing me to study the MSc abroad, and also special thanks must go to **Dr. Rafiq Siddiqui** for his advice and assistance while I was looking for acceptance and thank you also for introducing me to the best supervisor in the catalysis field.

I would like to acknowledge **Mrs. Kim Wilson** for her assistance in performing CHN analysis, **Mr. Jim Gallagher** for his help and advice with the SEM and **Mr. Andy Monaghan** for his patience in helping me with several techniques.

It is pleasure to record my special thanks to **Mr. Abdulrahman Al-harhi** for his friendship, support, encouragement and advice during my MSc study.

I would like also to thank other members of the Hargreaves research group, particularly **Abbas Lafta**, **Anne-Marie Alexander** and **Alexander Munnoch** for their support and general advice.

I would like also to thank my friends and family, namely **Mohammed Al-shalwi**, **Abdullah Al-Swieleh**, **Khalid Al-otaibi**, **Warrad Al-shalwi** and **Dr. Bandar Al-shammari** for making the life in Britain enjoyable and productive and also for their help and support about several personal issues.

Finally, I gratefully acknowledge the Ministry of Higher Education in Saudi Arabia, and the Saudi Cultural Bureau in London for generously providing funding.

## **Author's Declaration**

I hereby declare that the work contained in this thesis is my own work, submitted for a degree of MSc by research, except where due reference is made to the contribution of others. This work has not been previously submitted for a degree at Glasgow University or any other university.

---

Matar Al shalwi

# **Chapter 1: Introduction**

## **1.1 General Introduction**

Transition metal carbides, nitrides, oxynitrides and oxycarbides are of widespread interest [1-8] . The reasons for this can be attributed to their chemical and physical properties including their extreme mechanical hardness, thermal stability, their refractory nature, their corrosion and poisoning resistance, their superconductivity and their surface reactivity [9-15]. These features have succeeded in making some transition metal carbides, nitrides, oxynitrides and oxycarbide industrially applicable. For example, they have been used as cutting tools [16, 17], superconductors [18, 19], coatings and structural materials [20] as well as being used in optical and magnetic devices [5]. Furthermore, a wide range of studies have been conducted since Boudart and Levy. proposed that some transition metal carbides and nitrides have unique catalytic properties which are comparable with those of noble metals [21]. Molybdenum is one of the transition metal carbide and nitride systems which has been extensively studied in terms of its characteristics, synthesis, and catalytic behaviour. The advantages of using these materials rather than noble metals in catalytic reactions are their low cost and availability [22].

Molybdenum carbides, nitrides, oxynitrides and oxycarbides have been widely applied as catalysts [23, 24]. Whilst analogies have been drawn between the behaviour of the nitride and carbide with that of noble metals [7, 25], the nitride systems also possess the added functionality of basicity and some attention has been directed towards this aspect [1, 26].

## 1.2 Crystal Structure and Composition

The structure and composition of molybdenum nitride, carbide, oxynitride and oxycarbide have been widely studied by various techniques, and are well documented [1]. These compounds can be described as interstitial in nature wherein the non-metal atoms, for example C, N and O are located in the interstitial space between the relatively large atoms of the parent metal [20]. The presence of these interstitial atoms results in an increase in the lattice parameter [1]. As reported by Oyama [12], the two fundamental factors that influence these systems are geometric and electronic considerations. In terms of geometry, the empirical rule by Hägg specifies that non-metals (N, C, O) can occupy the interstitial sites of a metal structure when the radius ratio of non-metal to metal ( $r = r_x / r_{\text{metal}}$ ) is less than 0.59; consequently, the resultant phases are restricted to face centered cubic (fcc), hexagonal closed packed (hcp) or simple hexagonal (hex) structures, as illustrated in Figure 1.1. The non-metals often reside in the largest interstitial site available between metal atoms which is the octahedral site in face centered cubic (fcc) and hexagonal closed packed (hcp) metal atom arrangements [20]. The metal sub-lattice is generally formed by the close-packed layering in the arrangement of metal atoms which follow the sequence: -ABCABC- or -ABABAB- for the face centered cubic and hexagonally close packed systems respectively [9].

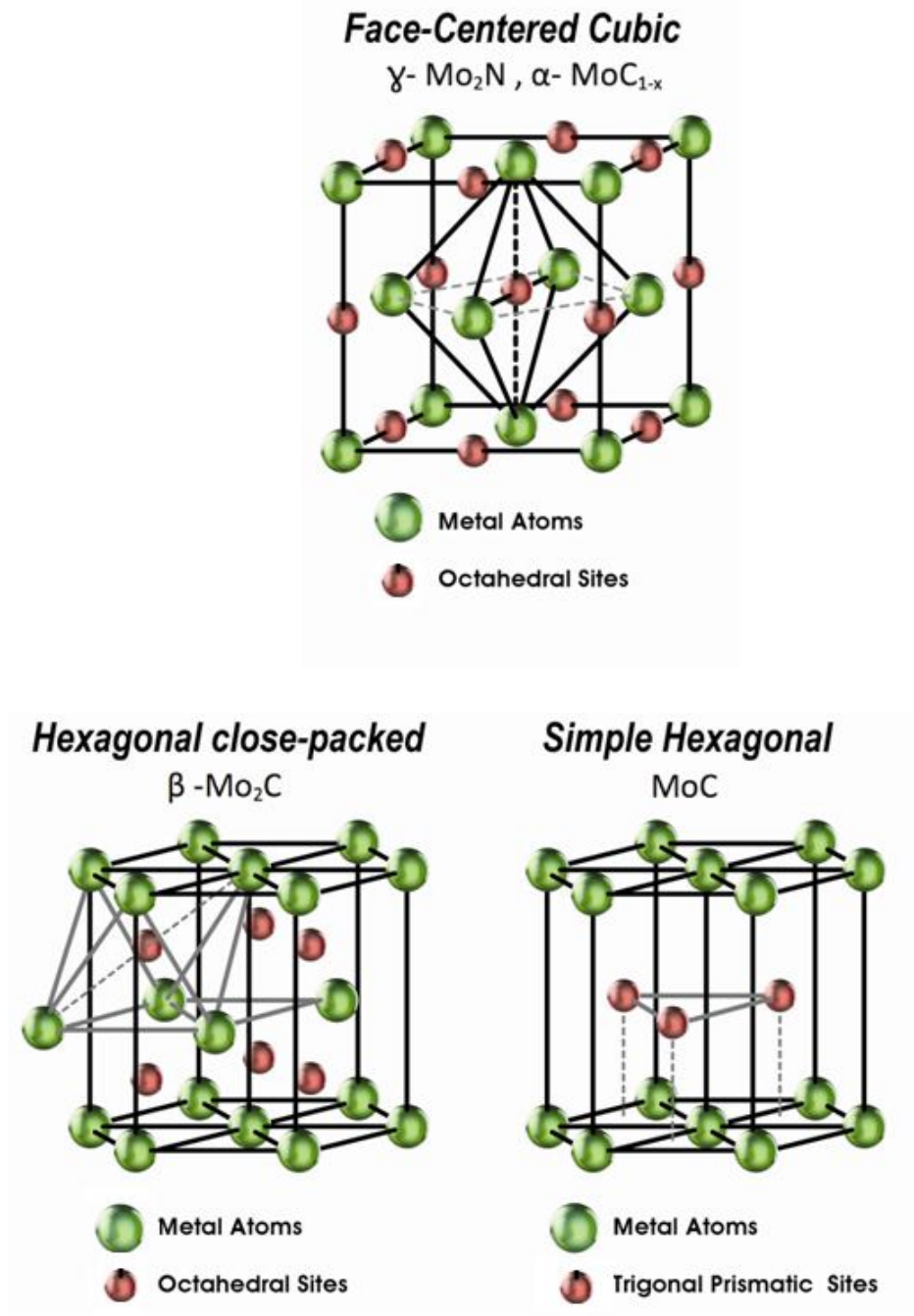


Figure 1.1: Crystal structure of common binary molybdenum nitrides and carbides  
[9, 20]

In terms of the electronic factor, the change of the parent metal structure can be driven by electronic effects. Engel-Brewer theory can be applied to explain this concept [12]. The structure of a metal or substitutional alloy is based on the s-p electron count which is defined by the number of s-p valence electrons per atom ( $e/a$ ). The bcc structure is formed when  $e/a = 1-1.5$ , the hcp structure is formed when  $e/a = 1.7-2.1$ , and when  $e/a = 2.5-3$  the fcc structure is formed [12]. Conversion of the structure from bcc to hcp to fcc is dependent on the mixing of the metal s-p-d orbitals and the non-metal s-p orbitals. Thus, the consequential s-p electron count may follow the sequence: parent metal < carbide < nitride. For instance, the structural conversion of molybdenum has the sequence: Mo (bcc) < Mo<sub>2</sub>C (hcp) < Mo<sub>2</sub>N (fcc) [13].

In addition, due to a deficiency of carbon or nitrogen atoms in some molybdenum systems, oxygen atoms can supplement the crystal system forming oxycarbides, oxynitrides and oxycarbonitrides [1]. These compounds are often non-stoichiometric, which makes a precise definition of non-atom sub-structure very difficult. However, the binary and ternary phases of molybdenum that contain nitrogen or carbon may play an important role in the catalysis field.

### 1.3 Physical and Electronic Properties

Molybdenum carbide and nitride, as well as their oxygen containing analogues, are compounds which exhibit extreme hardness and strength. They are also known for their very high melting points which are similar to those of ceramics. The melting points of Mo, Mo<sub>2</sub>C and Mo<sub>2</sub>N are 3156 °C, 2520 °C and 1950 °C respectively [12].

Their mechanical properties, such as hardness and Young's modulus, are similar to those in ceramic materials but differ from those for metals. For the hardness, which is defined as a measure of a material's resistance against deformation, the values regarding Mo, Mo<sub>2</sub>C and Mo<sub>2</sub>N are 250 Kg mm<sup>-2</sup>, 1500 Kg mm<sup>-2</sup> and 1700 Kg mm<sup>-2</sup>, respectively. In terms of Young's modulus, the values regarding the Mo and Mo<sub>2</sub>C are 320 GPa and 230 GPa, respectively [12].

The electronic properties of nitrides and carbides are different from their parent metals. They are often described in terms of covalent, ionic and metallic behaviour [13]. For example, they exhibit the high hardness values and brittleness of a covalent solid, the simple crystal structure and very high melting temperature of ionic systems and they possess the electronic and magnetic characteristics of transition metals [9, 10]. Moreover, theoretical band calculations of transition metal carbides and nitrides have suggested that bonding involves simultaneous contributions from metallic, covalent and ionic bonding. The metallic bond participation is ascribed to re-ordering of the metal-metal band. The covalent involvement is due to the formation of covalent bonds.

In general, there are two significant electronic properties related to (1) orientation and extent of charge transfer and (2) the impact of the carbide and nitride formation on metal d-band [13]. In terms of charge transfer, investigation of molybdenum carbide and nitride by X-ray photoelectron spectroscopy (XPS) and near-edge X-ray absorption fine structure (NEXAFS) shows evidence for electronic charge transfer directly from metal to non-metal [9, 10, 12]. Alexander and Hargreaves have reported that the surface investigation of those compounds by others has indicated that the carbides and nitrides surface have a low level of ionicity [3], perhaps due to the presence of the

electronegative interstitial atoms [9]. Regarding the d-band modification of the parent metal observed during the formation of carbides and nitrides (which is attributed by some to the increase of catalytic properties), one simple interpretation is the expansion of metal lattice during the formation of interstitial compounds, which in turn increases the metal-metal distance. For example, after formation of the carbide, the lattice parameters of molybdenum are expanded from 0.27 nm to 0.30 nm and for niobium and vanadium they are expanded from 0.33 nm to 0.45 nm and from 0.26 nm to 0.42 nm, respectively [9, 10, 13].

#### **1.4 Catalytic Applications**

As mentioned, molybdenum carbides, nitrides, oxycarbides and oxynitrides have received considerable attention as catalysts which, in some cases, have been proposed to resemble noble metals in terms of performance. They can be prepared so that they exhibit high specific area [9, 10, 13, 16, 27]. In some instances these catalysts are more desirable than noble metals due to their resistance to poisoning and enhanced selectivity in some reactions [3, 13, 20]. Accordingly, the activity, selectivity and performance of such compounds have been documented for a myriad of reactions. The most popular reactions that have been investigated using molybdenum carbide and nitride are hydrodenitrogenation (HDN) [28, 29], hydrodesulfurisation (HDS) [1, 30-32] and hydrodeoxygenation (HDO) [33], with interest being driven by industrial application and environmental considerations. Regarding the petroleum refining industry, such compounds could replace commercial catalysts and enhance the properties of resultant petroleum product. For example, in HDN reactions  $\text{Mo}_2\text{C}$  and  $\text{Mo}_2\text{N}$  have a hydrodenitrogenation activity greater than that of commercial sulfided Ni-Mo /  $\text{Al}_2\text{O}_3$  in the absence of sulfur containing components [28, 29]. Regarding HDS, such molybdenum nitrides and carbides are more active than conventional catalysts. However, on the basis of unit catalysis weight  $\text{Mo}_2\text{C}$  and  $\text{Mo}_2\text{N}$  are inferior to conventional catalysts [1].

Furthermore, molybdenum nitride and carbide are known as active catalysis for ammonia synthesis [25, 34]. Historically, a doubly-promoted iron catalyst was used as a commercial catalyst in the main process for the synthesis of ammonia, which is known as the Haber - Bosch Process. Up until now, this route is still one of the most important industrial processes for producing most commodities. In recent years, Ru has attracted interest as an alternative highly active catalyst with a Ru/C catalyst being commercialised [35]. Molybdenum carbide and nitride were reported to be more active than Ru, but it was found that the doubly-promoted iron catalyst is more active than molybdenum carbide and nitride. At 401 °C and 0.1MPa the order of activity is as follows:  $\beta$ -Mo<sub>2</sub>C >  $\alpha$ -Mo<sub>2</sub>C<sub>1-x</sub> >  $\gamma$ -Mo<sub>2</sub>N. It has also been reported that using Cs<sup>+</sup> as a promoter in this system can increase the areal rate but decrease the surface area [35].

Recently, it has been reported that Co<sub>3</sub>Mo<sub>3</sub>N is more active than the doubly-promoted iron catalyst and they also were found Co<sub>3</sub>Mo<sub>3</sub>N catalyst promoted with Cs<sup>+</sup> (2 mol.%) had much better performance than all other catalysts, including the commercial catalyst [35].

In addition, molybdenum carbide and nitride have been extensively studied for hydrogenation and dehydrogenation reactions. It has been found that Mo<sub>2</sub>C was more active than molybdenum metal in the hydrogenation of benzene to cyclohexane, and its steady-state conversion rate was analogous to that of Pt or Ru [35]. Molybdenum carbide exhibited the highest initial activity and deactivation rate comparing with the other catalysts. In terms of dehydrogenation, n-butane was investigated over carbide and nitride catalysts at 450 °C and 101 kPa for reactant mixture containing 4% n-butane, 60% hydrogen and 36% helium. It was found that the order of activity was  $\gamma$ -Mo<sub>2</sub>N > W<sub>2</sub>C ~ WC > W<sub>2</sub>N > WC<sub>1-x</sub> > Mo<sub>2</sub>C > VN~VC > NbN~ NbC [35].

However, a number of studies have demonstrated that molybdenum carbide gives light hydrocarbons, alcohols and CO<sub>2</sub> in the Fischer-Tropsch reaction [36-38] and also it exhibits high activity. Molybdenum nitride and carbide have been also tested for alkene hydrogenation [39, 40] and removal of NO [23, 25].

## 1.5 Lattice Reactivity

It may be possible to apply molybdenum carbides, nitrides, oxycarbides and oxynitrides as reservoirs of activated carbon and nitrogen which could be transferred to reactants and replenished from gas-phase sources. This concept was inspired by the Mars-van Krevelen oxidation mechanism which is effective in many oxidation reactions catalysed by oxide catalysts. In this mechanism, the lattice oxygen of the oxide acts as the oxidation agent to oxidise the substrate, yielding the oxidised product. Thus transient lattice oxygen vacancies occur within the oxide catalyst which can be replenished by gas phase oxygen containing sources such as  $O_2$ ,  $CO_2$  and  $H_2O$ . Scheme 1 shows the general type of process in which replenishment is achieved with  $O_2$  and where R-H represents an alkane.

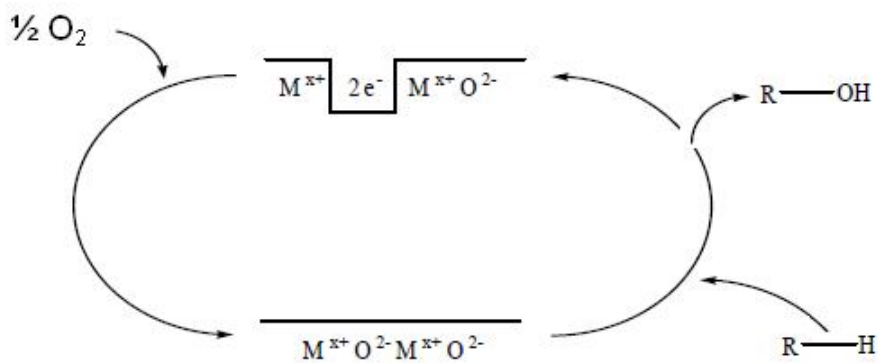


**Figure 1.2 Schematic diagram showing the Mars-van-Krevelen mechanism in oxidation catalysis [41]**

Regarding process considerations, this approach could result in the separation between substrate oxidation and catalyst re-oxidation steps, which may be desirable in some cases such as partial oxidations yielding unstable products [26]. Recently, in temporal analysis of products (TAP) reactor studies, Olea et al. have reported the participation of lattice nitrogen to the product from VAION catalysis during ammoxidation of propane [42]. In

addition, McKay et al. have demonstrated the lability of lattice nitrogen using temperature programmed reaction with a 3:1 H<sub>2</sub>: Ar mixture for some binary nitrides and ternary molybdenum containing nitrides. It was concluded that the main form of nitrogen lost was N<sub>2</sub>, with small amounts of NH<sub>3</sub> [26] and that this could lead to new nitrogen transfer pathways being developed.

In terms of carbides, some analogous studies have been made. Methane homologation is a case in point. The production of higher hydrocarbons directly from methane is highly desirable; however, it requires a temperature  $\geq 927^{\circ}\text{C}$ , due to thermodynamic restrictions. In this regard, Koerts et al. have studied the possibility of the formation a higher hydrocarbons from two-step direct conversion of methane at low temperature in the absence of oxygen [43]. They have reported that ethane, propane and pentane can be produced. As mentioned, this method consists of two steps; the first one was at a temperature around  $427^{\circ}\text{C}$ , wherein methane is adsorbed on a Group VIII transition metal, resulting in surface carbonaceous species and H<sub>2</sub>. The second step is described the ability of carbonaceous intermediate to produce alkanes by hydrogenation at around  $100^{\circ}\text{C}$  [43].

The small number of studies reported to date indicates that the study of lattice reactivity may be profitable. In particular, the direct hydrogenation of carbonitride materials as a source of nitrogen-containing hydrocarbons does not seem to have been considered.

## 1.6 Preparation

Molybdenum carbides, nitrides, oxycarbides and oxynitrides can be prepared by various synthetic approaches. Table 1.1 shows general methods as reported in the literature which have been applied to synthesise molybdenum carbides and nitrides.

**Table 1.1: General methods of synthesis molybdenum carbide and nitride**

Preparation method	Reaction	Phase	References
1) Direct reaction metal and non-metal	$\text{Mo} + \text{C}$	$\text{Mo}_2\text{C}$	[9, 12, 44]
2) The reaction of metal oxide in the presence of solid carbon	$\text{MoO}_3 + \text{C}$	$\text{Mo}_2\text{C}$	[9, 12, 44]
3) Reaction of metal or compounds with gas phase reagent	$\text{Mo} + \text{CO}$	$\text{Mo}_2\text{C}$	[12, 44]
	$\text{MoO}_3 + \text{CO}$	$\text{Mo}_2\text{C}$	[12, 44]
	$\text{MoO}_3 + \text{NH}_3$	$\text{Mo}_2\text{N}$	[12, 44]
4) Temperature-programmed methods	$\text{MoO}_3 + \text{CH}_4, \text{C}_2\text{H}_6,$ Toluene + $\text{H}_2$	$\text{Mo}_2\text{C}, \text{MoC}_{1-x}$	[4, 12, 31]
	$\text{MoO}_3 + \text{NH}_3$	$\text{Mo}_2\text{N}, \text{MoN}$	[12, 16]
	$\text{MoO}_3 + \text{H}_2/\text{N}_2$	$\beta\text{-Mo}_2\text{N}, \beta\text{-Mo}_2\text{N}_{0.78}$	[24, 26]
	$\text{MoO}_3 + \text{C}$	$\text{Mo}_2\text{C}$	[9, 12, 44]
5) The reaction with metal oxide vapour and solid carbon under vacuum	$\text{MoO}_3 + \text{C}$	$\text{Mo}_2\text{C}$	[9, 12, 44]
6) Pyrolysis of an organometallic complex under $\text{H}_2$	$\text{Cp}_2 + \text{Mo}_2(\text{CO})_4 (\text{dmad})$	$\text{Mo}_2\text{C}$	[12, 44]
7) Chemical vapour deposition	$\text{Mo}(\text{CO})_6 + \text{CO}, \text{H}_2$	$\text{Mo}_2\text{C}$	[9, 12, 44]
	$\text{MoCl}_5 + \text{CH}_4 + \text{H}_2$	$\text{Mo}_2\text{C}$	[45]
	$\text{MoCl}_5 + \text{NH}_3$	$\delta\text{-MoN}$	[46]
	$\text{MoCl}_5 + \text{Urea} + \text{N}_2$	$\text{Mo}_2\text{N}$	[47, 48]

Historically, methods such as direct carburisation or nitridation of metals or metal oxides at high temperature have been applied to produce molybdenum carbides or nitrides with low surface area. Due to surface area considerations in catalysis, these routes are now rarely used in catalyst preparation.

In recent times, temperature programmed reaction, which was developed by Boudart, is the most commonly applied technique to produce molybdenum carbides and nitrides with high surface area [9, 25]. In this method, high surface area  $\text{Mo}_2\text{C}$  and  $\text{Mo}_2\text{N}$  were formed by the reaction between  $\text{MoO}_3$  and  $\text{CH}_4/\text{H}_2$  to produce hexagonal  $\text{Mo}_2\text{C}$  with surface area of 50 to 100  $\text{m}^2/\text{g}$  or between  $\text{MoO}_3$  and  $\text{NH}_3$  to form  $\text{Mo}_2\text{N}$  which was pseudomorphic with the precursor and which had specific surface area up to 220  $\text{m}^2/\text{g}$  [16, 17, 22, 27]. The resultant materials are pyrophoric and are sensitive to exposure to air. Thus, a passivation step is required utilising diluted  $\text{O}_2$  at room temperature in order to form surface oxynitride and oxycarbide phases to prevent oxidation of bulk the desired phases [40].

In general, the preparation of such compounds with high specific surface area requires very controlled conditions which include high space velocities of reactant gas and low temperature ramp rates [9, 25]. Choi et al. have illustrated that the impact of the applied conditions, low ramp rate and high space velocity, are important factors to control the structural properties in molybdenum nitride via the temperature programmed reaction of  $\text{MoO}_3$  with  $\text{NH}_3$  [49]. An important consideration to produce high surface area materials was channeling the conversion of  $\text{MoO}_3$  through  $\text{H}_x\text{MoO}_3$  ( $x \leq 0.34$ ) and  $\gamma\text{-Mo}_2\text{O}_y\text{N}_{1-y}$  intermediates as summarised in Figure 1.3:

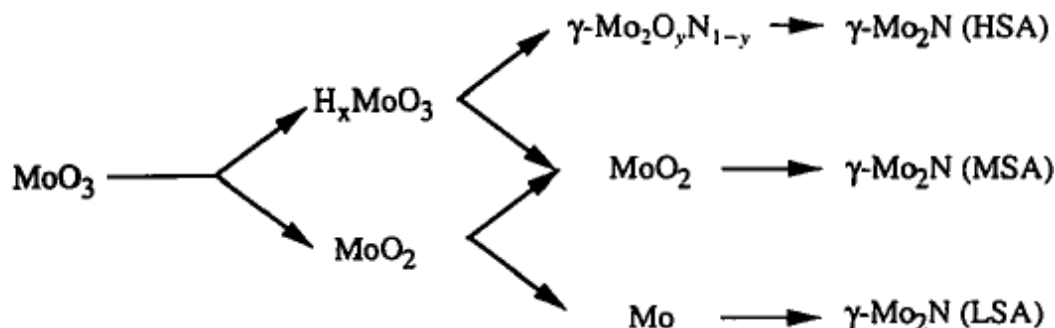


**Figure 1.3 Schematic diagram showing the conversion pathways during ammonolysis of  $\text{MoO}_3$ . The low, medium and high surface area catalysts are represented by LSA, MSA and HAS, respectively [49]**

However, a number of studies have investigated the effects of addition of small amounts of some transition metals such as Pd, Au, Ni and Cu upon the formation of molybdenum nitrides and carbides from direct conversion of molybdenum oxide precursors by temperature programmed reaction. Cairns et al. have studied the influence of addition of 1wt% Pd, Au, Ni and Cu upon a preparation of  $\beta\text{-Mo}_2\text{N}_{0.78}$  from the reaction of  $\text{MoO}_3$  with a 3/1  $\text{H}_2/\text{N}_2$  mixture at 750 °C [50]. It was reported that the addition of such metals on the precursor can lead to an increase in the specific surface area of the resultant molybdenum nitride. It was concluded that Pd dopant appears to enhance the formation of nitride, whereas Au impedes it. Cairns et al. have also studied the influence of dopants upon the denitridation of  $\beta\text{-Mo}_2\text{N}_{0.78}$  by using a 3/1  $\text{H}_2/\text{Ar}$  mixture. It was found that the addition of dopants lowered the quantity of ammonia produced under denitridation [50]. Impurity content of a precursor can strongly impact upon the morphology and the content of molybdenum in the final product. Cairns et al. have used two different sources of molybdenum trioxide to produce molybdenum nitride under a  $\text{N}_2/\text{H}_2$  gas mixture at 700 °C and 750 °C. It was concluded that the composition of product phase is a function of precursor purity [19].

In addition, Jung et al. have investigated the effect of addition of Pt, Pd, Ni, Cu and Co upon the formation of molybdenum carbide from the reaction of  $\text{MoO}_3$  with a reacting gas mixture of  $\text{CH}_4/4\text{H}_2$  [51]. The influence of dopants was observed to enhance the

specific surface area, temperature of reduction and obtained phases of molybdenum carbides. It was reported that the addition of dopants increased the specific surface area of resulting carbides and reduced the initiation temperature of reduction. In terms of the obtained phase of molybdenum carbide, it was reported that a cubic  $\alpha$ - $\text{MoC}_{1-x}$  can be obtained from Pt, Pd, or Ni doped  $\text{MoO}_3$ , whereas the remainder of the metals doped formed hexagonal  $\beta$ - $\text{Mo}_2\text{C}$ , which was similar to the phase produced by the conventional method under same conditions without any metal loading [51].

Li et al. have studied the impact of reactant gas on the transformation of  $\text{MoO}_3$  by temperature programmed reaction to form molybdenum carbide and nitride. The gases used were  $\text{H}_2$  and  $\text{NH}_3$  and the mixtures of  $\text{CH}_4$  or  $\text{CO}$  and  $\text{H}_2$  ( $\text{CH}_4/\text{H}_2$  1/4), ( $\text{CO} / \text{H}_2$  1/4) and ( $\text{N}_2/\text{H}_2$  1/3 and 3/1). It was concluded that using reacting gas mixtures of ( $\text{CH}_4/\text{H}_2$  1/4) and ( $\text{CO}/\text{H}_2$  1/4) led to the production of  $\beta$ - $\text{Mo}_2\text{C}$ , whilst ( $\text{N}_2/\text{H}_2$ ) resulted in  $\beta$ - $\text{Mo}_2\text{N}$ . It was also concluded that the solid-state transformation of  $\text{MoO}_3$  to molybdenum nitride by reaction with  $\text{NH}_3$  was topotactic and pseudomorphic. In contrast,  $\text{MoO}_3$  took a non-topotactic pathway by reaction with the  $\text{N}_2/\text{H}_2$  gas mixtures. It was concluded that it was necessary for the nitridation or carburisation to occur in the early stages of reduction at low temperature for topotactic conversion [24].

A number of studies have indicated that molybdenum nitride, carbide and oxycarbonitride can be prepared by thermal treatment of single source precursors. Afanasiev studied the thermal decomposition of a chemically homogeneous molecular precursor generated by reaction of hexamethylenetetramine (HMT) with ammonium heptamolybdate (AHM). The resultant material was  $(\text{HMT})_2(\text{NH}_4)_4 \text{Mo}_7\text{O}_{24} \cdot 2\text{H}_2\text{O}$  which was decomposed under an argon atmosphere in the temperature range 550-800 °C. It was observed that crystalline  $\text{Mo}_2\text{N}$  can be obtained at a temperature higher than 650 °C by this method. The surface area was decreased from around 139  $\text{m}^2/\text{g}$  at 650 °C to roughly 71  $\text{m}^2/\text{g}$  at 800 °C [52].

In addition, Wang et al. have reported that  $\beta\text{-Mo}_2\text{C}$  can be prepared by mixing HMT and  $(\text{HMT})_2(\text{NH}_4)_4 \text{Mo}_7\text{O}_{24} \cdot 2\text{H}_2\text{O}$  at a 7:1 molar ratio and reacting at 700 °C in an argon atmosphere. They have emphasised that temperature, which must be  $\geq 700^\circ\text{C}$ , is an important condition to synthesise  $\beta\text{-Mo}_2\text{C}$ . They also have indicated that the advantages of using this method to prepare molybdenum carbide are : 1) the low cost of the starting materials, 2) that the procedure of preparation is simple and facile, 3) that it does not require high flow rates of gaseous hydrocarbons and low temperature ramp rates [31]. Furthermore, single source precursor routes comprising HMT and AHM have been investigated under  $\text{H}_2$  atmosphere by Wang et al. They studied the influence of AHM and HMT molar ratios in the precursors, the influence of the heat treatment and the influence of the preparation method of the precursors on the final products. In terms of the influence of AHM and HMT, they found that pure  $\text{Mo}_2\text{C}$  can be obtained when the molar ratio of AHM and HMT reaches 1:4 in the precursors whilst the precursors with molar ratio 1:2 may produce nitride, carbide and carbonitride composite materials. Regarding the influence of the treatment temperature, they showed that  $\text{Mo}_2\text{N}$  becomes the major product phase at lower temperatures (e.g. 500 °C). In contrast,  $\text{Mo}_2\text{C}$  was produced at higher temperature (650 °C).

In terms of the influence of the preparation method, they prepared the precursors by two different methods. The first followed the method reported by Afanasiev [52]. The second method involved mechanically mixing AHM and HMT with a molar ratio of 1:4. They found that the former method yielded  $\text{Mo}_2\text{C}$  whilst, the second method produced metallic Mo and  $\text{MoO}_2$  [32].

McCandlish et al have patented novel molybdenum oxycarbonitride compositions prepared by thermal decomposition of the single source precursor ethylenediammonium molybdate. They found that a phase of composition  $\text{MoO}_{0.43}\text{C}_{0.31}\text{N}_{0.33}$  can be obtained under a helium atmosphere at  $650\text{ }^\circ\text{C}$ . They also found that the phases produced at low temperature (below  $650\text{ }^\circ\text{C}$ ) were amorphous or poorly crystalline [53].

## **1.7 Aim**

The aim of this work was to investigate the synthesis molybdenum carbides, nitrides or oxycarbonitrides by single source routes under various reaction atmospheres. In addition, initial studies aimed at determining the reactivity of the lattice species have been undertaken. This work is directed towards the possible production of important nitrogen containing organic products (e.g. amines) by the controlled reduction of carbonitride phases.

## **Chapter 2: Experimental**

### **2.1 Introduction**

The experimental techniques applied in this work are presented in four discrete sections: preparation of precursors, reactor design, experimental procedure and characterisation of resultant products.

### **2.2 Preparation of precursors**

There were two different precursors that have been employed in order to synthesise the desired compounds. The first precursor was ethylenediammonium molybdate and the second was hexamethylenetetramine molybdate.

#### **2.2.1 Preparation of ethylenediammonium molybdate**

Ethylenediammonium molybdate was prepared by mixing 5 g of molybdic acid ( $\text{H}_2\text{MoO}_4$  Sigma Aldrich,  $\geq 85$ ), and 75 ml of ethylenediamine (Sigma Aldrich BioXtra  $\geq 99.5$ ) which were then refluxed under stirring at 120 °C for around 16 hours, resulting in white - coloured product which was filtered. The resultant product was then washed with ethanol in order to remove any un-reacted ethylenediamine, after which the sample was dried overnight in an oven at 110 °C to remove the residual ethanol.

Powder X-ray diffraction and C H N analysis confirmed production of desired the phase as indicated in previous literature.[53]

#### **2.2.2 Preparation of hexamethylenetetramine molybdate**

Hexamethylenetetramine molybdate was synthesised by reacting hexamethylenetetramine (HMT) (Sigma Aldrich, 99.9 %) with  $(\text{NH}_4)_6\text{Mo}_7\text{O}_{24}\cdot 4\text{H}_2\text{O}$  (AHM) (Sigma Aldrich, 99.9 %). 3.5 g of AHM was dissolved in 50 ml of distilled water and 6 g of HMT was dissolved in 50 ml of distilled water. The HMT solution was then added to the AHM solution with stirring for several minutes. The reactants were left

overnight in air at room temperature, and colourless crystals precipitated. The crystals were filtered using filter paper (Whatman size 2). The obtained precursor was washed with a small quantity of deionised water, and dried in air. Powder X-ray diffraction and C H N analysis confirmed the phase as indicated in previous literature [52].

## **2.3 Reactor design**

In this work, various different precursors have been investigated. The hexamethylenetetramine molybdate and ethylenediammonium molybdate are the main precursors that have been investigated extensively in terms of temperature, ramp rate, flow rate and reaction atmosphere.

### **2.3.1 Decomposition of precursors**

The decomposition of all materials was performed in microreactor. A fixed bed microreactor as shown in Figure 2.1 was used. The material to be reacted was held centrally in a quartz tube (1cm internal diameter) between quartz wool plugs housed in a tube furnace (Carbolite MTF 10/25/130). A variety of gas mixtures were employed in these studies and flow control was achieved using a mass flow controller (Brooks Model 5850 SE) controlled with a control box (Brooks Model 5878). The various gases used for experiments were 3:1 H<sub>2</sub>:N<sub>2</sub> (BOC, H<sub>2</sub> 99.998%, N<sub>2</sub> 99.995%), 3:1 H<sub>2</sub>/Ar (BOC, H<sub>2</sub> 99.998%, Ar min 99.99%), Ar (BOC, 99.998%), 1:3 H<sub>2</sub>:N<sub>2</sub> (BOC, H<sub>2</sub> 99.998%, N<sub>2</sub> 99.995%) and N<sub>2</sub> (BOC 99.995%). The output gas from the reaction was passed through a water bubbler. All gases were vented through a fume cupboard.

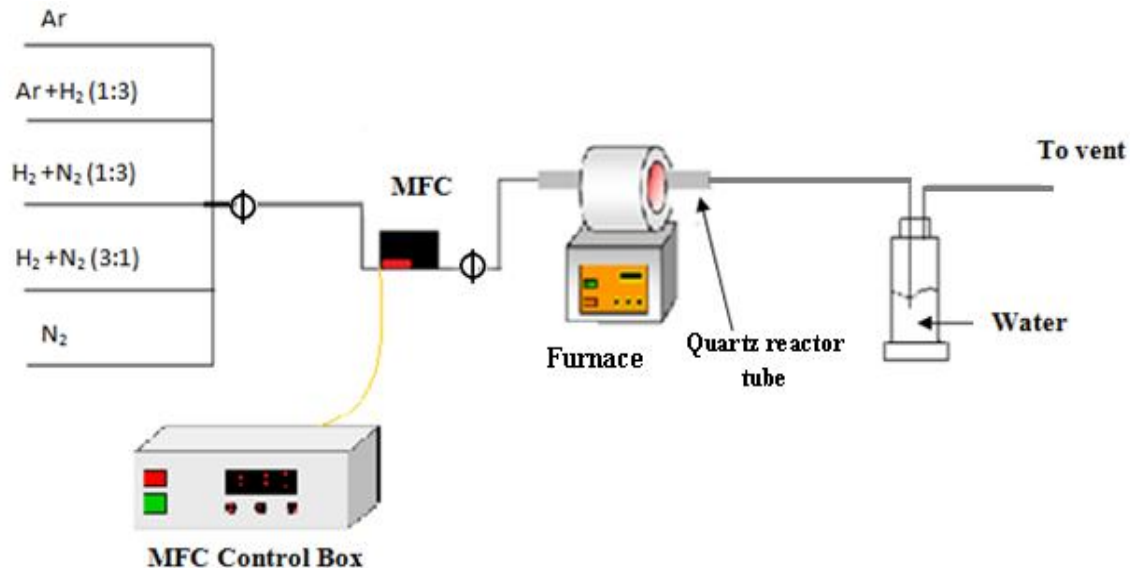


**Figure 2.1 Reactor for thermal decomposition preparation**

In these studies, different amounts of precursors were used and a variety of reaction atmospheres and temperature ramp rates were applied. Prior to discharge, all materials were passivated by back-diffusion of air overnight. Summaries of the conditions used are presented in Tables 2.1, 2.2 and 2.3.

**Table 2.1 : Conditions used for the decomposition of hexamethylenetetramine molybdate**

sample code	Mass g	Reaction Atmosphere	flow rate ml/min	Max. Temp.°C	Ramp rate °C/min	dwelt time hour
I-4	1.00	Ar	60	800	10	2
I-7 <i>in-situ</i>	1.00	Ar	60	800	10	2
I-6	1.00	Ar	10	800	10	2
I-12	1.00	Ar	10	700	10	2
I-10	1.00	Ar	60	700	10	2
I-14	1.00	Ar	94	700	10	2
I-21	1.00	Ar	125	700	10	2
I-17	1.00	Ar	60	700	2	2
I-16	1.00	Ar	60	700	5	2
I-28	1.00	N <sub>2</sub>	60	700	10	2
I-22	1.00	H <sub>2</sub> /N <sub>2</sub> 1 : 3	60	700	10	2
I-24	1.00	H <sub>2</sub> /N <sub>2</sub> 3 : 1	60	700	10	2
I-26	1.00	H <sub>2</sub> /Ar 3 : 1	60	700	10	2

**Table 2.2 : Conditions used for the decomposition of different precursors**

sample code	precursor	Mass g	Reaction Atmosphere	flow rate ml/min	Max. Temp.°C	Ramp rate °C/min	dwelt time hour
M-1	MoO <sub>3</sub>	1.00	H <sub>2</sub> /N <sub>2</sub> 1 : 3	60	700	10	2
M-2	MoO <sub>3</sub>	1.00	H <sub>2</sub> /N <sub>2</sub> 3 : 1	60	700	10	2
M-3	MoO <sub>3</sub>	0.40	H <sub>2</sub> /N <sub>2</sub> 3 : 1	60	650	10	2
M-4	MoO <sub>3</sub>	0.40	H <sub>2</sub> /N <sub>2</sub> 3 : 1	60	700	10	2
M-5	MoO <sub>3</sub>	0.40	H <sub>2</sub> /N <sub>2</sub> 3 : 1	60	750	10	2
M-6	MoO <sub>3</sub>	0.40	H <sub>2</sub> /N <sub>2</sub> 3 : 1	60	800	10	2
H-1	H <sub>2</sub> MoO <sub>4</sub>	1.00	H <sub>2</sub> /N <sub>2</sub> 1 : 3	60	700	10	2
H-2	H <sub>2</sub> MoO <sub>4</sub>	1.00	H <sub>2</sub> /N <sub>2</sub> 3 : 1	60	700	10	2
A-1	AHM	1.00	H <sub>2</sub> /N <sub>2</sub> 1 : 3	60	700	5	2
A-2	AHM	1.00	H <sub>2</sub> /N <sub>2</sub> 3 : 1	60	700	10	2
A-3	AHM	1.00	H <sub>2</sub> /Ar 3 : 1	60	700	10	2

**Table 2.3 : Conditions used for the decomposition of ethylenediammonium molybdate**

sample code	Mass g	Reaction Atmosphere	flow rate ml/min	Max. Temp.°C	Ramp rate °C/min	dwelt time hour
E-5	0.75	Ar	60	800	10	2
E-8 <i>In-situ</i>	0.75	Ar	60	800	10	2
E-9	0.75	Ar	10	800	10	2
E-11	0.75	Ar	60	700	10	2
E-13	0.75	Ar	10	700	10	2
E-15	0.75	Ar	94	700	10	2
E-18*	1.00	Ar	60	700	10	2
E-19*	1.00	Ar	60	700	10	2
E-29	0.75	N <sub>2</sub>	60	700	10	2
E-23	0.75	H <sub>2</sub> /N <sub>2</sub> 1 : 3	60	700	10	2
E-25	0.75	H <sub>2</sub> /N <sub>2</sub> 3 : 1	60	700	10	2
E-27	0.75	H <sub>2</sub> /Ar 3 : 1	60	700	10	2

E – 18\* a physical mixture of ethylenediammonium molybdate with MoO<sub>3</sub> where the molar ratio was 1: 1

E - 19\* a segregated bed of ethylenediamine and molybdenum trioxide in which the ethylenediamine was placed upstream of the MoO<sub>3</sub> where the molar ratio was 1: 1

### 2.3.2 Lattice nitrogen reactivity studies

A modification of previously described microreactor was used to study the reactivity of lattice nitrogen to generate  $\text{NH}_3$  for selected materials. A fixed bed microreactor as shown in Figure 2.2 was applied. The material to be reacted was held centrally in a quartz tube (1cm internal diameter) between quartz wool plugs housed in tube furnace (Carbolite MTF 10/25/130).  $\text{H}_2/\text{Ar}$  was employed in these studies and flow control was achieved using a mass flow controller (Brooks Model 5850 SE) controlled with a control box (Brooks Model 5878). In these studies, approximately 0.4g of precursors (I – 21, I – 22 or E – 23) were loaded in the reactor and treated with 60 ml/min of 3:1  $\text{H}_2/\text{Ar}$  (BOC,  $\text{H}_2$  99.998%, Ar min 99.99%). The temperature profile used is illustrated in Figure 2.3 and a temperature ramp rate of  $10^\circ\text{C}/\text{min}$  was applied. The output gas from the reaction was passed through 200 ml of an  $\text{H}_2\text{SO}_4$  solution (0.00108 M). The decline in conductivity, corresponding to the reaction between  $\text{H}^+$  and  $\text{NH}_3$  to form  $\text{NH}_4^+$  ions, was measured using a conductivity meter (EDT instrument BA 380). All gases were vented through a fume cupboard.

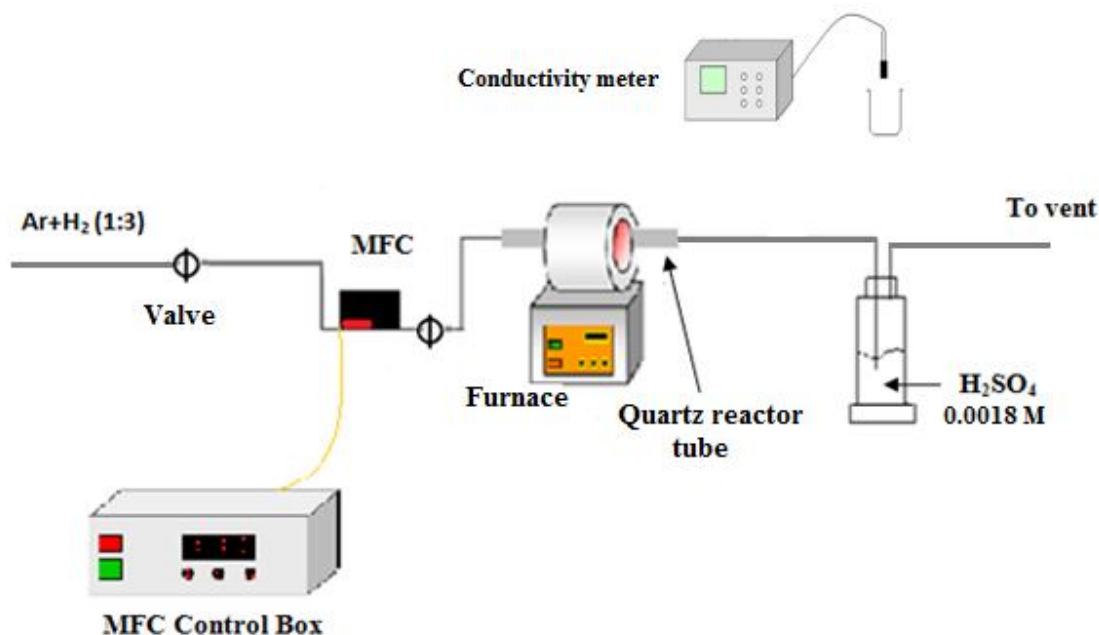
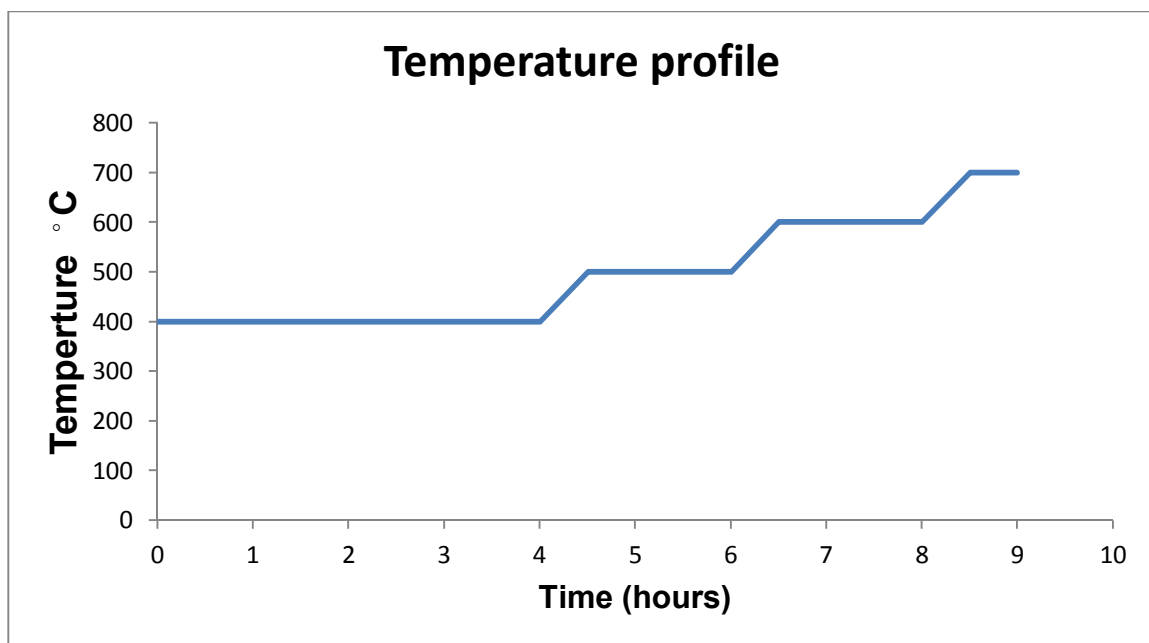


Figure 2.2 Apparatus employed for studies of the reactivity of lattice nitrogen



**Figure 2.3: Temperature profile of the lattice nitrogen reactivity studies**

### **2.3.3 Stability studies**

The stability studies were investigated using the same apparatus illustrated in Figure 2.1. Approximately 0.15g of the material of interest (I – 22 or E – 23) was packed in the reactor and was treated with 60 ml/min of either 3:1 H<sub>2</sub>/Ar (BOC, H<sub>2</sub> 99.998%, Ar min 99.99%) or pure Ar (BOC, 99.998%). The temperature profile and gases used are illustrated in Figure 2.4 and 2.5. A 10 °C/ min ramp rate was used. The output gas from the reaction was passed through a water bubbler. All gases were vented through a fume cupboard.

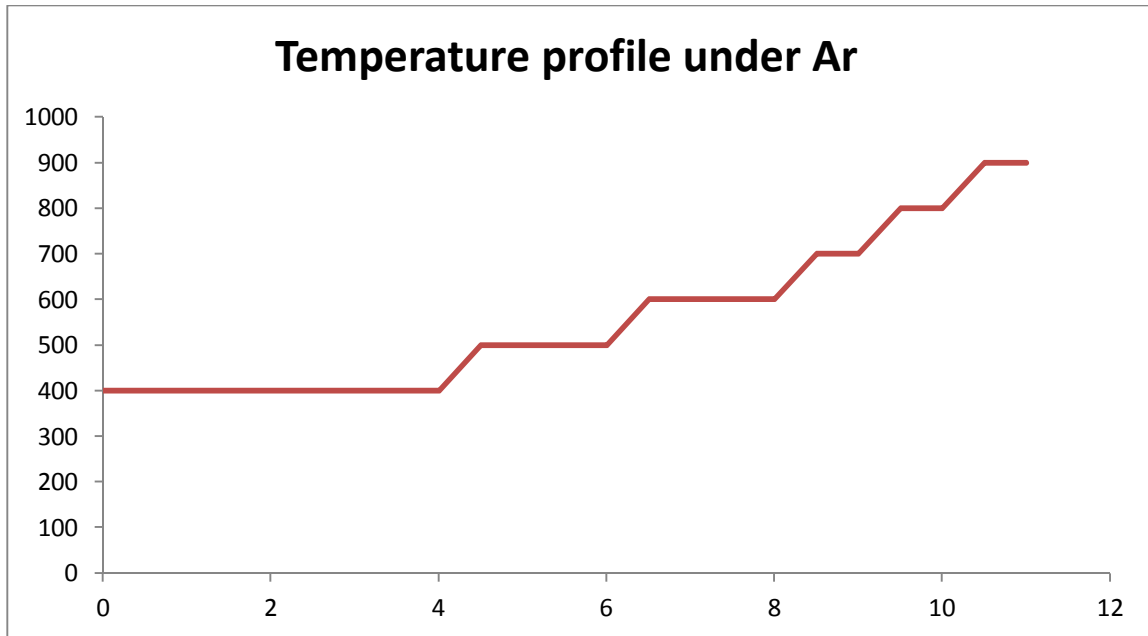


**Figure 2.4: Temperature profile of the stability studies under Ar**

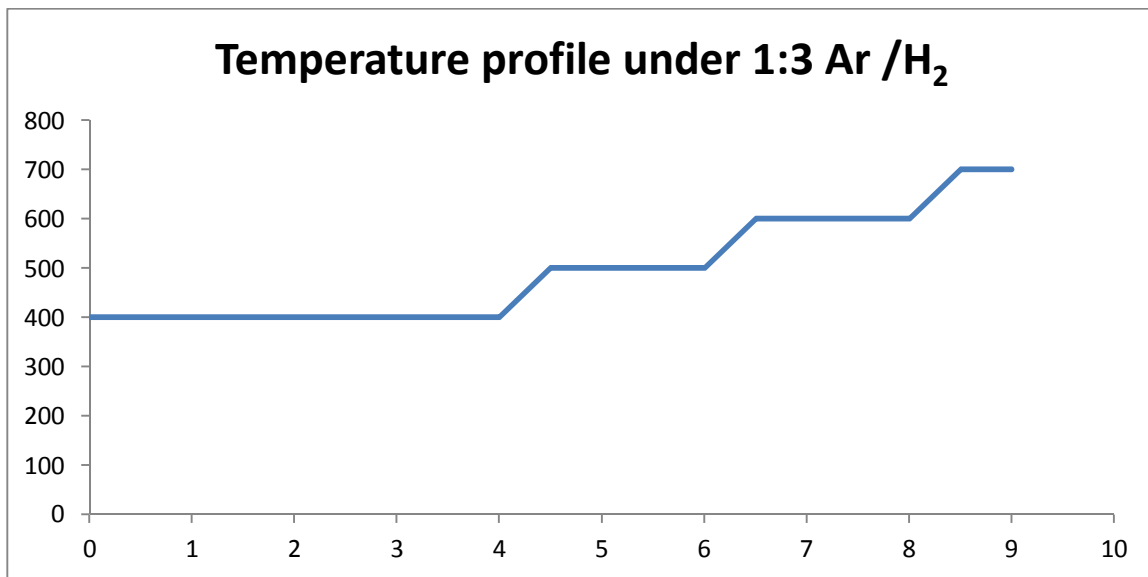


**Figure 2.5: Temperature profile of the stability studies under 1:3 Ar /H<sub>2</sub>**

## 2.4 Characterisation methods

In this project there were several techniques that were used in order to prove, describe and characterise the properties of materials.

### 2.4.1 Powder X-ray diffraction (XRD)

Powder X-ray diffraction was used to identify phases of the pre- and post-reaction samples. The apparatus used to obtain the X-ray patterns was a Siemens D5000 X-ray diffractometer (40kV, 40mA) using a CuK $\alpha$  X-ray source (1.5418Å). The patterns were collected over a scanning range of  $5^\circ < 2\theta < 85^\circ$  with a step size of  $0.02^\circ$  and counting time of 1s per step. *In-situ* XRD was carried out under an argon atmosphere using an Antonn-Parr XRK cell fitted to the diffractometer.

### 2.4.2 Surface Area Determination

The surface area for each sample was determined by using a Micrometrics Gemini III 2375 Surface Area Analyser. Approximately 0.04g of sample was loaded in a vessel and degassed in a flow of nitrogen overnight at 110°C. Then, the sample was weighed to determine the actual weight of the sample after removing any adsorbed moisture by degassing. Subsequently, the vessel was charged into the instrument to measure its surface area. The surface area was calculated by applying the BET equation [54] to the N<sub>2</sub> physisorption isotherm determined at -196 °C.

$$\frac{P}{V_{total}(P-P_0)} = \frac{1}{V_{mono}C} + \frac{c-1}{V_{mono}C} \left( \frac{P}{P_0} \right)$$

Where:  $V_{total}$  = volume of gas adsorbed at equilibrium pressure P,

$V_m$  = monolayer capacity,

$P_0$  = saturated vapour pressure of the adsorbed gas at the temperature of measurement,

C = a constant,

### **2.4.3 Thermogravimetric Analysis**

Thermogravimetric analysis of hexamethylenetetramine molybdate and ethylenediammonium molybdate precursors were carried out in a SDT Q600 series combined TGA-DSC instrument supplied by TA Instruments. In each case, approximately 0.005g of sample was loaded in a sample pan and heated from room temperature to 900 °C under a flowing Ar atmosphere (100 ml/min) at a ramp rate of 10 °C /min.

### **2.4.4 Determination of Carbon, Hydrogen and Nitrogen Content**

C H N (Carbon, Hydrogen and Nitrogen) analysis was kindly conducted by Mrs Kim Wilson at the University of Glasgow. This technique involved combustion of each sample in an Exeter Analytical CE- 440 elemental analyser.

### **2.4.5 Scanning Electron Microscopy (SEM)**

Scanning Electron Microscopy (SEM) images of the all samples were performed by using a Philips XL30 ESEM. The samples were coated by using a Polarn SC7640 Auto high resolution sputter coater with a gold / palladium target. This technique was used to study the morphology and surface features of the samples.

## 2.4.6 Thermal volatilisation analysis (TVA)

Thermal volatilisation analysis was undertaken with the kind assistance of Dr. John Liggat and Miss Debbie Todd from the Department of Pure and Applied Chemistry, University of Strathclyde. Approximately 70 mg of the sample was pumped overnight on the TVA system prior to analysis in order to reduce the background levels of carbon dioxide and water within the system. The heating rate applied was 10°C/min and samples were held isothermally at 850 °C for thirty minutes with continual cryogenic collection of the extracted volatiles. Sub-ambient differential distillation of collected volatiles was performed by increasing the temperature of the primary cold trap from -196 °C to 30 °C. The volatiles were separated into four secondary cold traps and transferred to IR and GC-MS sample cells. A combination of GC-MS, FTIR spectroscopy and MS was used to analyse the separated volatiles. Figure 2.6 shows a schematic of the system for thermal volatilisation and sub-ambient differential distillation analysis (TVA).

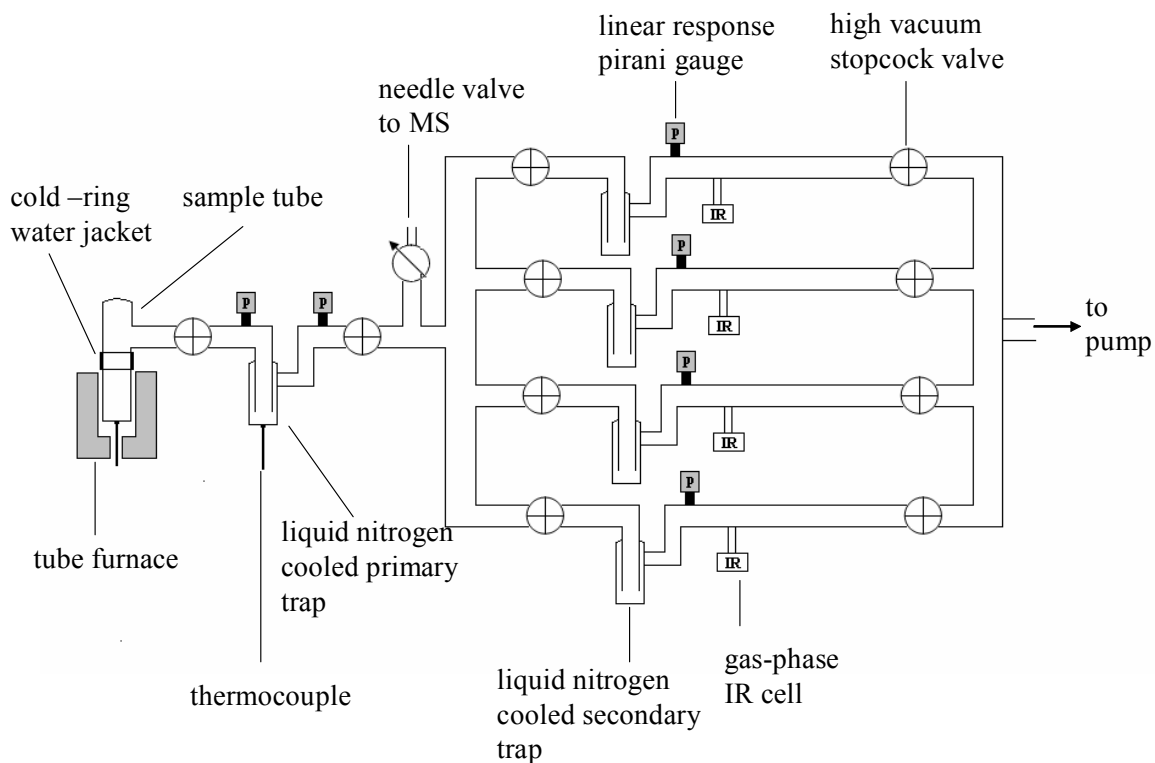


**Figure 2.6: Schematic diagram of the TVA apparatus**

### **2.4.7 X-Ray photoelectron spectroscopy (XPS)**

XPS analysis was kindly undertaken by Dr. David Morgan at the EPSRC XPS access facility at Cardiff University using a Kratos Axis Ultra-DLD photoelectron spectrometer equipped with a delay-line-detector (DLD). Analysis was performed using a monochromatic Al  $K_{\alpha}$  source ( $h\nu = 1486.6$  eV) and at pass energies of 160 eV for survey scans and 40 eV for the high resolution region scans; the step size for these scans was 1 eV and 0.1 eV respectively. Multiple scans were performed to increase the signal to noise ratio. The system was operated in the hybrid spectroscopy mode which utilises both magnetic and electrostatic transfer lenses for enhanced sensitivity, and the analysis area in this mode is approximately 300x400 microns. Sputtering was achieved using a minibeam I reseating ion source, using argon ions at 4 keV over an area of approximately 4 mm. Subsequent analysis was performed at the same position each time in the centre of the sputtered area. Charge neutralisation was performed using an immersion lens system, resulting in a 2-3 eV shift to lower energy which was then corrected through calibration to the C1s line for adventitious carbon with assigned energy of 284.7 eV. Spectra were quantified using CasaXPS software v2.3.15, and corrected for analyser transmission. Elemental sensitivity factors were supplied by the manufacturer.

### **Chapter 3: Hexamethylenetetramine molybdate single source route**

Hexamethylenetetramine molybdate has been widely used for the preparation of molybdenum nitride and carbide [32, 52]. The HMTA precursor acts as a nitrogen and a carbon source and also the carbon source can act as reducing agent to remove oxide species from the precursor in unreactive atmospheres. The final products that are generated from this precursor rely on a number of parameters such as the crystallinity of the precursor, the gas flow rate applied, the mass of sample used and the amount of H<sub>2</sub>O generated from the precursor [55]. Moreover, various products were obtained from the thermal decomposition of hexamethylenetetramine molybdate precursor under different reaction gases. Afanasiev prepared molybdenum nitride by using the precursor under an Ar atmosphere at 800°C [52]. Furthermore, another study by Chouzier et al. has documented the preparation of molybdenum carbide and molybdenum nitride using the same precursor, where the molybdenum carbide is obtained when H<sub>2</sub> containing reaction gas is employed, and molybdenum nitride is alternatively obtained when either Ar or NH<sub>3</sub> is employed [55].

In this work, thermal decomposition of hexamethylenetetramine molybdate under various reaction atmospheres has been undertaken in order to obtain molybdenum carbonitrides that may be of interest as reagents for the preparation of nitrogen containing organic compounds.

### 3.1 Investigation of hexamethylenetetramine molybdate

Hexamethylenetetramine molybdate (designated I) was prepared as described in Section 2.2.2. Chemical analysis was undertaken and it was found that I contained 9.60 wt. % carbon and 10.94 wt. % nitrogen. This result agrees with the stoichiometric composition  $(\text{HMT})_2(\text{NH}_4)_4\text{Mo}_7\text{O}_{24}\cdot 2\text{H}_2\text{O}$  as documented by Afanasiev where it was also reported that precursor I has a complex low symmetry unit cell [52]. Powder X-ray diffraction of the precursor was undertaken and the resultant pattern is shown in Figure 3.1.

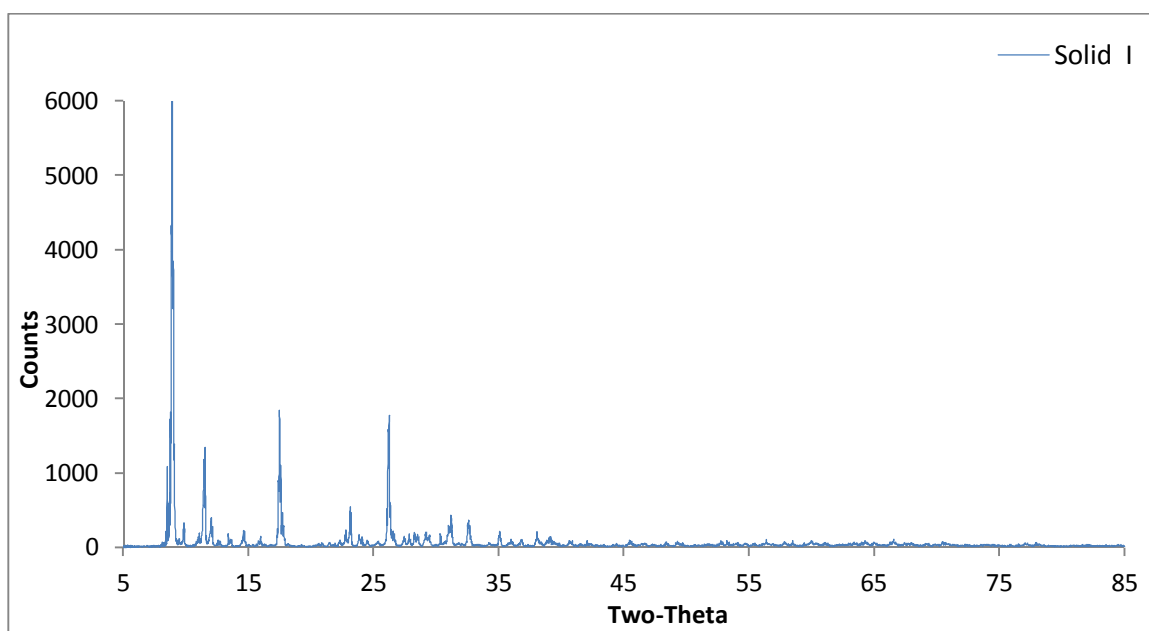


**Figure 3.1 XRD pattern of precursor I**

TGA-DSC analysis of the precursor I was also performed under an argon atmosphere, as shown in Figure 3.2. The TGA analysis showed that the total weight loss was 50.1% corresponding to formation of  $\text{Mo}_2\text{N}$  as determined by the stoichiometric calculation presented in Appendix 1. It also indicated that the mass remained constant beyond 700 °C.

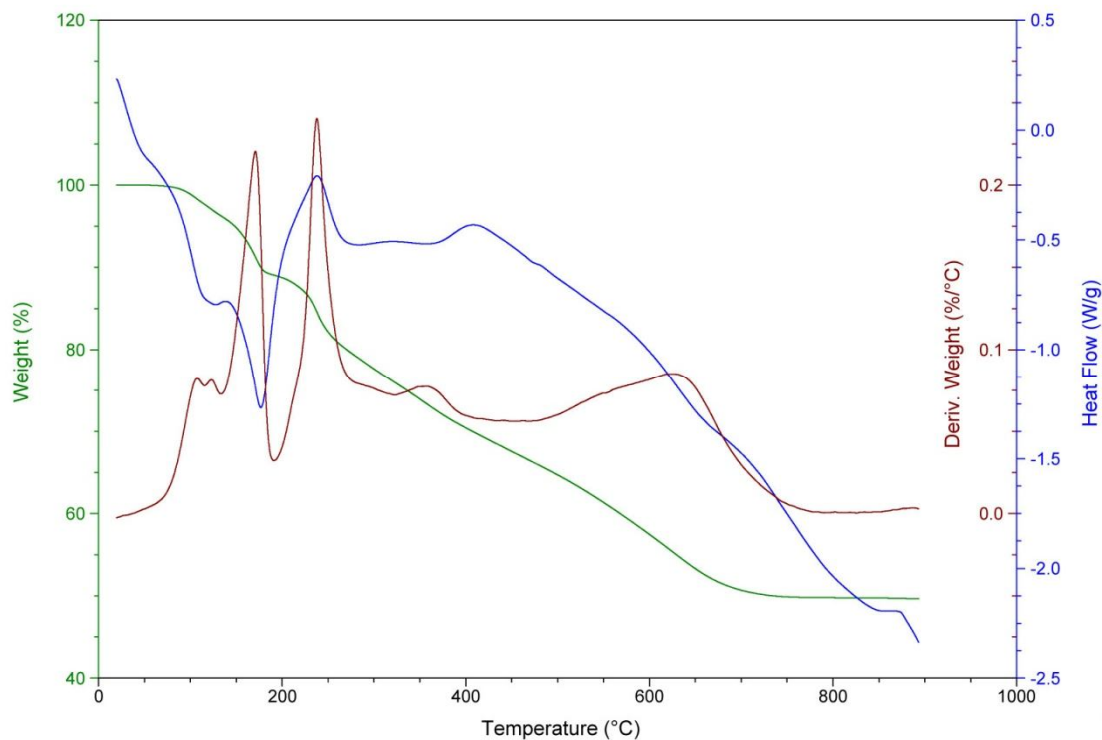


**Figure 3.2 TGA-DSC profile of precursor I under argon atmosphere**

An *in-situ* XRD experiment was performed to investigate the thermal decomposition process of precursor I. This experiment was conducted under a 60 ml/min flow of argon from room temperature to 800 °C. A scan was taken at each 100 °C interval. The results are presented in Figure 3.3 which shows the five most significant stages of transformation during the experiment. The progressive development of  $\beta$ -Mo<sub>2</sub>N<sub>0.78</sub> as function of temperature can be clearly seen as can a small reflection corresponding to the presence of Mo metal in the 800 °C pattern.

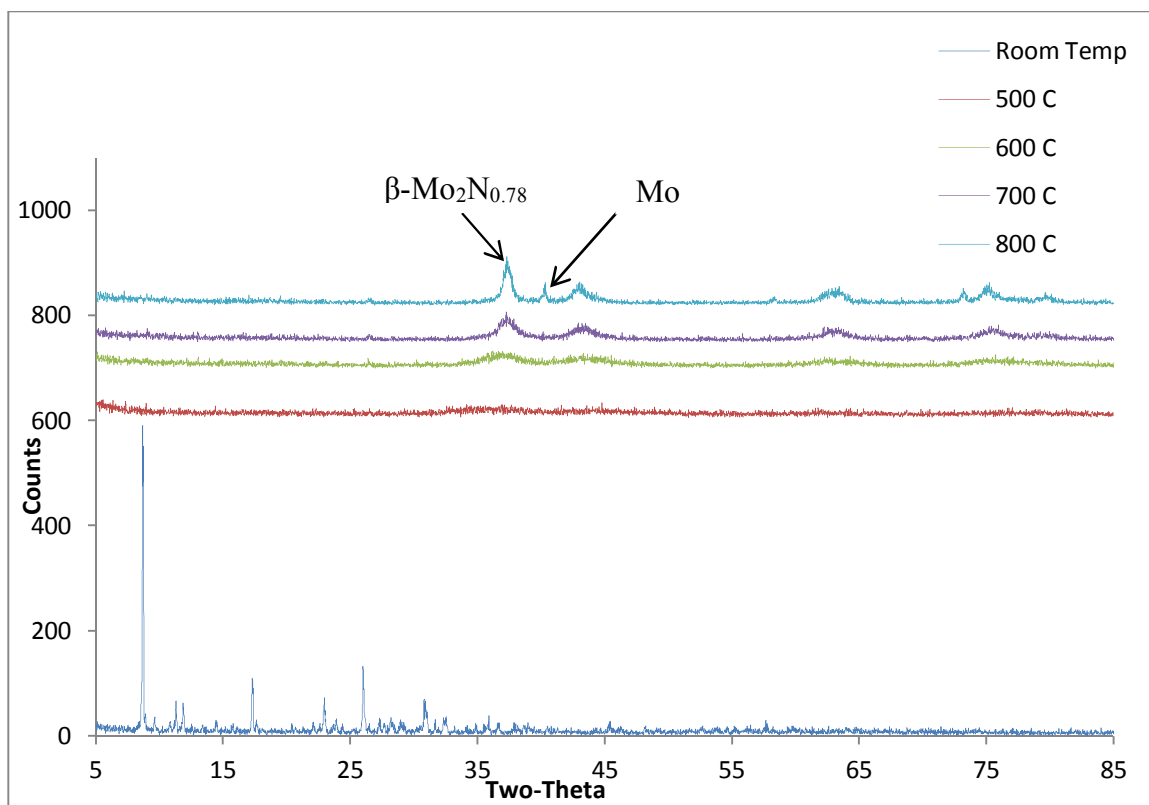


**Figure 3.3** *In-situ* XRD patterns at room temperature, 500 °C, 600 °C, 700 °C and 800 °C

As mentioned in experimental chapter, the thermal decomposition studies of precursor I were performed under a variety conditions. In this respect, the results are presented in three discrete sections: (i) decomposition under an argon atmosphere at 800 °C, (ii) decomposition under an argon atmosphere at 700°C and (iii) decomposition under different reaction atmospheres at 700°C.

### 3.1.1 Decomposition of precursor I under an argon atmosphere at 800 °C

As previously described in the experimental chapter, decomposition was undertaken using two different flow rates – 60ml/min (yielding sample I-4) and 10ml/min (yielding sample I-6).

#### 3.1.1.1 XRD patterns

Figure 3.4 presents the resultant XRD patterns of samples I-4 and I-6. The patterns can be matched to  $\beta$ -Mo<sub>2</sub>N<sub>0.78</sub> (e.g. a reflection signature is present at ca. 38° 2 $\theta$  consistent with JCPDS, 25-1368). MoO<sub>2</sub> is also evident as shown by its signature reflection at 26° 2 $\theta$  (JCPDS, 32-0671). It is interesting to note that the peak intensities of sample I-6 are much higher than those observed in sample I-4, particularly with respect to those for the MoO<sub>2</sub> phase.

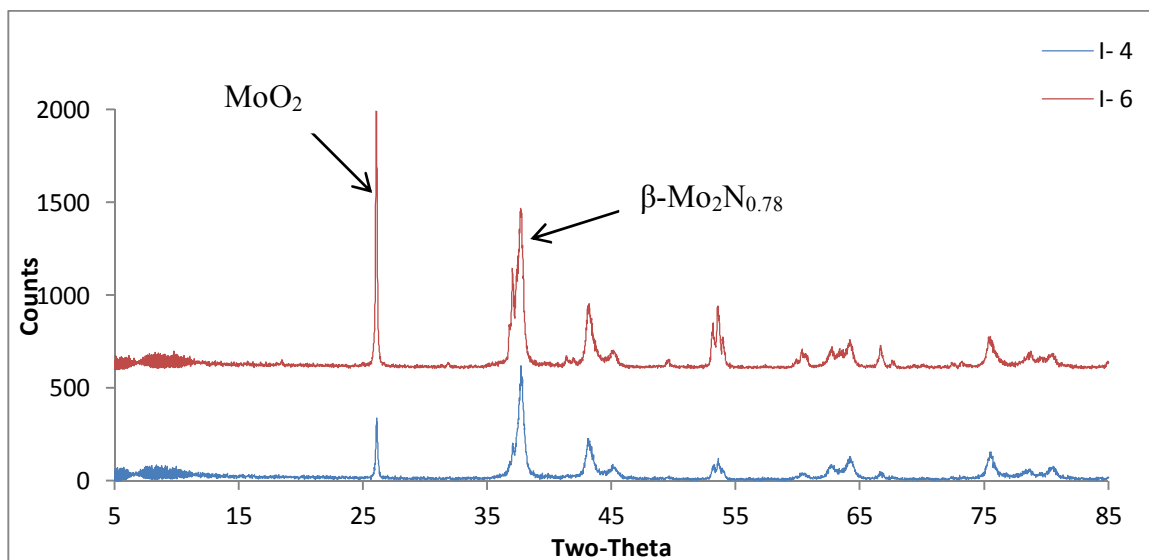


Figure 3.4 XRD patterns of samples I-4 and I-6

### 3.1.1.2 C H N analysis

The carbon and nitrogen content of all samples including that generated by the *in-situ* XRD reaction is presented in Table 3.1. These results indicate that sample I-4 contains a higher nitrogen content than sample I-6. It is also found that C H N and XRD results confirm that molybdenum nitride is the main product. It is worth noting that the nitrogen content of the *in-situ* XRD experiment (I-7) is close to that observed for sample I-4. As reported in the literature [50], the expected nitrogen content of the  $\beta$ -Mo<sub>2</sub>N<sub>0.78</sub> phase would be 5.38 wt.%. The presence of MoO<sub>2</sub>, which was evident in the XRD studies of I-4 and I-6, would lead to a reduction of N content of both samples.

**Table 3.1: Carbon and nitrogen content of sample I-4, I-6 and I-7 *in-situ***

Sample Code (Ar, 800 °C)	Flow rate ml/min	Post-reaction analysis	
		Carbon (wt. %)	Nitrogen ( wt.% )
I-4	60	0	4.22
I-7 <i>in-situ</i>	60	0.32	4.31
I-6	10	0	3.42

### 3.1.1.3 BET surface area measurements

Table 3.2 presents the BET surface areas of samples I-4, I-6 and I-7. These results confirm that using a higher flow rate results in a material of higher area than that generated at lower flow rate.

**Table 3.2: BET surface area of samples I- 4, I- 6 and I- 7**

Sample Code	BET surface area ( m <sup>2</sup> /g )
I -4	13.5
I-7 <i>in-situ</i>	13.7
I-6	6.9

### 3.1.1.4 SEM images

SEM images of all the samples are shown in Figure 3.5. The morphology of sample I-4 and I-7 *in-situ* resemble that of their precursor. It can be seen that sample I- 6 exhibits a different crystal size which is smaller than the other samples. It should be noted that the “whiskers” seen in some of the images relate to an artifact corresponding to the presence of residual SiO<sub>2</sub> wool in post-reactor samples.

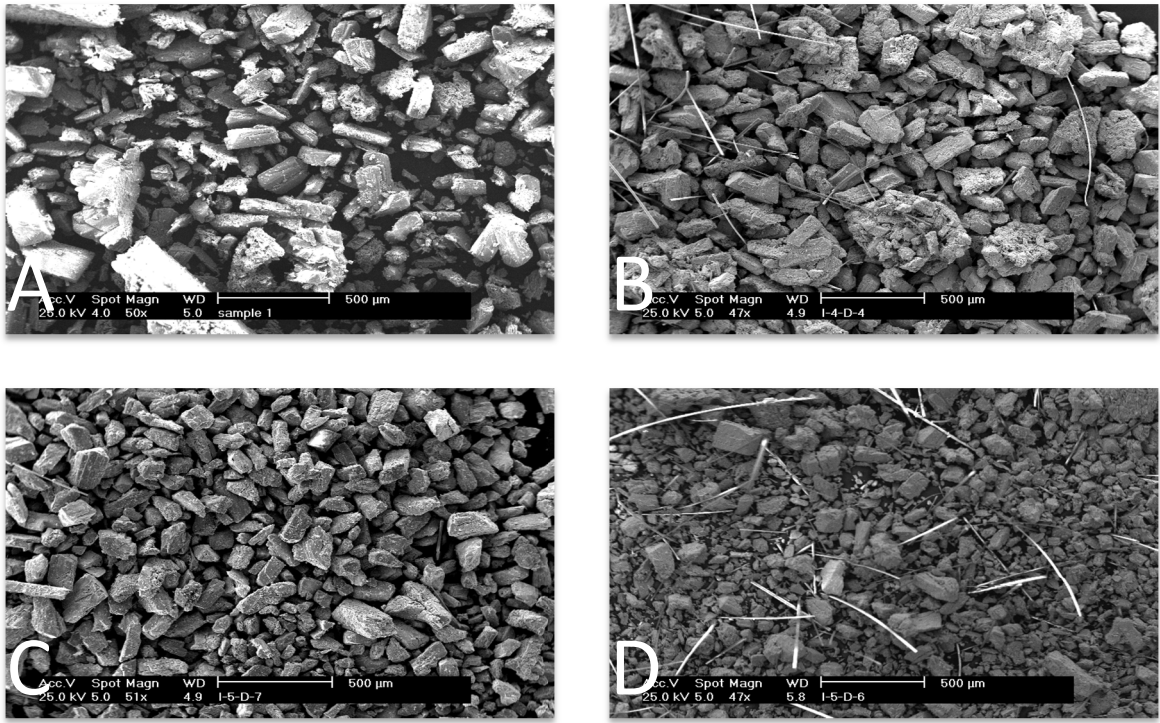


**Figure 3.5: SEM images of A) precursor I, B) sample I-4, C) sample I-7 *in-situ* and D) sample I- 6. All images correspond to the same magnification**

### 3.1.1.5 Summary

It can be noted that the applied conditions are related to those reported in the literature in which the formation of phase pure  $\text{Mo}_2\text{N}$  was described [52]. However, the preparation of molybdenum nitride phase is known to be very sensitive to the effects of precursor [19] and also sample mass and reactant gas flow rate. In general, the  $\beta\text{-Mo}_2\text{N}_{0.78}$  and  $\text{MoO}_2$  phases are present to varying degrees in the current study. The oxidation-reduction process that occur during the decomposition of ammonium salts of molybdenum oxides leads to some intermediate reduced oxides, for instance,  $\text{Mo}_5\text{O}_{11}$  or  $\text{MoO}_2$  [52, 56]. It is well known that the final temperature is an important factor to prepare a pure phase of  $\beta\text{-Mo}_2\text{N}_{0.78}$  [31]. It is also documented that minimization of the partial pressure of water vapour is important for the production of high surface area materials through reduction of hydrothermal sintering [6, 17]. In the current study, there is good agreement between the results obtained from XRD and those obtained by C H N analysis.

In the current study the nitrogen content of the resultant product was increased at the higher flow rate applied. Furthermore, at the higher flow rate the particle size of the product was found to be closer to the precursor than in the case of the lower flow rate.

### 3.1.2 Decomposition under an argon atmosphere at 700 °C

According to the *in-situ* XRD data and TGA analysis, the pure phase of molybdenum nitride starts forming at 700 °C. However, the aim of this section was to study the effect of flow rate on the final product. As described in experimental chapter, different argon flow rates were applied at a reaction temperature of 700 °C. The sample codes I-12, I-10, I-14 and I-21 correspond to flow rates of 10, 60, 94 and 125 ml/min, respectively.

#### 3.1.2.1 XRD patterns

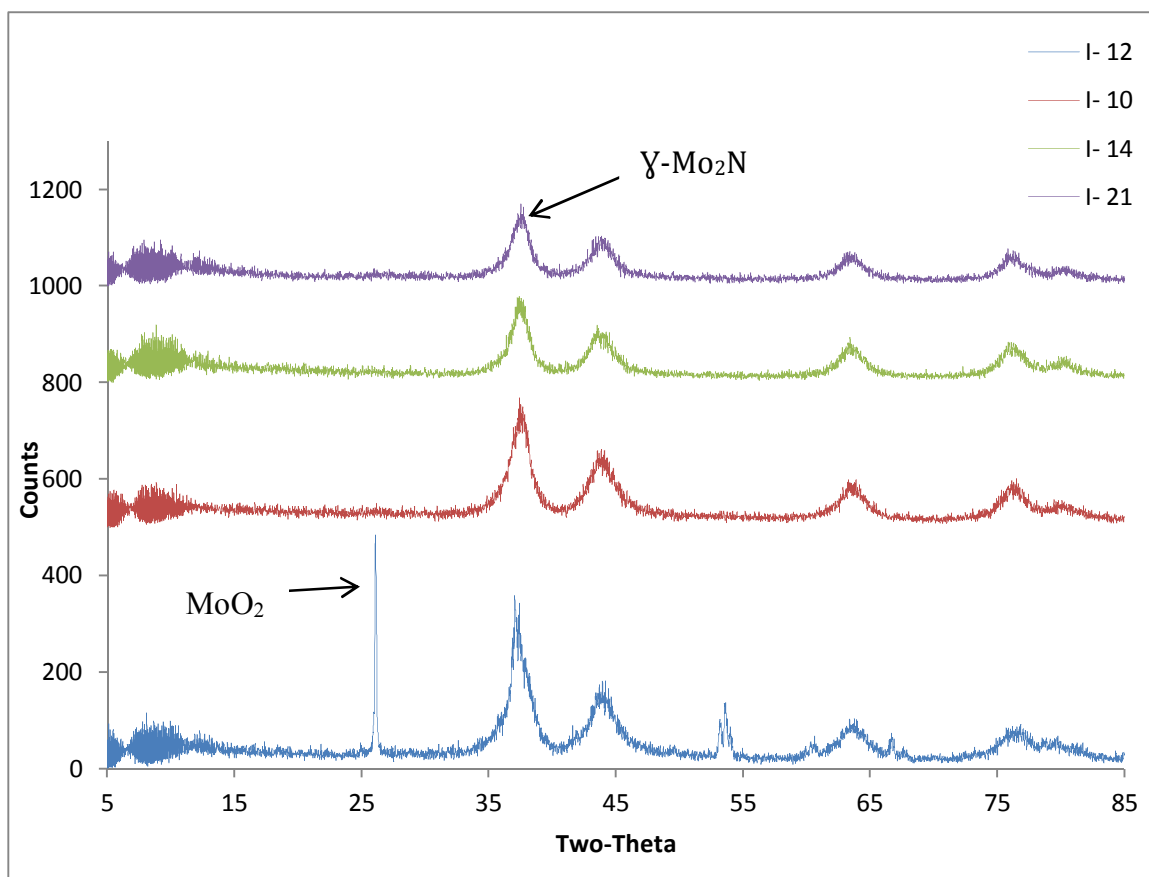


Figure 3.6 XRD patterns of samples I-12, I- 10, I-14 and I-21

The XRD analysis of samples I-12, I-10, I-14 and I-21 is shown in Figure 3.6. In all cases,  $\gamma$ -Mo<sub>2</sub>N appears to be the main phase except for sample I-12 which contains reflections corresponding to MoO<sub>2</sub>. The strong diffraction peaks of  $\gamma$ -Mo<sub>2</sub>N can be seen clearly at 37.36°, 43.41°, 63.17°, 75.68°, 79.82° 2 $\theta$  consistent with JCPDS 25-1366 [57].

### 3.1.2.2 C H N analysis

The influence of applying different flow rates can be observed clearly in the C H N results as shown in Table 3.3. These results indicate that the nitrogen content rises steadily with increasing flow rate. It should also be noted that all results exhibit a lower nitrogen content than that expected on the basis of  $\gamma$ -Mo<sub>2</sub>N (which would be 6.80 w.t. %).

**Table 3.3: Carbon and nitrogen content of samples I-12, I-10, I-14 and I-21**

Sample Code (Ar, 700 °C)	Flow rate ml/min	Post-reaction analysis	
		Carbon (wt. %)	Nitrogen ( wt.% )
I-12	10	0	3.76
I-10	60	0	4.45
I-14	94	0	4.54
I-21	125	0	4.65

### 3.1.2.3 BET surface area measurements

The influence of applying different flow rates on specific surface area, as shown in Table 3.4, seemed to be generally reversed for the nitrogen content observed by C H N analysis. The observation may be interrelated to higher surface area materials being more reactive upon exposure to ambient conditions upon discharge from the reactor, leading to a greater degree of surface oxidation/ loss of nitrogen.

**Table 3.4: BET surface area of samples I-12, I-10, I-14 and I-21**

Sample Code	BET surface area ( m <sup>2</sup> /g )
I-12	59.4
I-10	59.5
I-14	49.0
I-21	31.1

### 3.1.2.4 SEM images

Figure 3.7 shows the morphology of the samples. It can be observed that the increase of flow rate led to an increase in the particle size of the final product corresponding to the reduction in BET surface area described above. It should be noted that the “whiskers” seen in some of the images relate to artifacts corresponding to the presence of residual SiO<sub>2</sub> wool in post-reactor samples.

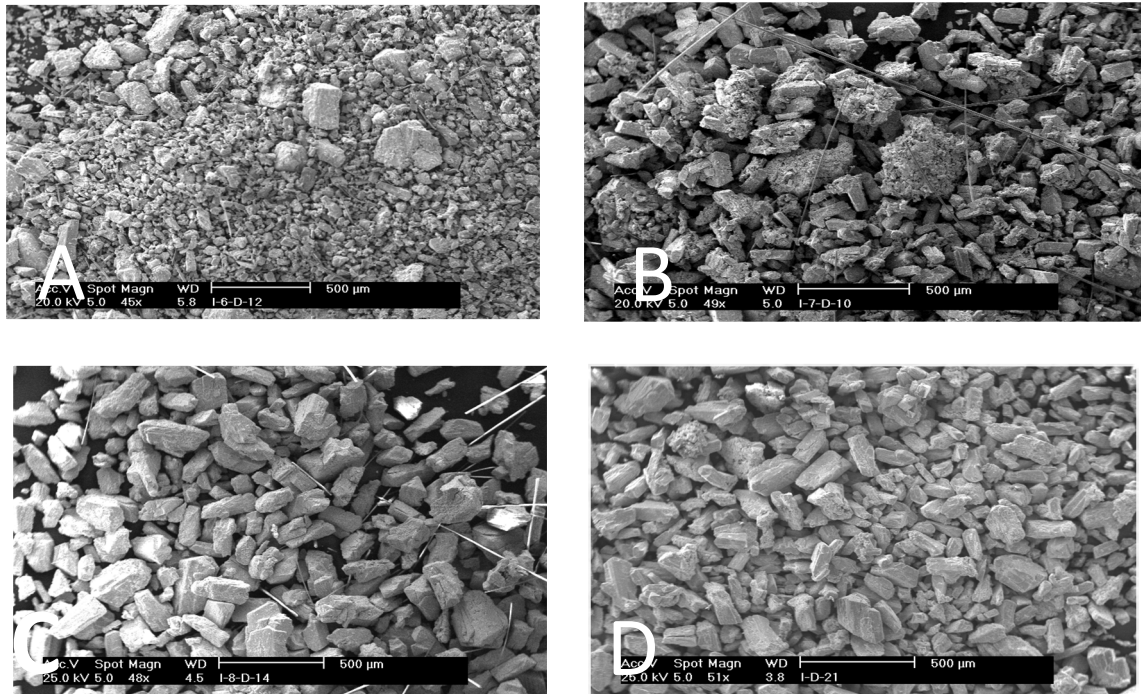


**Figure 3.7: SEM images of A) sample I-12, B) sample I-10, C) sample I-14 and D) sample I-21. All images correspond to the same magnification.**

### 3.1.2.5 Summary

The main conclusion of the decompositions conducted under Ar is the apparent influence of flow rate on the nitrogen content. However, a degree of caution must be exercised in making the phase analysis.  $\beta$ -Mo<sub>2</sub>N<sub>0.78</sub> and  $\gamma$ -Mo<sub>2</sub>N possess similar XRD patterns with the former comprising additional reflections as a result of lowering of symmetry ( $\gamma$ -Mo<sub>2</sub>N is an fcc based system, whilst  $\beta$ -Mo<sub>2</sub>N<sub>0.78</sub> is body centred tetragonal based). Given that the 700°C derived samples possess reflections of much greater width (possibly as a consequence of smaller coherent diffraction domain size and / or greater degree of disorder) reflection overlap may occur, obscuring the additional reflections expected for the  $\beta$ -phase. It can be seen from XRD patterns presented in Figures 3.4 and 3.6 that the increase of temperature from 700 °C to 800 °C possibly induces transformation from the  $\gamma$ -Mo<sub>2</sub>N to  $\beta$ -Mo<sub>2</sub>N<sub>0.78</sub> phase. Wei and co-workers have investigated the transformation of  $\gamma$ -Mo<sub>2</sub>N under a helium atmosphere. They have observed that  $\gamma$ -Mo<sub>2</sub>N transforms to  $\beta$ -Mo<sub>2</sub>N<sub>0.78</sub> and metallic Mo at elevated temperatures up to 1000°C [58]. It should be noted that using low flow rates at both final temperatures (700 °C and 800 °C) leads to the production of MoO<sub>2</sub>.

It is clear from C H N results that nitrogen content increases with increasing flow rate. It can be also observed that the nitrogen value is lower than the stoichiometric values anticipated on the basis of  $\gamma$ -Mo<sub>2</sub>N and  $\beta$ -Mo<sub>2</sub>N<sub>0.78</sub>. This may be associated with oxidation and/or presence of molybdenum metal which may or may not be apparent by XRD analysis. However, BET analysis shows a reduced value of specific surface area with increase in flow rate for samples prepared at 700 °C, and this is possibly consistent with a lower degree of surface oxidation.

### 3.1.3 Decomposition under an argon atmosphere at 700°C using different ramp rate.

In this section, different ramp rates were applied at 700°C in order to study the influence of heating rate on the final product. The sample codes I-17 and I-18 correspond to ramp rates of 2°C/min and 5°C/min, respectively.

#### 3.1.3.1 XRD patterns

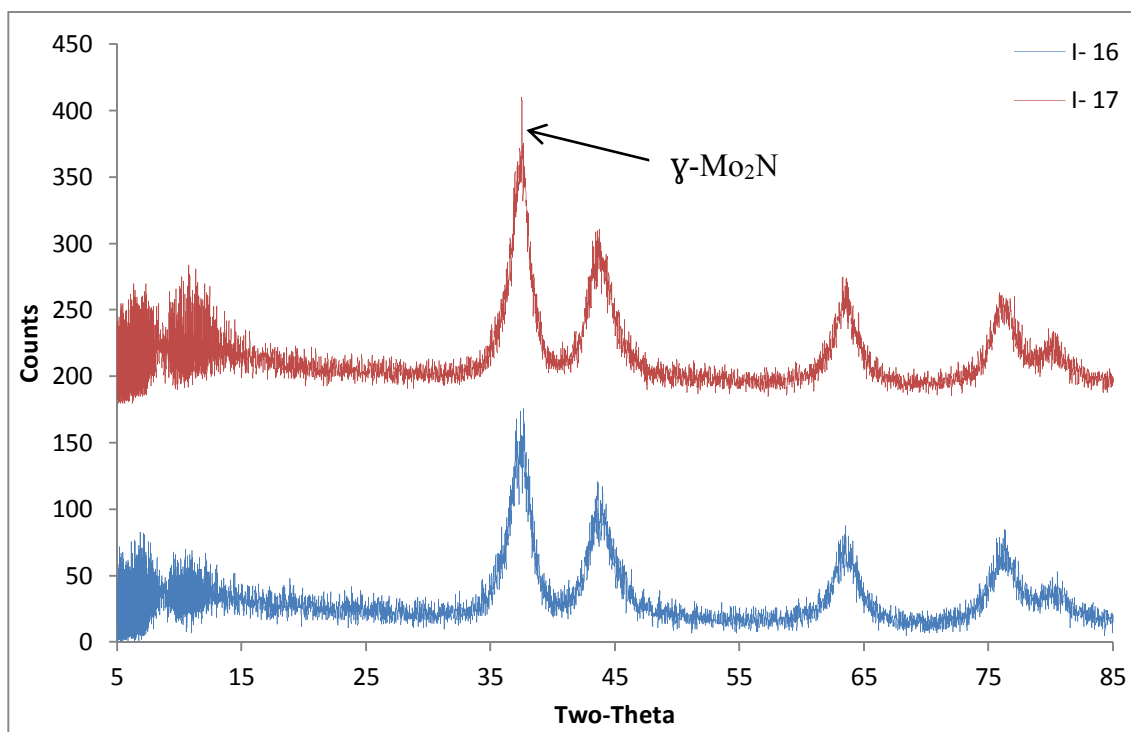


Figure 3.8 XRD patterns of samples I-16 and I-17

Figure 3.8 presents XRD patterns of samples I-16 and I-17 after reaction. It can be seen that  $\gamma$ -Mo<sub>2</sub>N, JCPDS 25-1366, is the phase observed for both samples.

### 3.1.3.2 C H N analysis

Table 3.5 presents the carbon and nitrogen content of the samples. It indicates that there could possibly be a small difference between sample I-17 and sample I-16 in terms of nitrogen value, where using the lower ramp rate shows an apparently slightly higher nitrogen content than that observed when the higher ramp rate is applied.

**Table 3.5 Carbon and nitrogen content of samples I-17 and I-16**

Sample Code (Ar, 700°C, 60 ml/min)	Ramp rate °C/min	Post-reaction analysis	
		Carbon (wt. %)	Nitrogen ( wt.% )
I-17	2	0	4.50
I-16	5	0	4.40

### 3.1.3.3 BET surface area measurement

Table 3.6 shows the BET surface areas of samples I-17 and I-16. These results indicate that both samples exhibit also a small, possibly insignificant, difference in the specific surface areas.

**Table 3.6 BET surface area of samples I-17 and I-16**

Sample Code	BET surface area ( m <sup>2</sup> /g )
I-17	50.8
I-16	49.8

### 3.1.3.4 SEM images

Figure 3.9 shows the SEM images depicting morphology of samples I-17 and I-16. These images indicate that there is a wide distribution of particle size in the case of sample I-17, whilst sample I-16 shows similar size particles. The differences observed are larger than would be anticipated on the basis of the comparable surface areas. It should be noted that the “whiskers” seen in some of the images relate to an artifact corresponding to the presence of residual SiO<sub>2</sub> wool in post-reactor samples.

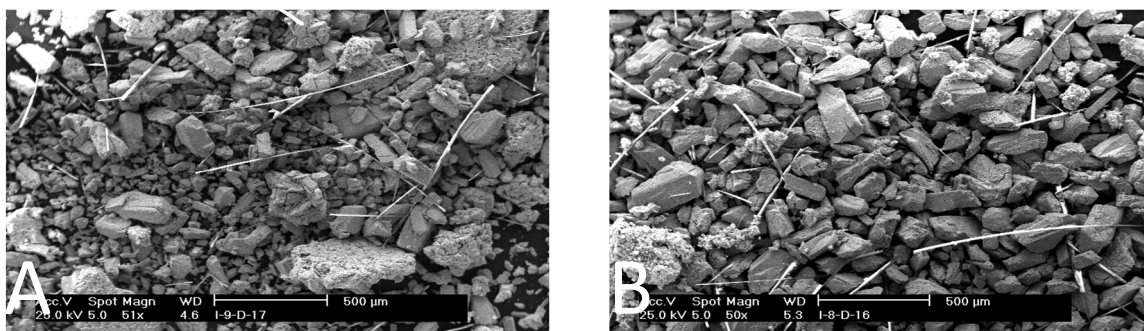


**Figure 3.9: SEM images of A) sample I-17 and B) sample I-16. All images correspond to the same magnification**

### 3.1.3.5 Summary

Although the preparation of molybdenum nitride with high specific area using conventional methods requires the application of low temperature ramp rates [9, 25], it was found that applying a low temperature ramp rate has little effect on the specific surface area of the product using the single source precursor route. This is in a good agreement with the work of Wang et al.[31], where a low temperature ramp rate was not necessary when using the single source route to prepare molybdenum carbide or nitride with high specific surface area.

### 3.1.4 Decomposition under different reaction atmospheres at 700°C.

As previously described in the experimental chapter, the reaction of precursor I was investigated under N<sub>2</sub>, H<sub>2</sub>/N<sub>2</sub> 1:3, H<sub>2</sub>/N<sub>2</sub> 3:1 and Ar/H<sub>2</sub> 1:3 atmospheres which are represented by sample codes I-28, I-22, I-24 and I-26, respectively.

#### 3.1.4.1 XRD patterns

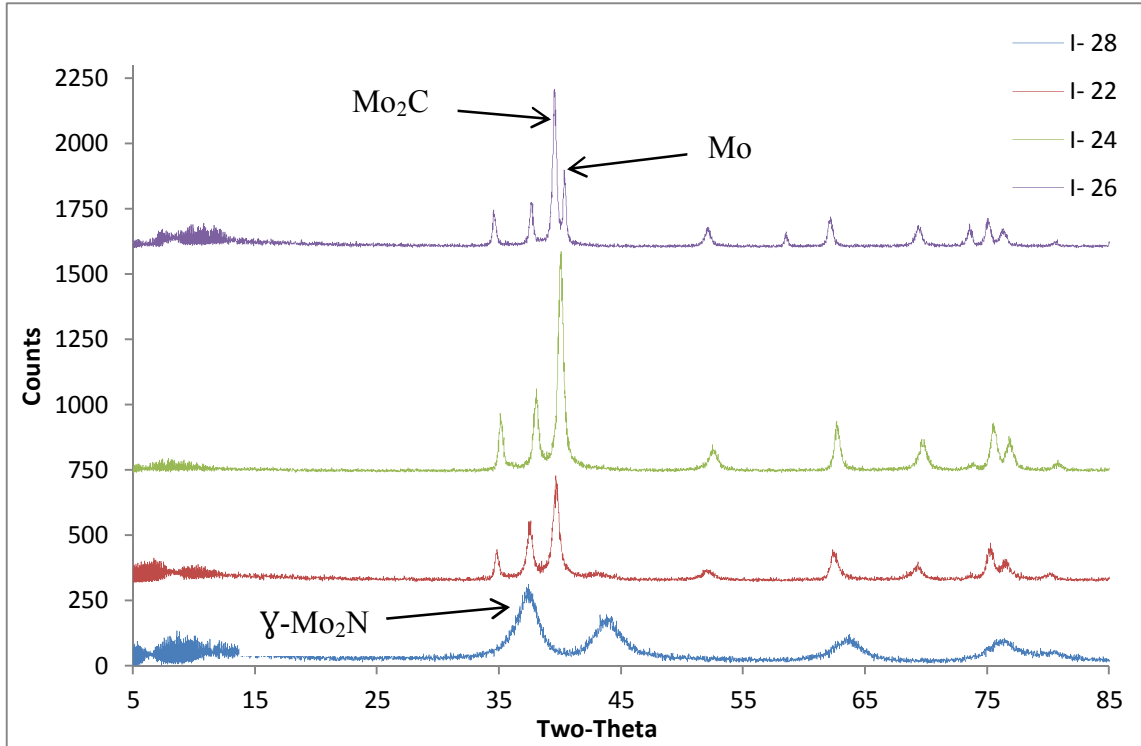


Figure 3.10 XRD patterns of samples I-28, I-22, I-24 and I-26

Figure 3.10 presents XRD patterns of I-28, I-22, I-24 and I-26 after reaction. These results have indicated that the Mo<sub>2</sub>C phase, (JCPDS, 11-0680) occurs most commonly being formed with all H<sub>2</sub> containing gas mixtures. In addition, metallic Mo is evident when a 1:3 Ar/H<sub>2</sub> atmosphere was used. It should be noted that there was small shift in the position of molybdenum carbide reflections compared with the standard pattern, which suggests that the products may not be pure carbides. In the case of N<sub>2</sub>,  $\gamma$ -Mo<sub>2</sub>N is formed and the very broad reflections indicate small coherent diffraction domains and/or the presence of disorder.

### 3.1.4.2 C H N analysis

Table 3.7 presents the carbon and nitrogen content of the samples. It is readily apparent that, despite Mo<sub>2</sub>C being evident in the XRD patterns of I-22, I-24 and I-26, the N contents are very high and the C contents are very low (the stoichiometric C content of Mo<sub>2</sub>C is 5.88 w.t.%). In the case of the sample I-28 which shows a  $\Upsilon$ -Mo<sub>2</sub>N phase in the XRD result, the nitrogen value is less than would expected stoichiometrically for a pure phase which is 6.80 wt. %.

**Table 3.7: Carbon and nitrogen content of sample I-28, I-22, I-24 and I-26**

Sample Code ( 700 °C, 60 ml/min)	Reaction Atmosphere	Post-reaction analysis	
		Carbon (wt. %)	Nitrogen ( wt.% )
I-28	N <sub>2</sub>	0	4.31
I-22	H <sub>2</sub> /N <sub>2</sub> 1 : 3	1.55	4.45
I-24	H <sub>2</sub> /N <sub>2</sub> 3 : 1	2.45	3.43
I-26	H <sub>2</sub> /Ar 3 : 1	2.37	2.34

### 3.1.4.3 BET surface area measurements

Table 3.8 presents the BET surface areas of the samples. The areas of samples I-22, I-24 and I-26 were too low to be reliably determined. However, sample I-28 which corresponds to the  $\Upsilon$ -Mo<sub>2</sub>N phase has a reasonably large surface area which is higher than that measured for  $\Upsilon$ -Mo<sub>2</sub>N in the previous sections in this chapter, and which may be consistent with the broad reflections in its XRD pattern.

**Table 3.8: BET surface area of samples I-28, I-22, I-24 and I-26**

Sample Code	BET surface area ( m <sup>2</sup> /g )
I-28	72.4
I-22	low
I-24	low
I-26	low

### 3.1.4.4 SEM images

Figure 3.11 shows the morphology of the samples illustrating the effect of employing different reaction gases. It can be also observed that sample I-22 and sample I-24 show a wide distribution of particle size and also are not pseudomorphic with their precursor. However, sample I-28 has totally different morphology which shows very small particle size, and is again not pseudomorphic with its precursor. Sample I-26 shows similar features to the corresponding materials produced under the argon atmosphere, and is pseudomorphic with precursor I.

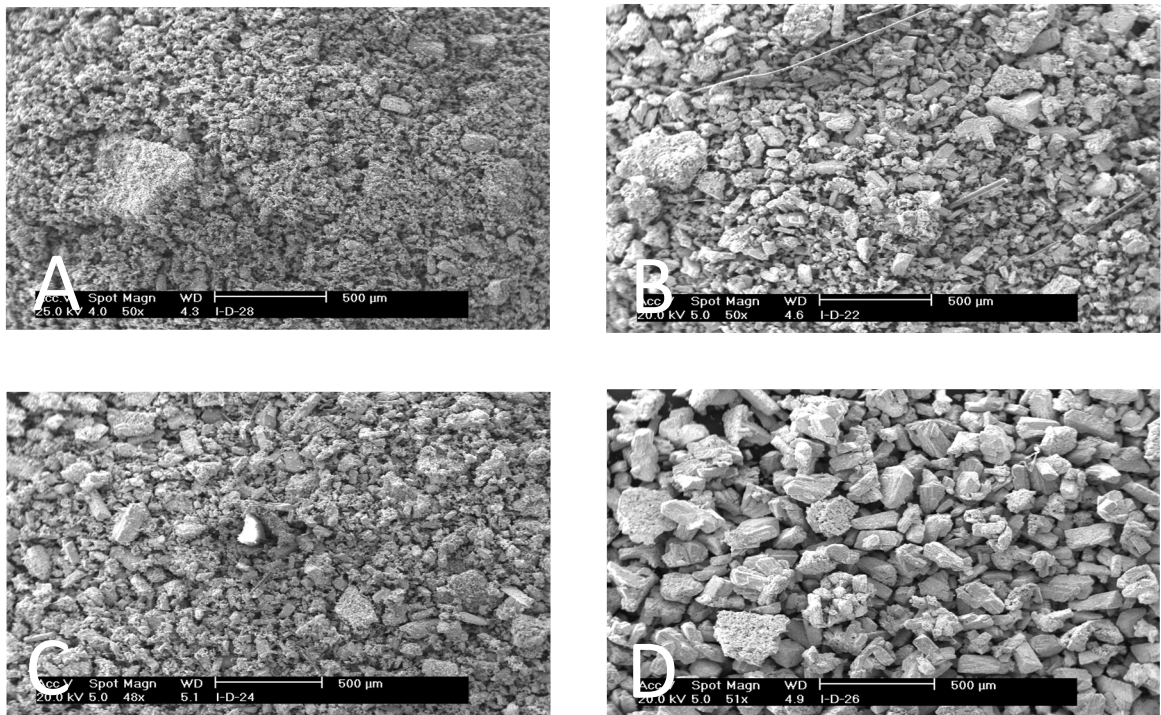


**Figure 3.11: SEM images of A) sample I- 28, B) sample I-22, C) sample I-24 and D) sample I-26. All images correspond to the same magnification**

### 3.1.4.5 Summary

The reactant gas atmosphere exerts a significant influence on the resultant phase formed from hexamethylenetetramine molybdate. By looking more closely at the power X-ray diffraction patterns of samples I-22, I-24 and I-26, which correspond to  $\text{Mo}_2\text{C}$ , small shifts in the positions of most of the reflections are evident. This could be explained by the presence of nitrogen, as confirmed by CHN analysis, leading to the formation of carbonitride phases which are isostructural with  $\text{Mo}_2\text{C}$ . The atomic radii of C and N, which are 0.078 nm and 0.074 nm respectively [59], are similar resulting in small shifts upon substitution [32]. However, it is well-known that the decomposition of hexamethylenetetramine molybdate under an argon atmosphere can form a reduced phase, which was achieved by reduction from the carbon source present in the precursor and subsequent nitridation occurs by utilising the nitrogen also present in the precursor. A striking observation in the current study is that carbides, or carbonitrides, are formed when  $\text{H}_2$ -containing reaction atmospheres are employed. This is most likely due to the fact that  $\text{H}_2$  acts as a more effective reductant meaning that the carbon content of the precursor is not exhausted by reaction with its lattice oxygen and is consequently available for incorporation into the molybdenum containing product phase. This suggestion is indirectly supported by the low surface area of the resultant products which may arise as a consequence of hydrothermal sintering associated with enhanced partial pressure of water generated upon reaction [3, 32, 52, 56].

The SEM images indicate sample morphology is also a function of reactant gas. This phenomenon can be explained by differences in the reduction-carbide and nitridation mechanism that occur during the reaction [19]. Figure 3.12 presents a schematic diagram summarising the resultant phase from thermal decomposition of hexamethylenetetramine molybdate under different atmospheres.

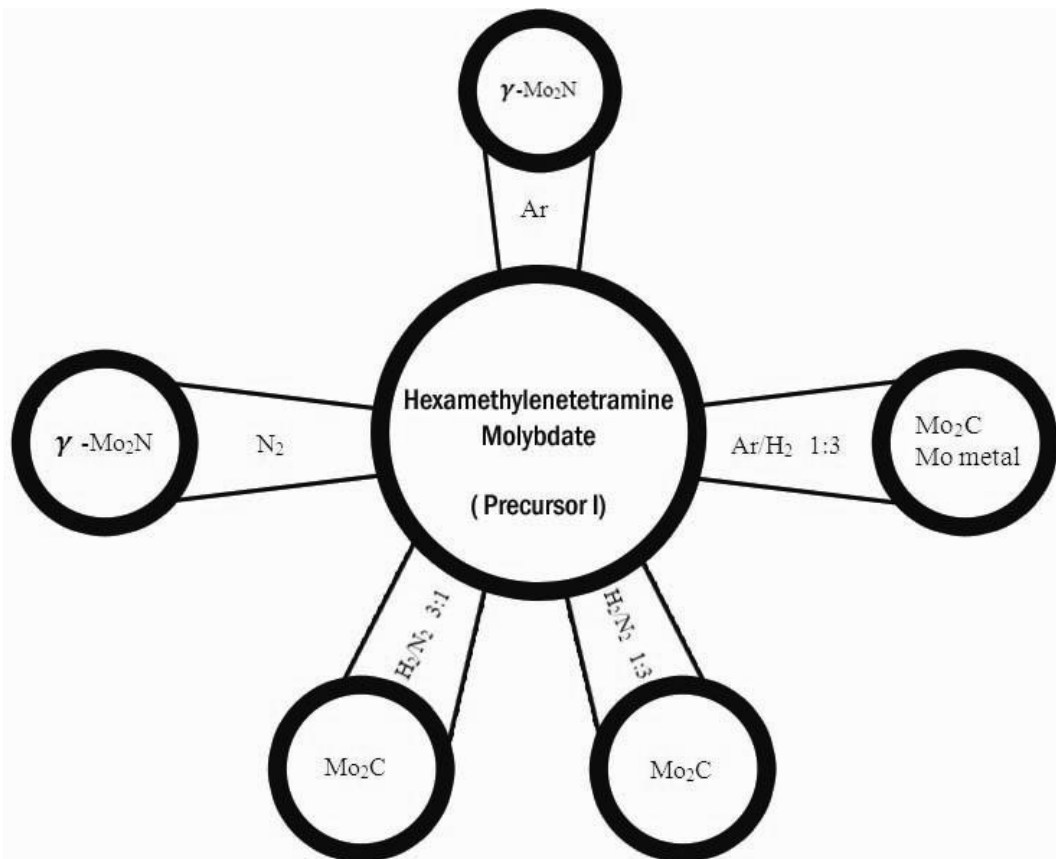


**Figure 3.12 Schematic diagram showing the resultant materials from thermal decomposition of hexamethylenetetramine molybdate under different atmospheres**

## 3.2 Investigation of various precursors

The transformation products resulting from the reaction of molybdenum trioxide ( $\text{MoO}_3$ ), ammonium heptamolybdate (AHM) and molybdic acid ( $\text{H}_2\text{MoO}_3$ ) under different gas-mixtures was also investigated. As previously described in the experimental chapter, these materials were used as initial reagents to prepare precursor I and precursor E (to be described in the following chapter). In this respect, comparison between these materials and precursor I and precursor E was undertaken.

### 3.2.1 Molybdenum trioxide ( $\text{MoO}_3$ )

1g of  $\text{MoO}_3$  was reacted under  $\text{H}_2/\text{N}_2$  feeds with 1:3 and 3:1 ratio at 700 °C, corresponding to samples M-1 and M-2 respectively. Reactions were also undertaken using 0.4g with 3:1  $\text{H}_2/\text{N}_2$  at 650°C, 700°C, 750°C and 800°C to yield sample M-3, M-4, M-5 and M-6 respectively.

#### 3.2.1.1 XRD patterns

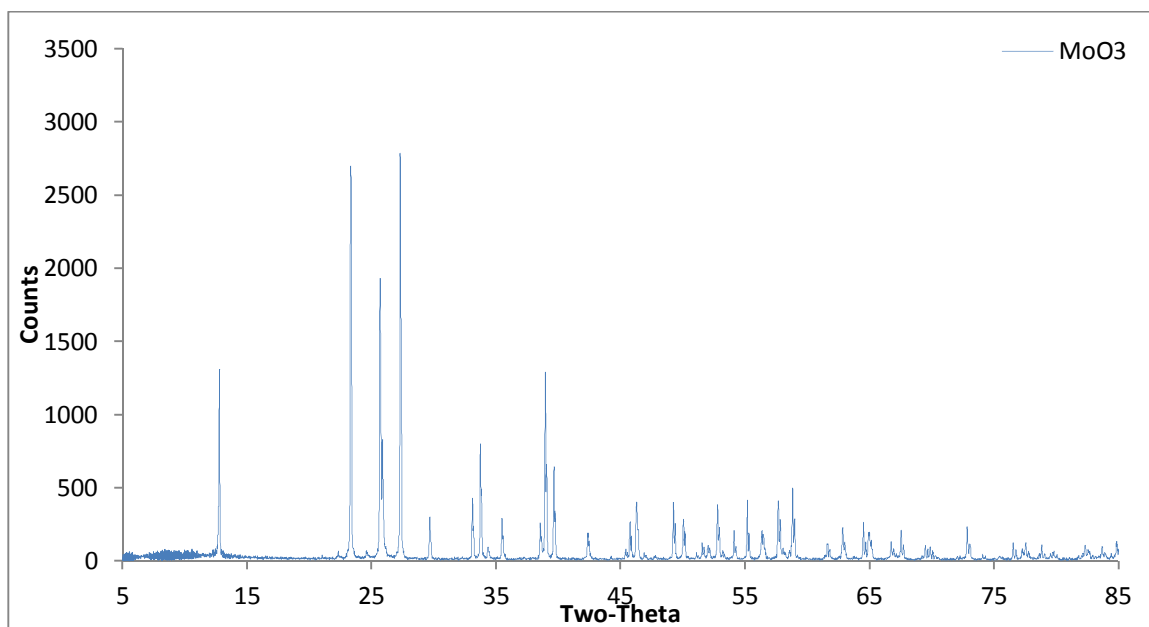


**Figure 3.13 XRD pattern of  $\text{MoO}_3$ . The pattern is consistent with that expected for the  $\text{MoO}_3$  phase.**

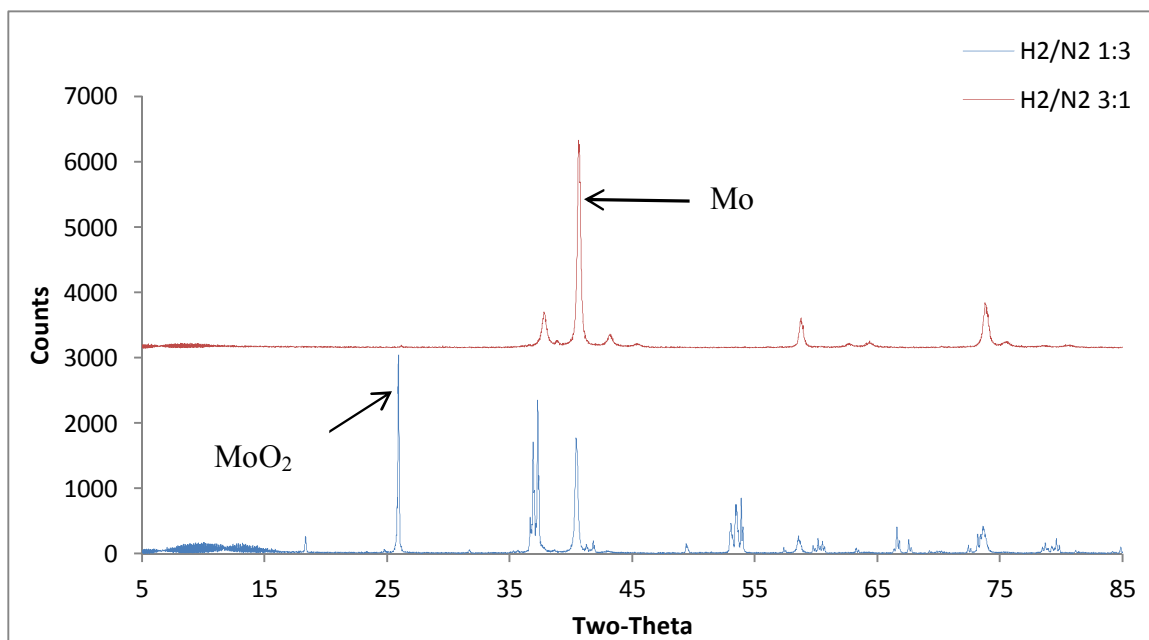


**Figure 3.14 XRD pattern of samples M-1 and M-2 prepared at 700 °C**

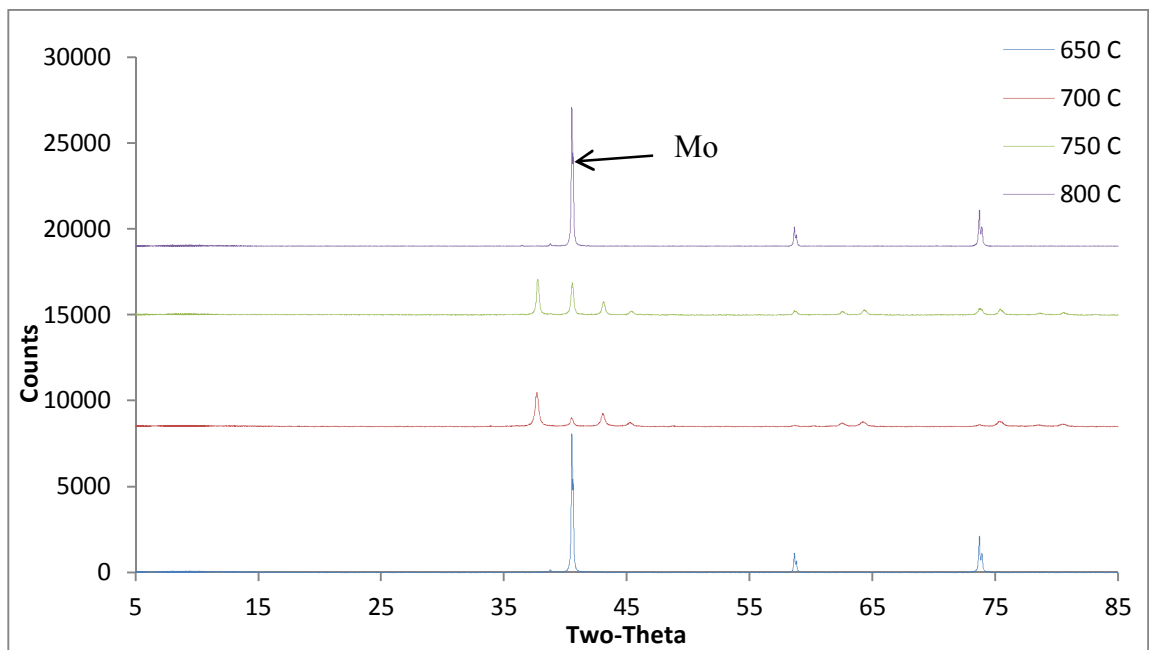


**Figure 3.15 XRD pattern of sample M-3, M-4, M-5 and M-6 prepared under H<sub>2</sub>/N<sub>2</sub> 3:1**

Figure 3.14 shows the XRD patterns of samples M-1 and M-2. In both cases, strong Mo reflections are apparent. It can be also observed that small diffraction peaks of beta-molybdenum nitride phase are apparent in the case of sample M-1, whilst M-2 appears to contain MoO<sub>2</sub> as a major phase.

Figure 3.15 also shows the XRD patterns of samples M-3, M-4, M-5 and M-6. Metallic Mo was the only phase evident after reaction at 650°C and 800°C and β-Mo<sub>2</sub>N<sub>0.78</sub> is observed after reaction at 700°C and 750 °C. This indicates β-Mo<sub>2</sub>N<sub>0.78</sub> to be metastable requiring a specific temperature window for its formation under this reaction atmosphere.

### 3.2.1.2 C H N analysis

Table 3.9 presents the nitrogen and carbon contents of the samples. It indicates that a very low nitridation level was achieved in sample M-2, whilst, no evidence of nitridation can be observed in sample M-1 as is consistent with the XRD result.

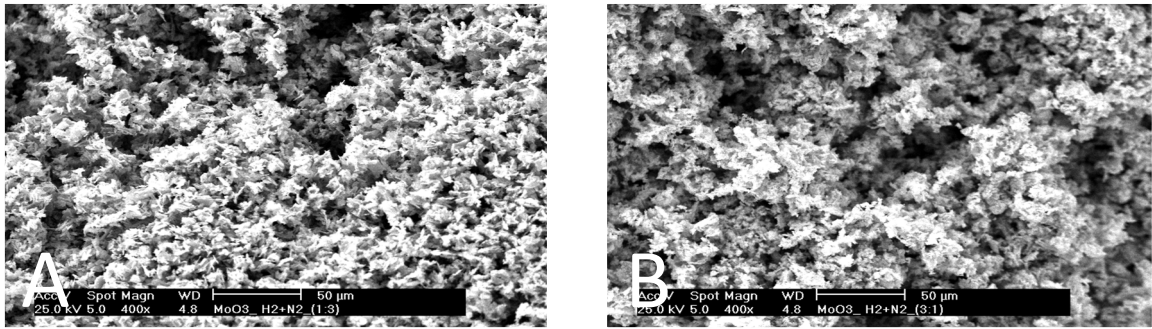
Table 3.9 also exhibits the weight percentages of nitrogen recorded in the samples M-3, M-4, M-5 and M-6. The nitrogen content of β-Mo<sub>2</sub>N<sub>0.78</sub> would be 5.38 wt.% as reported in the literature [19]. All of the values determined as shown in Table 3.9, fall below the theoretical value for pure phase of β- Mo<sub>2</sub>N<sub>0.78</sub>. It can be seen that the lowest nitrogen contents are achieved at the highest and lowest temperatures which is consistent with the XRD results although there is no evidence that a nitride is formed in the case of M-3. The sample formed at 700°C contains the highest N content which is reasonably close to, but still below, that expected for stoichiometric β-Mo<sub>2</sub>N<sub>0.78</sub>.

**Table 3.9: Carbon and nitrogen content of samples M-1, M-2, M-3, M-4, M-5 and M-6**

Sample Code	Post-reaction analysis	
	Carbon (wt. %)	Nitrogen ( wt.% )
M-1	0	0
M-2	0	1.82
M-3	0	2.03
M-4	0	5.00
M-5	0	3.61
M-6	0	0

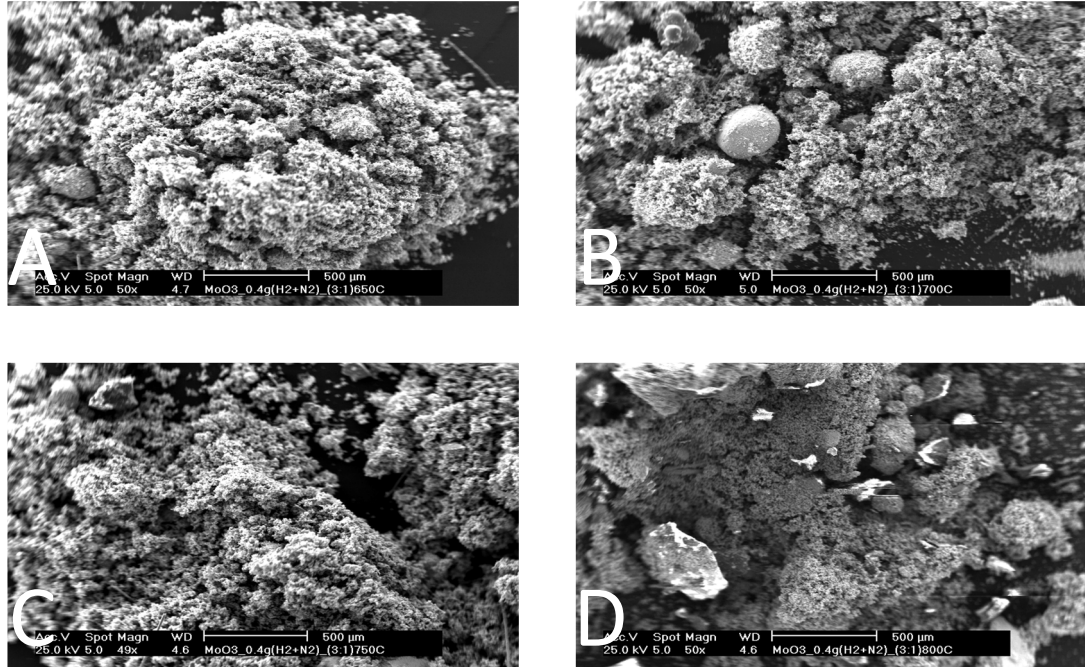
### 3.2.1.3 SEM images

Figure 3.16 presents the images of samples M-1 and M-2. It indicates that the morphologies of both samples are similar.



**Figure 3.16: SEM images of A) sample M-1 and B) sample M-2. All images correspond to the same magnification**

Figure 3.17 shows the features of samples M-3, M-4, M-5, and M-6. The images indicate that all samples exhibit same morphology except sample M-6 which also shows regions of high contrast which may correspond to metallic content.



**Figure 3.17: SEM images of A) sample M-3, B) sample M-4, sample M-5 and sample M-6. All images correspond to the same magnification**

### 3.2.1.4 Summary

It is well-known that  $\beta$ -  $\text{Mo}_2\text{N}_{0.78}$  can be prepared from the reaction of  $\text{MoO}_3$  with  $\text{H}_2/\text{N}_2$  3:1 at 750 °C [50]. The reason for conducting these experiments was to compare the effect of precursor on reduction-nitridation steps and the applied conditions so that comparisons with related single source routes can be made.

### 3.2.2 Ammonium heptamolybdate (AHM)

AHM was investigated under three different reactant gases as described in the experimental chapter.  $H_2/N_2$  in ratios of 1:3 and 3:1 and also a  $H_2/Ar$  3:1 atmosphere were used at 700 °C, generating product samples denoted as A-1, A-2 and A-3 respectively.

#### 3.2.2.1 XRD patterns

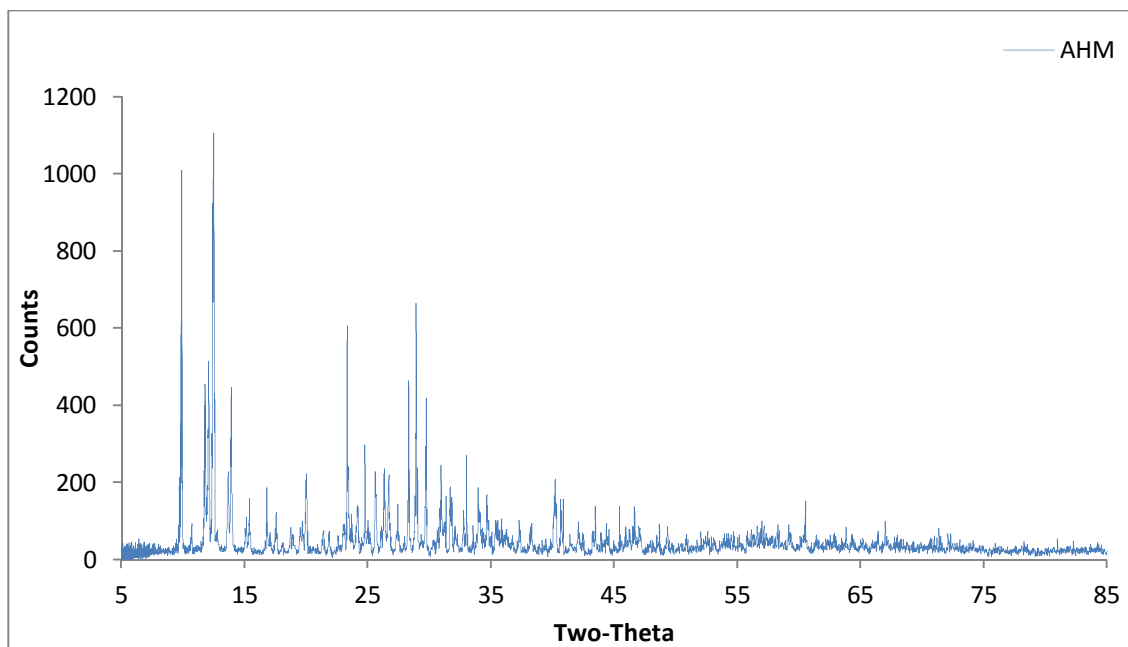


**Figure 3.18 XRD pattern of AHM. The pattern is consistent with that expected for the AHM phase**

Figure 3.19 shows the XRD patterns of samples A-1, A-2 and A-3, which indicate that all samples contain a Mo metal phase.  $\beta\text{-Mo}_2\text{N}_{0.78}$  was also observed in the case of sample A-2, and  $\text{MoO}_2$  is found to be present in sample A-3.

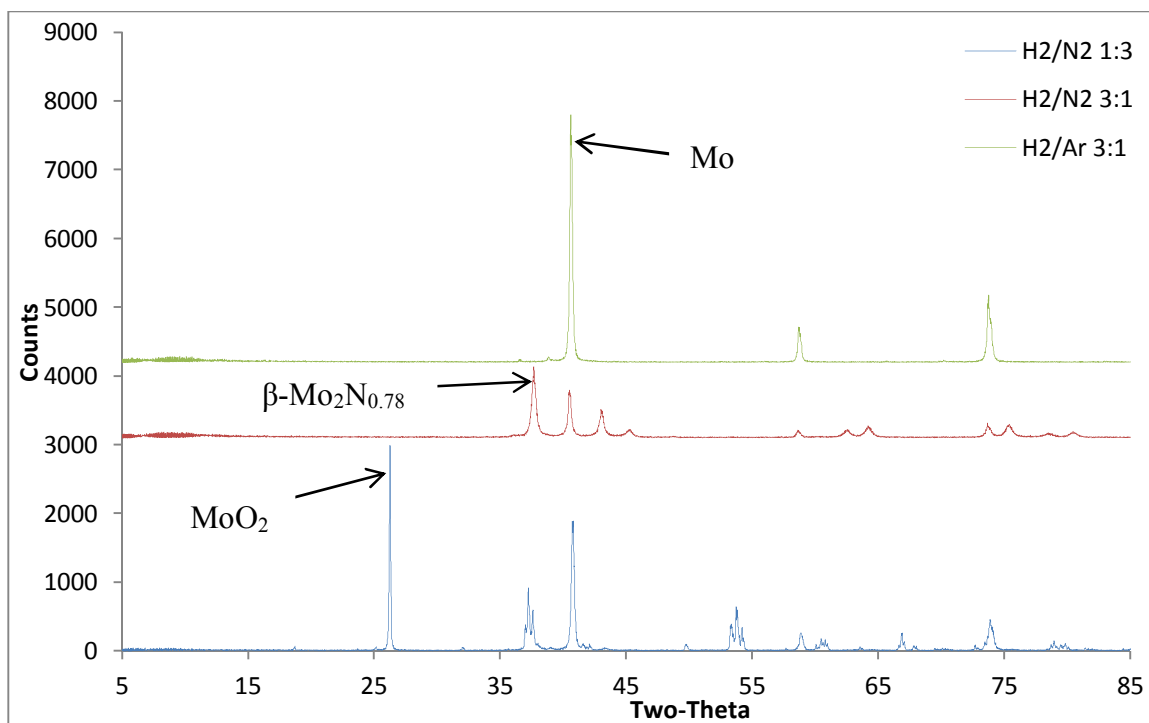


**Figure 3.19 XRD patterns of samples A-1, A-2 and A-3**

### 3.2.2.2 C H N analysis

Table 3.10 shows the C H N results of samples A-1, A-2 and A-3, and confirms that only sample A-2 was achieved a good level of nitridation. Although A-2 has 4.34 wt. % nitrogen, it is below the stoichiometric value (5.38 w.t. %) expected for β-Mo<sub>2</sub>N<sub>0.78</sub> which is not surprising considering that Mo is also present in its XRD pattern.

**Table 3.10: Carbon and nitrogen content of samples A-1, A-2 and A-3**

Sample Code	Post-reaction analysis	
	Carbon (wt. %)	Nitrogen ( wt.% )
A-1	0	0.25
A-2	0	4.34
A-3	0	0

### 3.2.2.3 SEM images

Figure 3.20 shows the features of samples of pure AHM, A-1, A-2, and A-3. The images indicate that all samples exhibit different particle sizes. These differences can be attributed to the gas ratio that was applied. In terms of sample A-3, a very small particle size evident compared to its precursor and the other samples.

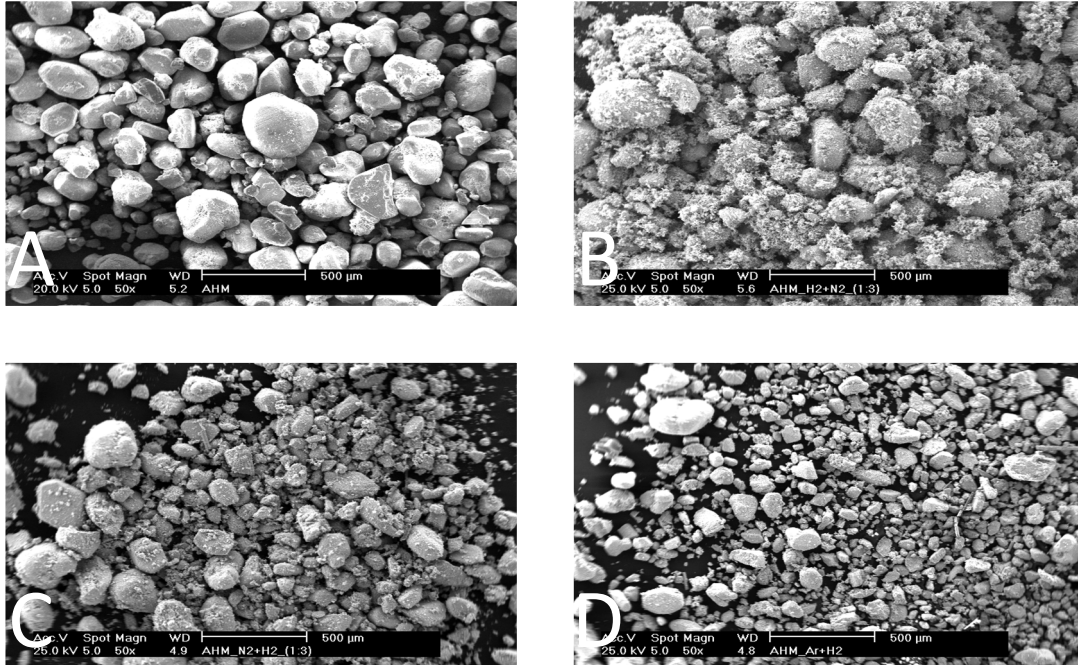


**Figure 3.20: SEM images of A) pure AHM, B) sample A-1, C) sample A-2 and D) sample A-3**

### 3.2.2.4 Summary

Although experiments were not optimised to obtain the beta-molybdenum nitride phase, treatment of AHM under 3:1  $H_2/N_2$  results in a phase comparable to that obtained by the conventional route of nitridation of  $MoO_3$  with  $H_2/N_2$  mixtures as described in section 3.2.1. It is worth noting that AHM decomposition is sufficient to produce some nitrogen [56], but this is not enough for completing the nitridation steps.

### 3.2.3 Molybdic acid ( $\text{H}_2\text{MoO}_4$ )

The transformation of  $\text{H}_2\text{MoO}_4$  was investigated under  $\text{H}_2/\text{N}_2$  mixtures in ratios of 1:3 and 3:1, at 700 °C yielding samples designated H-1 and H-2, as described in the experimental chapter.

#### 3.2.3.1 XRD patterns

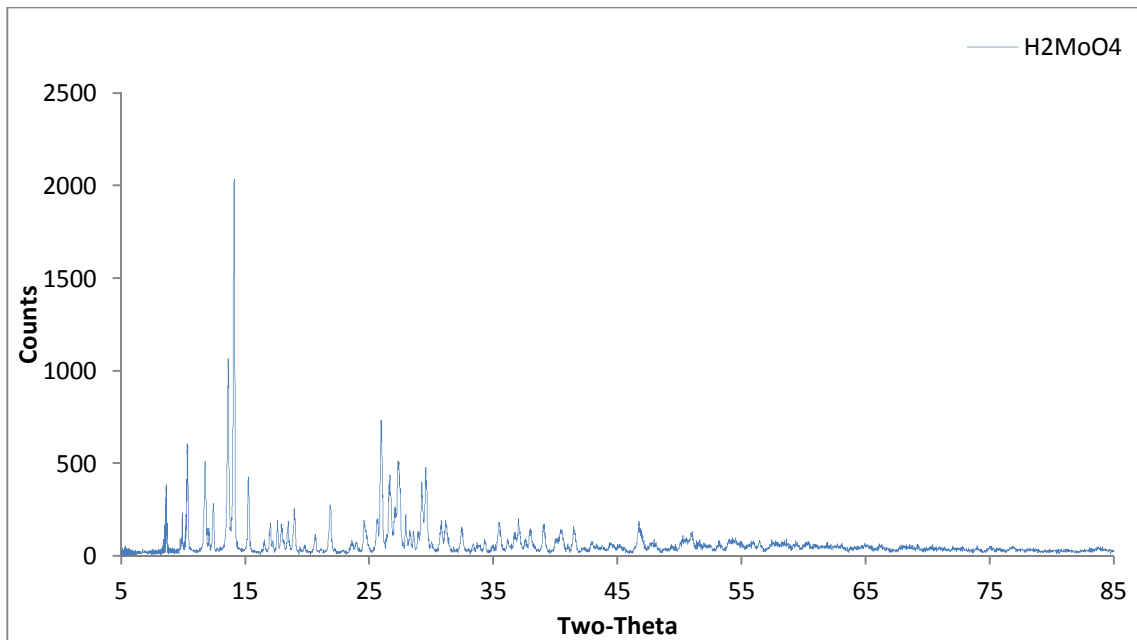


**Figure 3.21 XRD pattern of pure  $\text{H}_2\text{MoO}_4$ . The pattern is consistent with that expected for the  $\text{H}_2\text{MoO}_4$  phase**

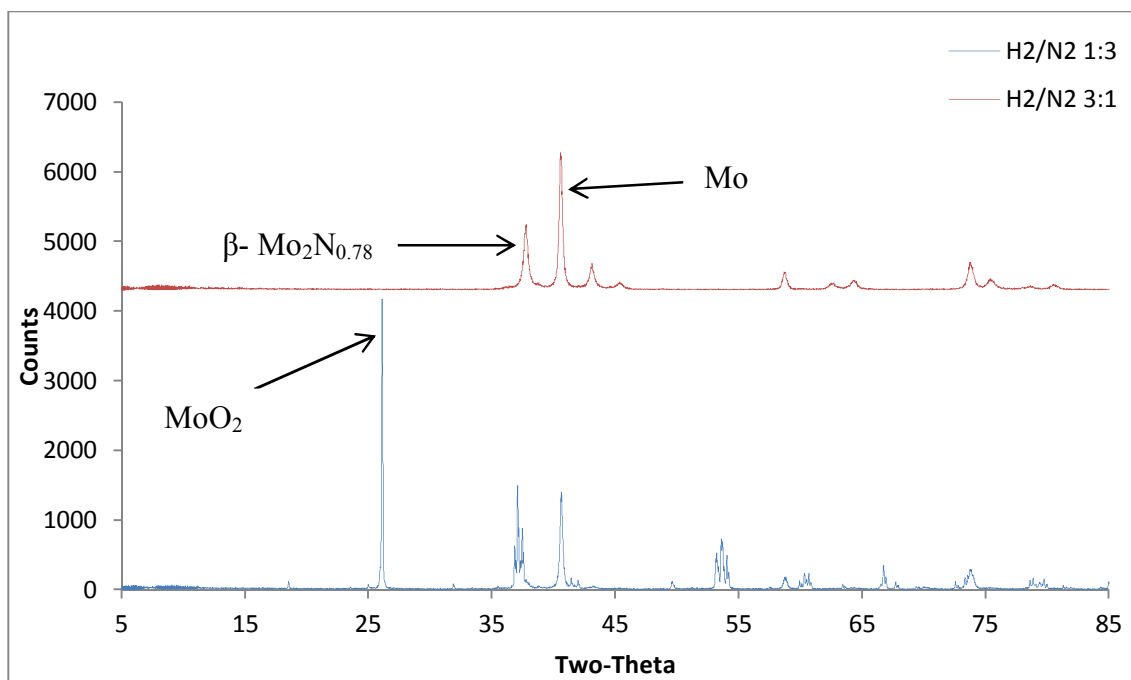


**Figure 3.22 XRD patterns of samples H-1 and H-2**

Figure 3.22 presents the XRD patterns of samples H-1 and H-2. It can be observed from these results that both samples contain reflections corresponding to molybdenum metal. It can be also observed that sample H-2 shows diffraction peaks corresponding to  $\beta$ -Mo<sub>2</sub>N<sub>0.78</sub>, whilst the additional reflections for sample H-1 correspond to the presence of a MoO<sub>2</sub> phase.

### 3.2.3.2 C H N analysis

Table 3.11 presents the C H N results of samples H-1 and H-2. The results indicate that the degree of nitridation of sample H-2 does not correspond to the presence of pure  $\beta$ -Mo<sub>2</sub>N<sub>0.78</sub> as is to be expected on the basis of the additional Mo phase apparent in its XRD pattern.

**Table 3.11: Carbon and nitrogen content of samples H-1 and H-2**

Sample Code	Post-reaction analysis	
	Carbon (wt. %)	Nitrogen ( wt.% )
H -1	0	0
H -2	0	3.00

### 3.2.3.3 SEM images

Figure 3.23 shows the morphologies of A) pure  $\text{H}_2\text{MoO}_4$ , B) sample H-1 and C) sample H-2. It indicates that all samples comprise particles which have spherical shape although different particle sizes are apparent.

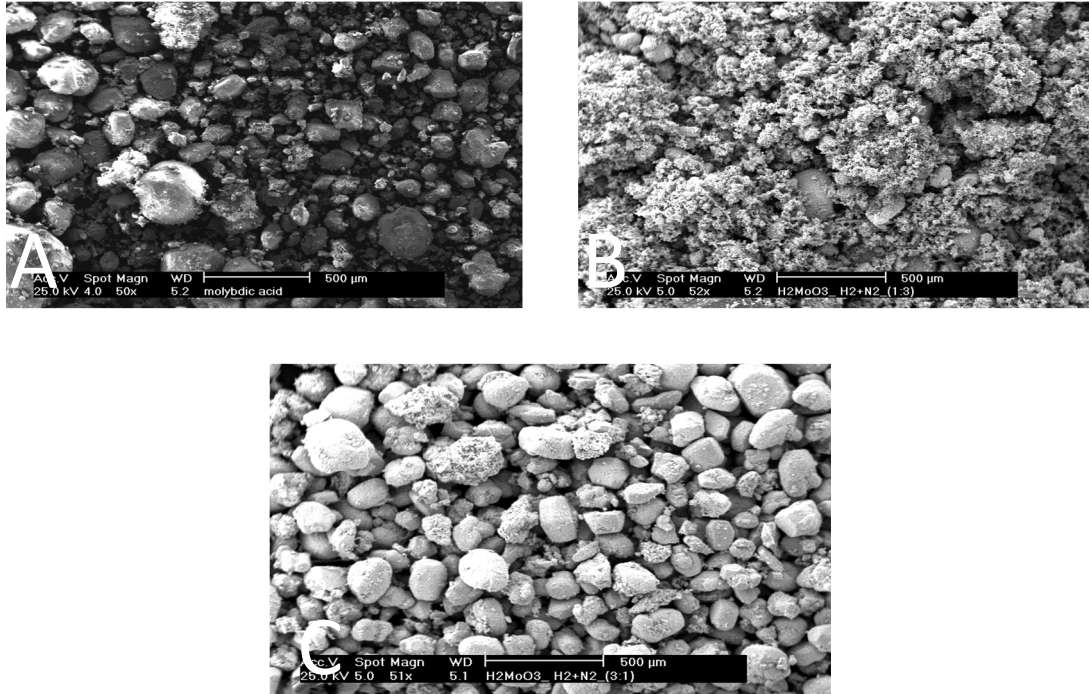


Figure 3.23: SEM images of A) pure  $\text{H}_2\text{MoO}_4$ , B) sample H-1 and C) sample H-2

### 3.2.3.4 Summary

From above data, it is apparent that  $\beta\text{-Mo}_2\text{N}_{0.78}$  can be prepared from  $\text{H}_2\text{MoO}_4$  under  $\text{H}_2/\text{N}_2$  3:1 at  $700^\circ\text{C}$ . However, the overall degree of nitrogen content, (and presumably of  $\beta\text{-Mo}_2\text{N}_{0.78}$  phase fraction) is lower than when the AHM precursor is used, although it is greater than with  $\text{MoO}_3$ .

### 3.3 Conclusion

Thermal decomposition of hexamethylenetetramine molybdate (precursor I) produces various materials. However, several factors can play an important role in the obtained products. The obtained results suggest that gas atmosphere, final temperature and flow rate are important parameters. In terms of gas atmosphere, it can be concluded that decomposition of precursor I under Ar and N<sub>2</sub> leads to production of molybdenum nitride. In contrast, molybdenum carbide/carbonitride was obtained under H<sub>2</sub>/N<sub>2</sub> 1:3, 3:1 and Ar/ H<sub>2</sub> 1:3. It can be noted that carbides/carbonitride are formed when H<sub>2</sub>-containing reaction atmospheres are employed because H<sub>2</sub> acts as a more effective reductant meaning that the carbon content of the precursor is not exhausted by reaction with its lattice oxygen. It can be also concluded that the reaction gas can influence morphology. The results indicated that the obtained materials are not pseudomorphic with their precursor when H<sub>2</sub>-containing and N<sub>2</sub> reaction atmospheres are employed, except for Ar/H<sub>2</sub>. Applying different temperatures (700 °C, 800 °C) under the same gas atmosphere (Ar) can affect the transformation product. The results suggested that γ-Mo<sub>2</sub>N transforms to β-Mo<sub>2</sub>N<sub>0.78</sub> when the temperature is increased from 700 °C to 800 °C.

In terms of flow rate, applying low flow rates leads to production of MoO<sub>2</sub> and reduces the nitrogen content, whilst high flow rates favour the generation of pure molybdenum nitride with higher nitrogen contents.

## **Chapter 4: Ethylenediammonium molybdate single source route**

Ethylenediammonium molybdate precursor has been used for the preparation of molybdenum oxycarbonitride [53]. Although, ethylenediammonium molybdate contains slightly lower Mo/C and Mo/N ratios than those present in hexamethylenetetramine molybdate, where the carbon and nitrogen are responsible for the reduction and carbidation-nitridation steps, there is a lack of research available in the literature that that has been performed for investigation of the possibility of producing molybdenum carbide or nitride from ethylenediammonium molybdate precursors.

McCandlish and co-workers have patented a novel molybdenum oxycarbonitride phase generated from ethylenediammonium molybdate precursor prepared under helium atmosphere for Fischer-Tropsch catalysis [53].

In this work, the ethylenediammonium-molybdate precursor was investigated in a similar manner to that conducted for hexamethylenetetramine molybdate, as described in the previous chapter, in order to make comparison between them.

### **4.1 Investigation of ethylenediammonium molybdate**

Ethylenediammonium molybdate (E) was prepared as described in Section 2.2.1 and was investigated using the procedures described in section 3.1. The conditions used are listed in Table 2.3. Chemical analysis indicated that precursor E contained 11.90 wt. % carbon, 13.46 wt. % nitrogen and 3.96 wt. % hydrogen which is in a good agreement with the literature [53]. Figure 4.1 shows the X-ray diffraction pattern of precursor E.

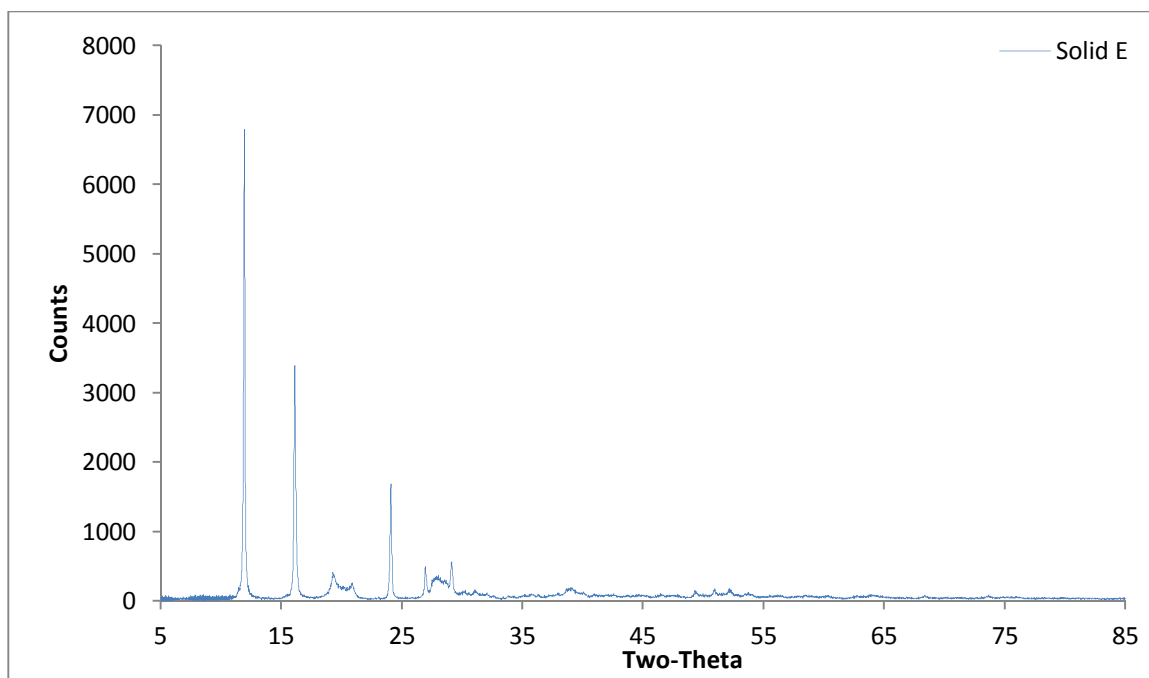


**Figure 4.1 XRD pattern of precursor E**

Precursor E was also studied by TGA-DSC analysis under an argon atmosphere, as shown in Figure 4.2. The TGA- DSC result showed that the total weight loss was 54 wt. %. McCandlish et al. investigated the decomposition of ethylenediammonium molybdate under a helium atmosphere. They suggested that the resulting composition had the empirical formula  $\text{MoO}_{0.43}\text{C}_{0.31}\text{N}_{0.33}$  and were that composition to be formed, the mass loss would be expected to be 51.32% which is close to, but not exactly, that observed herein. This is detailed in Appendix 2.

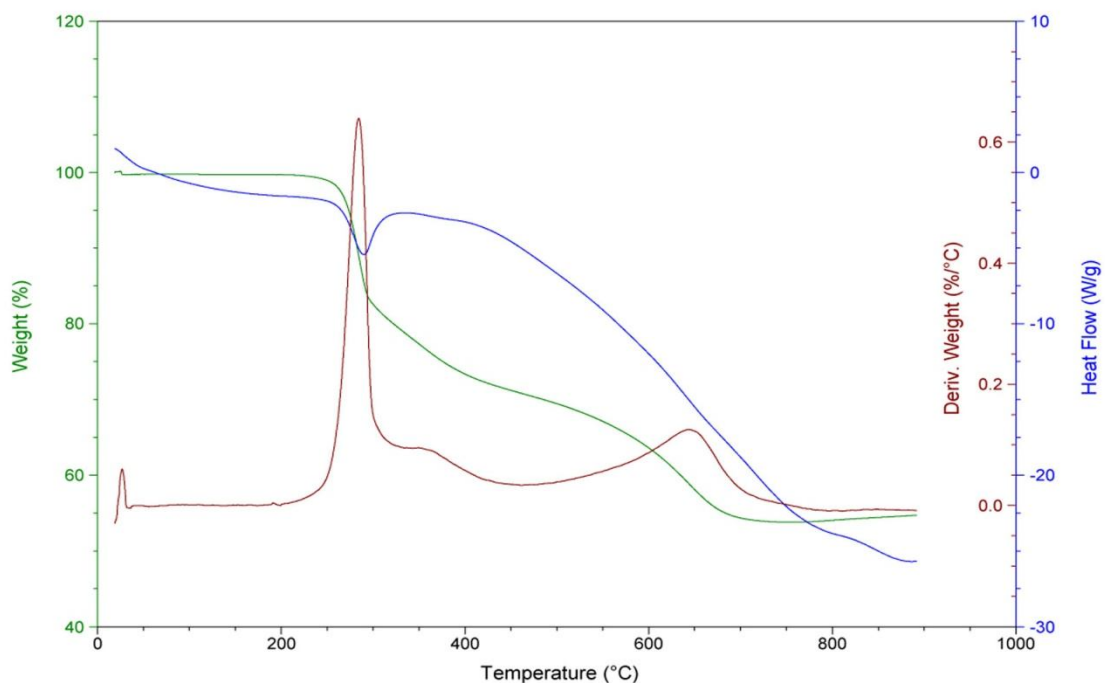


**Figure 4.2 TGA-DSC profile of precursor E conducted under an argon atmosphere**

An *in-situ* XRD experiment was carried out to investigate the thermal decomposition process of precursor E. This experiment was conducted under 60 ml/min argon and the temperature was increased from room temperature to 800 °C. A scan was taken at each 100 °C interval. The results are presented in Figure 4.3 which contains five patterns corresponding to the different phases observed. From this data, it can be seen that the characteristic reflections of molybdenum carbide are clearly observed at 800 °C (e.g. those observed at 34.41°, 38.08° 2θ as consistent in the powder diffraction index (JCPDS 11-0680)).

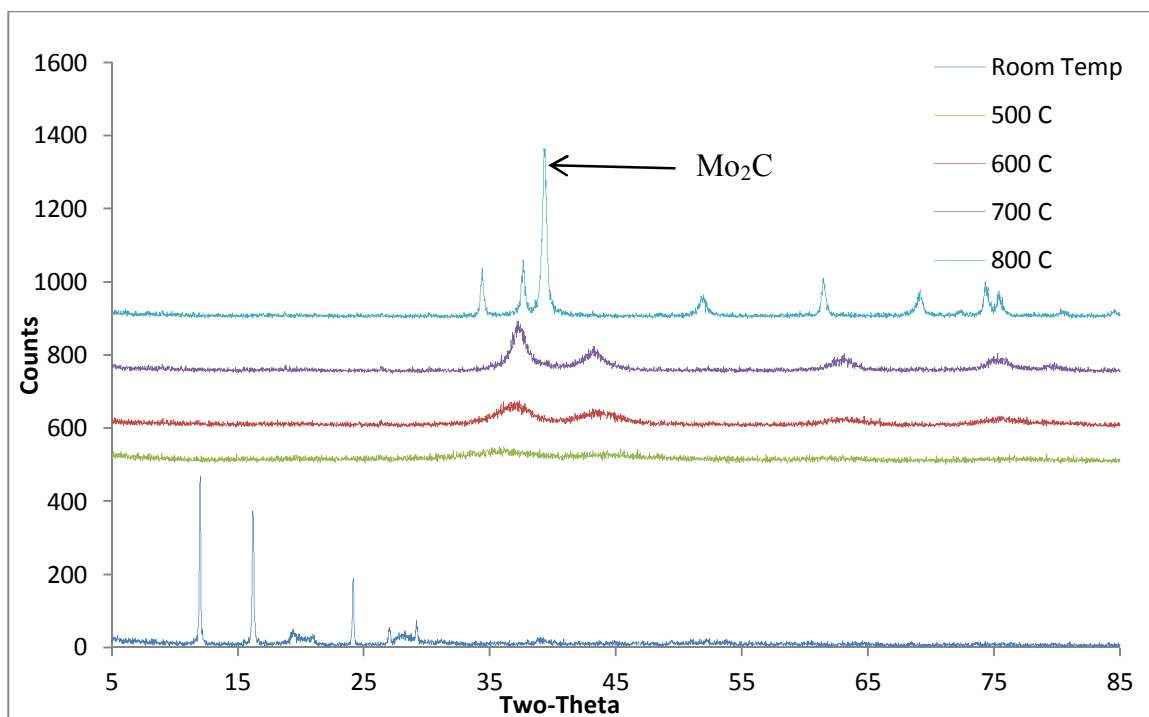


**Figure 4.3 *In-situ* XRD patterns at room temperature, 500 °C, 600 °C, 700 °C and 800 °C**

As mentioned in experimental chapter, the thermal decomposition studies of precursor E detailed within this thesis were performed under various conditions. In this regard, the work is presented in four discrete sections: (i) investigation of precursor E under an argon atmosphere at 800 °C, (ii) investigation of precursor E under an argon atmosphere at 700°C, (iii) Investigation of mixed precursor preparing by using mechanical mixture of MoO<sub>3</sub> with precursor E under an argon atmosphere at 700 °C and (iv) investigation of precursor E under different atmospheres at 700°C.

### 4.1.1 Investigation of precursor E under an argon atmosphere at 800 °C

Two different flow rates were introduced to the sample yielding E-5 (60ml/min) and E-9 (10ml/min). The details are described in the experimental chapter.

#### 4.1.1.1 XRD patterns

Figure 4.4 shows XRD patterns of samples E-5 and E-9. It can be observed that all samples show three different phases, Mo<sub>2</sub>C (JCPDS, 11-0680), Mo (JCPDS, 42-1120) and β-Mo<sub>2</sub>N<sub>0.78</sub> (JCPDS, 25-1368). There is a significant difference in the peak intensities of both samples. The relative peak intensities of Mo<sub>2</sub>C and β-Mo<sub>2</sub>N<sub>0.78</sub> regarding sample E-5 are much higher than those observed in sample E-9. In contrast, the intensity Mo metal peaks in the case of sample E-9 are higher than those observed in sample E-5.

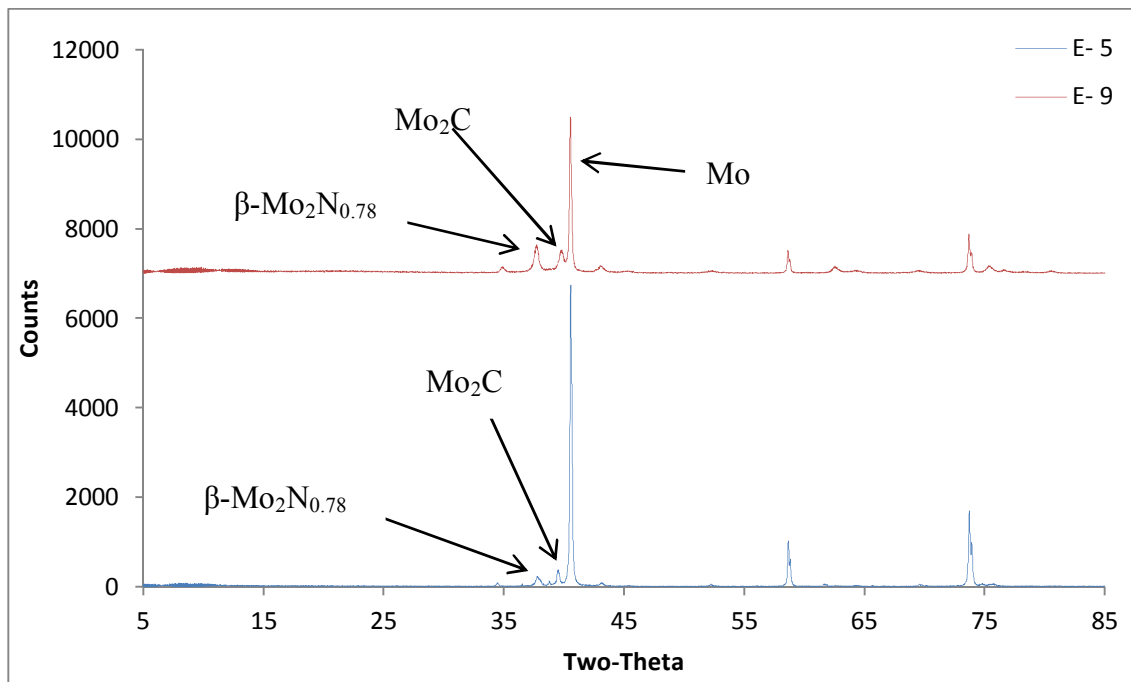


Figure 4.4 XRD patterns of samples E-5 and E-9

#### 4.1.1.2 C H N analysis

The carbon and nitrogen content of all samples including that generated by the *in-situ* XRD reaction is shown in Table 4.1. It can be observed that there is very low level of carbon and nitrogen content in samples E-5 and E-9. Although the *in-situ* experiment has a high carbon content, it is less than the expected carbon content for a pure stoichiometric phase of Mo<sub>2</sub>C which would be 5.88 w.t.%. As mentioned in the introduction chapter, the preparation of molybdenum carbide or nitride is sensitive to any variation of conditions resulting in modification of the final product and its carbon and nitrogen content.

**Table 4.1: Carbon and nitrogen content of samples E-5, E-9 and E-8 *in-situ***

Sample Code (Ar, 800 °C)	Flow rate ml/min	Post-reaction analysis	
		Carbon (wt. %)	Nitrogen ( wt.% )
E-5	60	0.62	0.31
E-8 <i>In-situ</i>	60	4.77	0.62
E-9	10	0.75	1.96

#### 4.1.1.3 BET surface area measurements

Table 4.2 shows the BET surface areas of samples E-5, E-9 and E-8 *in-situ*. It can be seen from this table that sample E-8 *In-situ* shows the highest surface area. It is interesting to note that applying high flow rate leads to an increase in the specific surface area. In this regard, sample E-9, which prepared using high flow rate, exhibited a higher specific surface area than sample E-5, although it is still low.

**Table 4.2: BET surface area of samples E-5, E-9 and E-8 *in-situ***

Sample Code	BET surface area ( m <sup>2</sup> /g )
E-5	2.9
E-8 <i>In-situ</i>	18.5
E-9	9.4

#### 4.1.1.4 SEM images

Representative SEMs of samples A, B, C and D corresponding to the precursor, E-5, E-8 *in-situ* and E-9 respectively are presented in Figure 4.5. All samples are pseudomorphic with the precursor. It can be seen that the morphologies of all samples take on a rough appearance. It can be noted that sample D contains some rods of silica wool which are observed together with the particles.

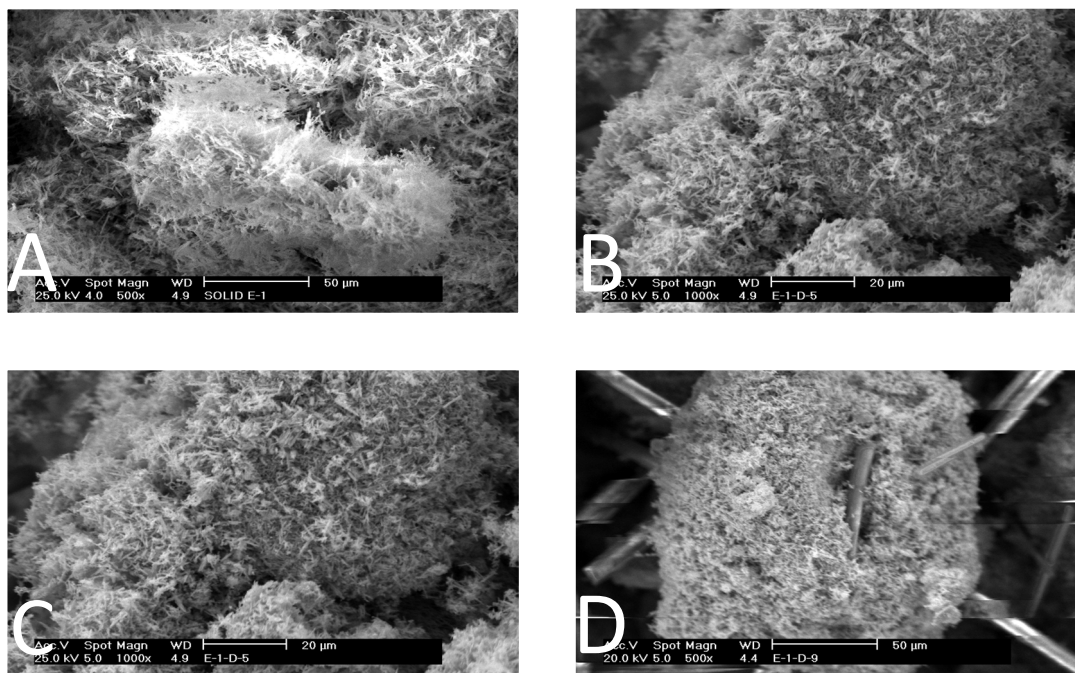


**Figure 4.5: SEM images of A) precursor E, B) sample E-5, C) sample E-8 *in-situ* and D) sample E-9; all images correspond to the same magnification**

#### 4.1.1.5 Summary

It is well known that the preparation of molybdenum carbide, nitride and oxycarbonitride by single source routes requires very controlled conditions in order to obtain specific desired products. High concentrations of water vapour can also change the nature of products [55].

The significant differences between the *in-situ* experiment and corresponding microreactor studies conducted under nominally the same conditions can be attributed to differences in reactor configuration and reaction procedure.

It is interesting to note that investigation of ethylenediammonium molybdate under a helium atmosphere produced molybdenum oxycarbonitride [53]. This is consistent with obtained results conducted in the microreactor using an argon atmosphere although oxygen analysis was not undertaken in the current study. However, there is a good agreement with the results obtained from XRD and those obtained by C H N analysis, which show high level of carbidation was achieved in both experiments.

## 4.1.2 Decomposition under an argon atmosphere at 700 °C

In this section, comparable experiments to those described for precursor I detailed in the previous chapter were undertaken to facilitate comparison. The aim of this section was to study the effect of flow rate on the final product phase. As described in the experimental chapter, different argon flow rates were applied at a reaction temperature of 700 °C. The sample codes E-13, E-11 and E-15 correspond to flow rates of 10, 60, 94 ml/min, respectively.

### 4.1.2.1 XRD patterns

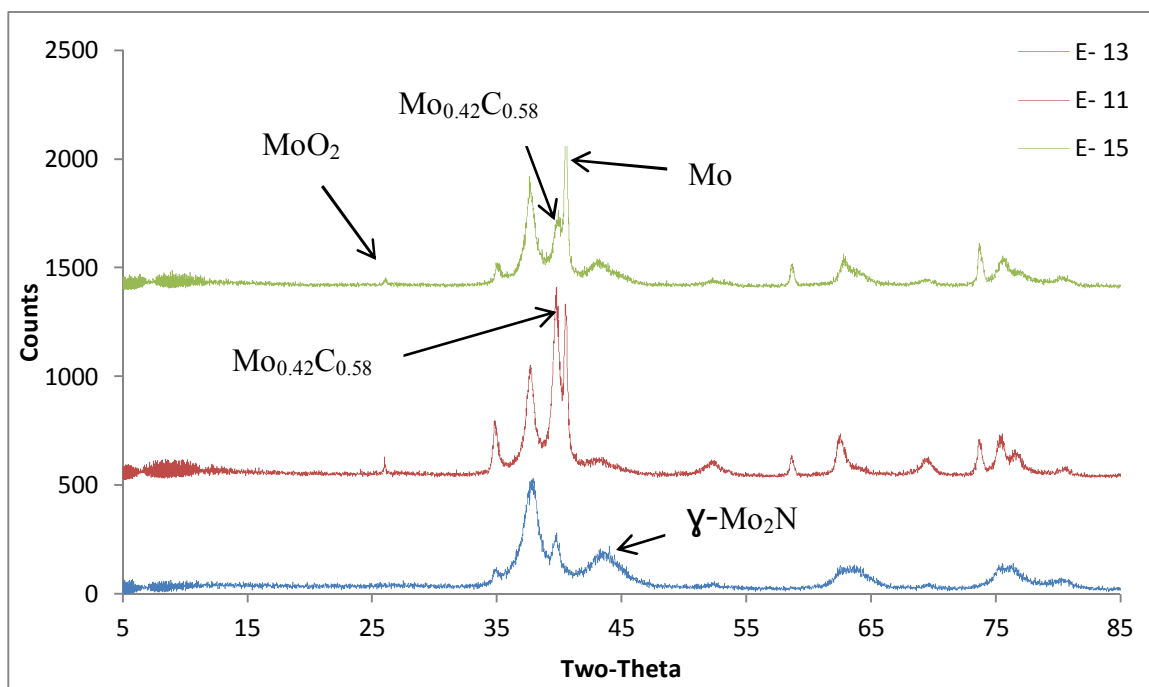


Figure 4.6 XRD patterns of samples E-13, E-11 and E-15

The XRD analysis of samples E- 13, E- 11 and E- 15 is shown in Figure 4.6. In all cases, molybdenum carbide is a major product phase. Moreover, samples E- 11 and E- 15 contain reflections corresponding to Mo metal and MoO<sub>2</sub>. The presence of Mo<sub>0.42</sub>C<sub>0.58</sub> is evident as shown by its signature reflections (e.g. at 39.7°) (JCPDS, 36-0863). It is worth noting that unequivocal determination of gamma- molybdenum nitride is difficult due to potential overlap of its very broad peaks with those of other phases.

#### 4.1.2.2 C H N analysis

Table 4.3 shows the carbon and nitrogen content of the samples. Although molybdenum carbide is evident in the XRD patterns of E- 13, E- 11 and E- 15, the nitrogen contents are very high and the carbon contents are very low (the stoichiometric carbon content of Mo<sub>0.42</sub>C<sub>0.58</sub> is 14.72 wt. %).

**Table 4.3: Carbon and nitrogen content of samples E- 13, E- 11 and E- 15**

Sample Code (Ar, 700 °C)	Flow rate ml/min	Post-reaction analysis	
		Carbon (wt. %)	Nitrogen ( wt.% )
E-13	10	1.39	3.82
E-11	60	1.46	3.18
E-15	94	0.77	3.78

#### 4.1.2.3 BET surface area measurements

Table 4.4 presents the BET surface areas of the samples. These results indicate that the specific surface area steadily rises with increasing flow rate.

**Table 4.4: BET surface area of samples E- 13, E- 11 and E- 15**

Sample Code	BET surface area ( m <sup>2</sup> /g )
E-13	7.0
E-11	11.1
E-15	19.8

#### 4.1.2.4 SEM images

Figure 4.7 presents representative SEM micrographs of the three samples. These images indicate that all samples have similar features and are not pseudomorphic with their precursor. It should be noted that the “whiskers” seen in some of the images relate to an artifact corresponding to the presence of residual SiO<sub>2</sub> wool in post-reactor samples.

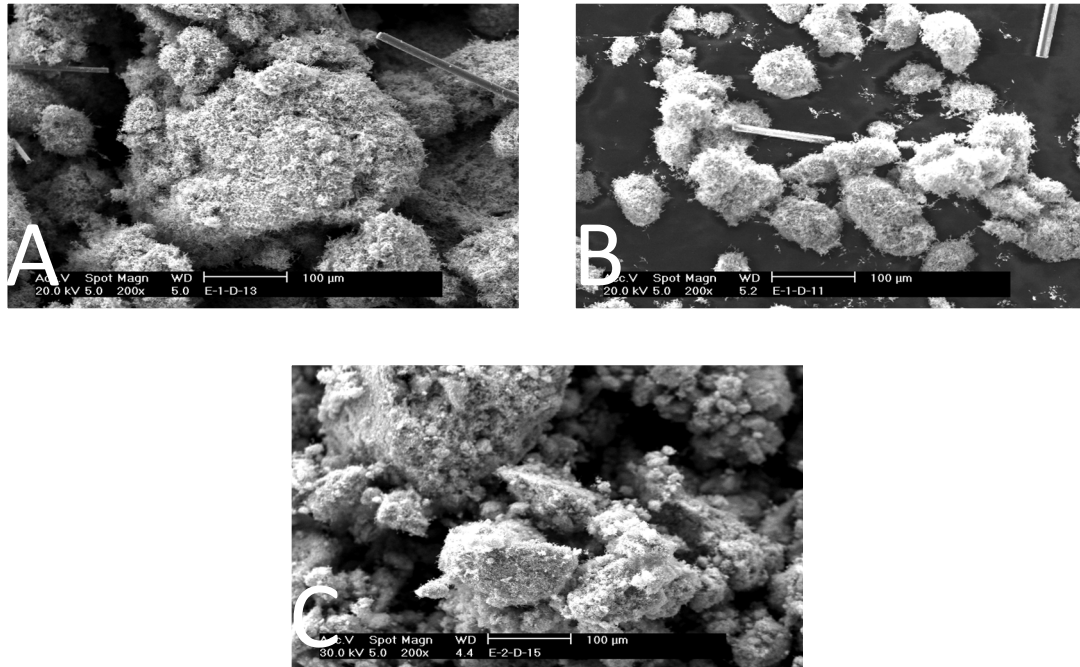


**Figure 4.7: SEM images of A) sample E- 13 B) sample E- 11 and C) sample E- 15; all images correspond to the same magnification**

#### 4.1.2.5 Summary

The decomposition of ethylenediammonium molybdate differs from that observed in the case of hexamethylenetetramine molybdate under the same conditions. However, three different phases are evident in the XRD patterns of the resultant materials corresponding to Mo metal, MoO<sub>2</sub> and Mo<sub>0.42</sub>C<sub>0.58</sub>. It was clear from C H N results that nitrogen content is much greater than carbon content which could be due to the formation of highly dispersed γ-Mo<sub>2</sub>N or amorphous nitride phase, and some evidence of γ-Mo<sub>2</sub>N with broad reflection widths is apparent. However, applying different flow rates was found to have a limited effect on the nitrogen and carbon content. When comparing between the final products of precursor I and precursor E treated under the same conditions it was found that the reaction of precursor I yielded molybdenum nitride and molybdenum dioxide at low flow rate, whereas in contrast, precursor E produces three different phases, Mo metal, MoO<sub>2</sub> and Mo<sub>0.42</sub>C<sub>0.58</sub>. In making comparison between the two precursors it is worth noting the differences in the Mo/N and Mo/C ratio. In the case of precursor I these are both 7/12, whereas for E they are 1/2. Upon increasing the flow rate, there was a little effect on the N and C content, although a general increase in surface area was apparent.

### 4.1.3 Investigation of mixed precursor preparing by using mechanical mixture of $\text{MoO}_3$ with precursor E under an argon atmosphere at $700^\circ\text{C}$ .

In this section, the precursor E was investigated by adding  $\text{MoO}_3$  to precursor E with 1:1 molar ratio by using two different pathways of preparation, as described in the experimental chapter. The purpose of this study was to investigate the effect of preparation methods on the final product phases. However, the sample E-18 represents a physical mixture of molybdenum trioxide and ethylenediamine molybdate whereas sample E-19 represents a segregated bed of ethylenediamine molybdate and molybdenum trioxide in which the ethylenediamine molybdate was placed upstream of the molybdenum trioxide.

#### 4.1.3.1 XRD patterns

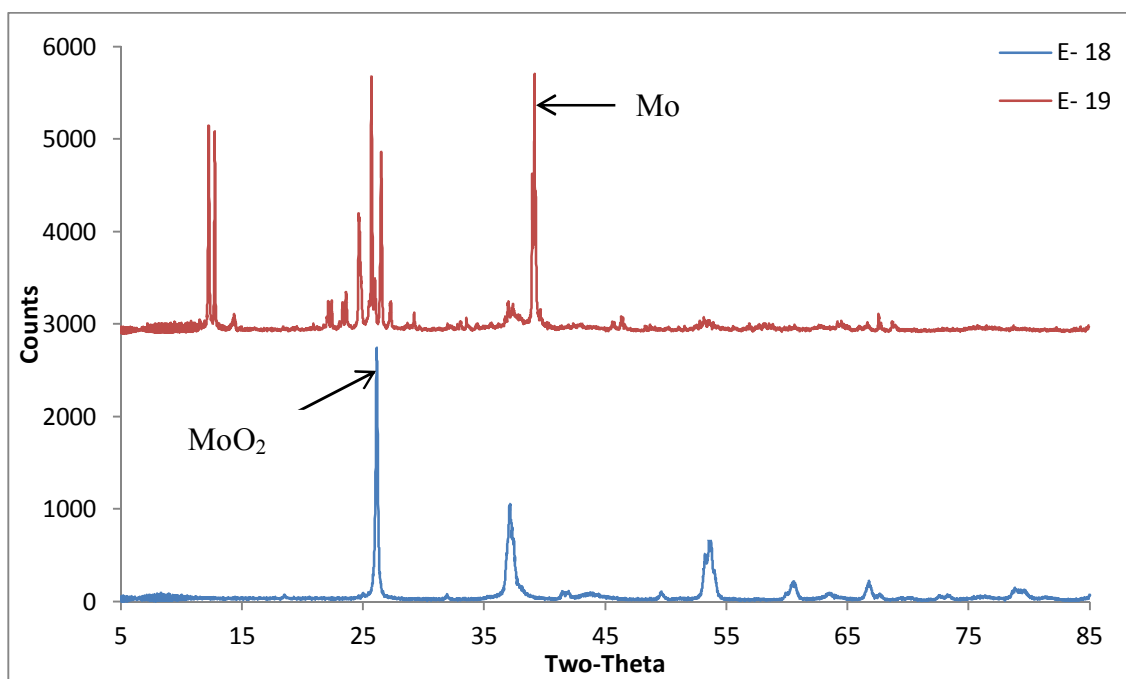


Figure 4.8 XRD patterns of samples E-18 and E-19

Figure 4.8 presents XRD patterns of samples E-18 and E-19 after reaction. It can be seen that molybdenum dioxide is evident in the case of sample E-18, while, sample E-19

contains reflections corresponding to molybdenum metal and molybdenum trioxide. E-18 may also contain some  $\beta\text{-Mo}_2\text{N}_{0.78}$ , although not all expected reflections are present.

#### 4.1.3.2 C H N analysis

Table 4.5 presents the C H N results of samples E-18 and E-19. The results indicate that low degree level of nitridation observed in the case of sample E-18 which possibly contains some  $\beta\text{-Mo}_2\text{N}_{0.78}$  and it is less than the nitrogen content observed in sample E-11, which is prepared using precursor E without adding molybdenum trioxide under similar conditions. In terms of sample E-19, a smaller amount of nitrogen content is present after reaction.

**Table 4.5: Carbon and nitrogen content of samples E-18 and E-19**

Sample Code (Ar, 60ml/min, 700°C)	Post-reaction	
	Carbon (wt. %)	Nitrogen ( wt.% )
E-18	0	1.39
E-19	0	0.85

#### 4.1.3.3 BET surface area measurements

Table 4.6 presents the BET surface areas of samples E-18 and E-19. It can be seen from this table that sample E-19 possesses a lower surface area than sample E-18.

**Table 4.6: BET surface area of samples E-18 and E-19**

Sample Code	BET surface area ( m <sup>2</sup> /g )
E-18	18.2
E-19	4.2

#### 4.1.3.4 SEM images

Figure 4.9 shows the morphology of samples E-18 and E-19. It can be observed from these images that there is a significant difference in the features of samples, where the morphology of sample E-18 is similar to that observed in sample E-11. The effect of the presence of molybdenum trioxide and molybdenum metal is apparent in the case of sample E-19, where the sample exhibited some contrast regions which can be attributed to the metallic content.

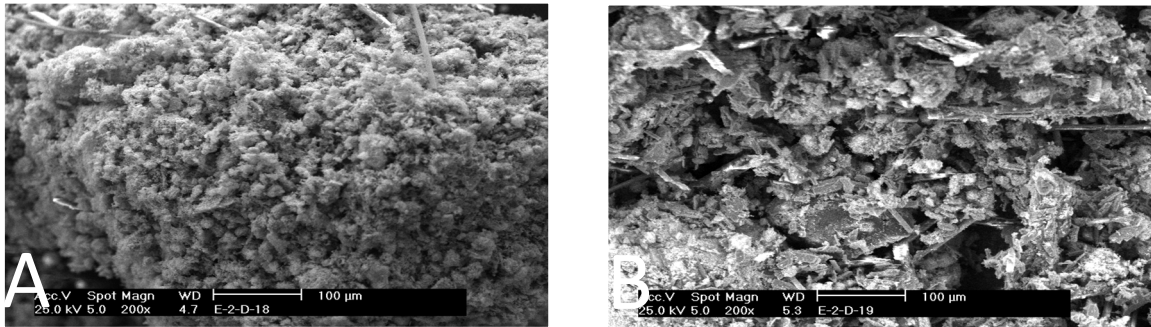


**Figure 4.9: SEM images of A) sample E- 18 and B) sample E- 19; all images correspond to the same magnification**

#### 4.1.3.5 Summary

In this section, the effect of the percentage of the carbon and nitrogen source to percentage of molybdenum, present in the precursor, can be seen to influence the final product. However, it is well known that sufficient carbon and nitrogen sources in the precursor are the most important factor to complete the reduction-nitridation or carbidation steps in the preparation of molybdenum carbide or nitride using the single source route method [3].

Mixing molybdenum trioxide with precursor E leads to decrease the percentage of carbon and nitrogen present in precursor and a corresponding increase in the percentage of molybdenum present also in precursor. Thus, the resultant materials exhibited mixed phases of molybdenum metal and molybdenum oxide with a small amount of molybdenum nitride, as was confirmed by XRD and which was consistent with the C H N results.

#### 4.1.4 Decomposition under different reaction atmospheres at 700°C

In this section the reaction of precursor E was investigated under N<sub>2</sub>, H<sub>2</sub>/N<sub>2</sub> 1:3, H<sub>2</sub>/N<sub>2</sub> 3: 1 and Ar/H<sub>2</sub> 1:3 atmospheres which are represented by sample codes E- 29, E-23, E-25 and E-27, respectively.

##### 4.1.4.1 XRD patterns

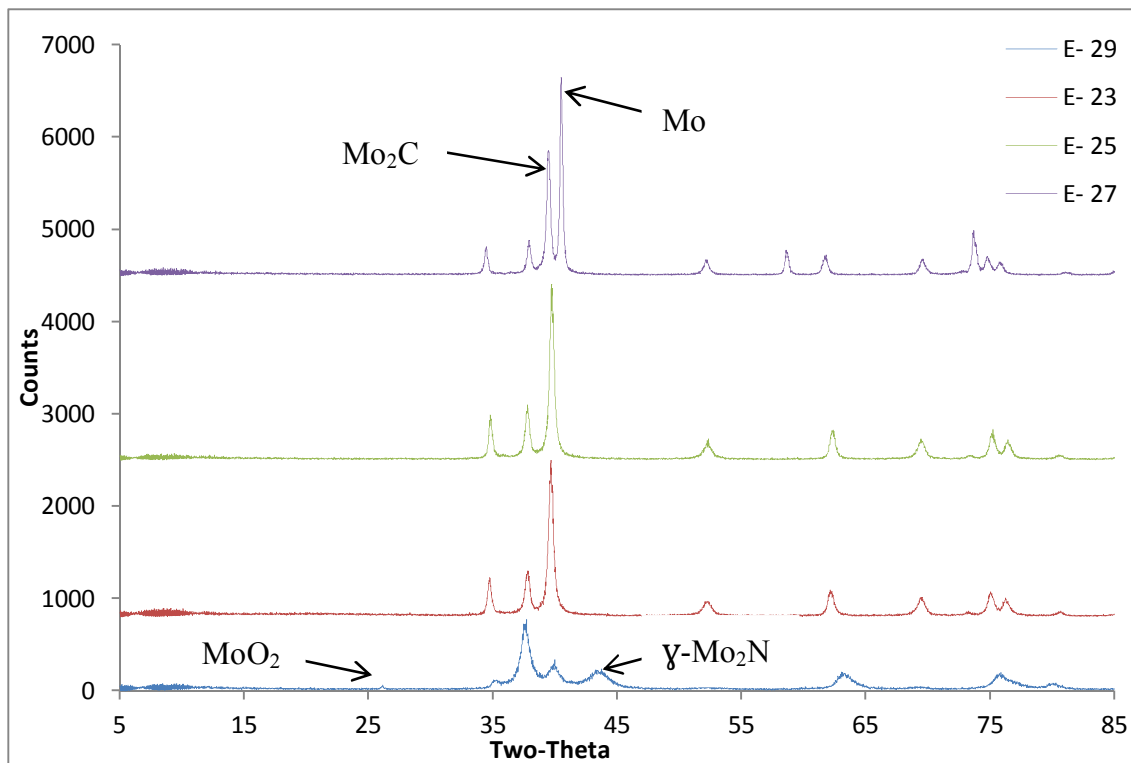


Figure 4.10 XRD patterns of samples E-29, E-23, E-25 and E-27

Figure 4.10 presents XRD patterns of E-29, E-23, E-25 and E-27 after reaction. It was clear from XRD results that Mo<sub>2</sub>C, (JCPDS, 11-0680) is a major phase in all cases. In addition, metallic Mo is evident in the case of sample E-27, which was formed under a 1:3 Ar/ H<sub>2</sub> atmosphere.

It should be noted that there was a similar observation in relation to the position of molybdenum carbide reflections as documented in the previous chapter for comparable samples generated from precursor I. Their reflections possessed small shifts compared with the standard pattern, indicating that the products may not be pure carbides. In the

case of sample E-29 which employed a N<sub>2</sub> atmosphere, a small diffraction peak corresponding to molybdenum dioxide can be clearly seen at 26° 2θ and also γ-Mo<sub>2</sub>N is formed.

#### 4.1.4.2 C H N analysis

Table 4.7 presents the carbon and nitrogen content of the samples. It is readily apparent that, despite Mo<sub>2</sub>C being evident in the XRD patterns of E-23, E-25 and E-27, the nitrogen content increased when the ratio of H<sub>2</sub> gas is increased for the N<sub>2</sub>/H<sub>2</sub> mixture; while the carbon content decreased (the stoichiometric C content of Mo<sub>2</sub>C is 5.88 %). Although, sample E-29 shows γ-Mo<sub>2</sub>N, MoO<sub>2</sub> and Mo<sub>2</sub>C phases in the XRD pattern, no evidence of the presence of carbon can be seen in C H N results. The nitrogen value is less than the expected value for pure phase of γ-Mo<sub>2</sub>N which is 6.80 wt. %.

**Table 4.7: Carbon and nitrogen content of samples E-29, E-23, E-25 and E-27**

Sample Code ( 700 °C, 60 ml/min)	Reaction Atmosphere	Post-reaction analysis	
		Carbon (wt. %)	Nitrogen ( wt.% )
E-29	N <sub>2</sub>	0	5.24
E-23	H <sub>2</sub> /N <sub>2</sub> 1 : 3	3.27	2.82
E-25	H <sub>2</sub> /N <sub>2</sub> 3 : 1	2.25	3.15
E-27	H <sub>2</sub> /Ar 3 : 1	2.75	0.35

#### 4.1.4.3 BET surface area measurements

Table 4.8 presents the BET surface areas of the samples. The areas of E-23, E-25 and E-27 were higher than those measured for samples generated from the precursor I, which were obtained under the same conditions. However, sample E-29 which corresponds to the mixed γ-Mo<sub>2</sub>N phase has a higher surface area compared with those obtained from the other gas mixtures, but it is lower than that measured for γ-Mo<sub>2</sub>N in the previous chapter.

**Table 4.8: BET surface area of samples E-29, E-23, E-25 and E-27**

<b>Sample Code</b>	<b>BET surface area ( m<sup>2</sup>/g )</b>
<b>E-29</b>	<b>18.8</b>
<b>E-23</b>	<b>8.3</b>
<b>E-25</b>	<b>7.8</b>
<b>E-27</b>	<b>5.2</b>

#### **4.1.4.4 SEM images**

Figure 4.11 shows the SEM images depicting the morphology of the samples. It can be seen from these images that all samples show a wide distribution of particle size and also are not pseudomorphic with their precursor.

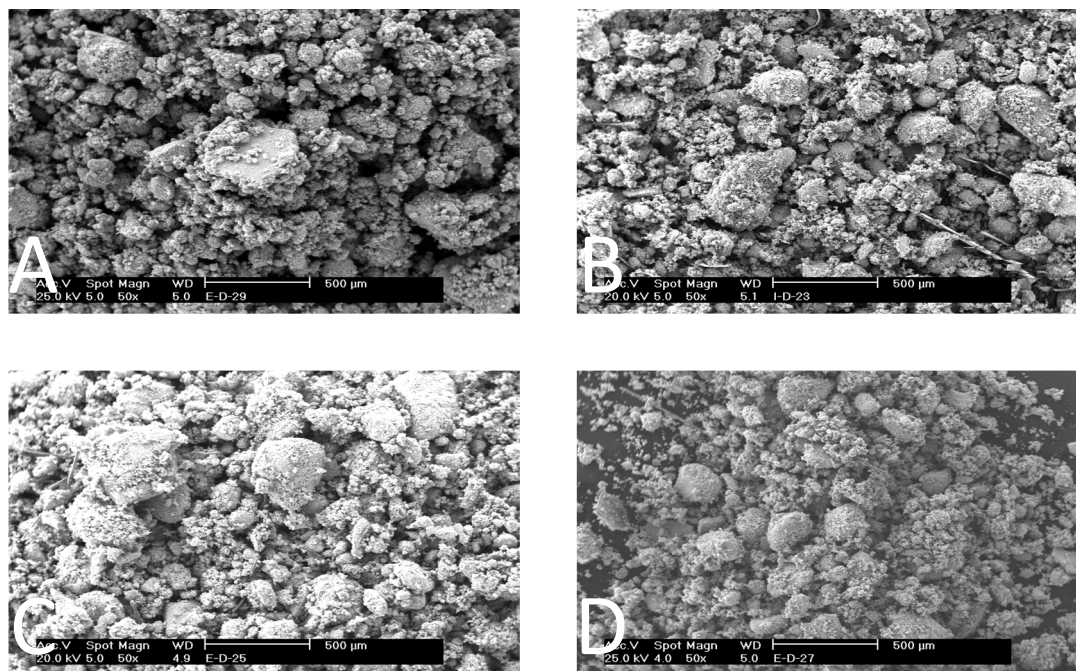


**Figure 4.11: SEM images of A) sample E- 29, B) sample E- 23, C) sample E-25 and D) sample E- 27. All images correspond to the same magnification**

#### 4.1.3.5 Summary

The influence of employing different reaction gases during the thermal decomposition of ethylenediamine molybdate (precursor E) was similar in some respects to that observed in the case of hexamethylenetetramine molybdate (precursor I). The XRD patterns obtained for the decomposition of ethylenediamine molybdate in hydrogen containing reaction atmospheres, which were represented by sample codes E-23, E-25 and E-27, show that molybdenum carbide is the main phase with a small shift of the reflection peaks being evident as has been discussed in Chapter 3. Despite the similarity of XRD patterns obtained from both precursors, there are significant differences in the C H N results and BET surface area measurements. In the reactions conducted under  $H_2/N_2$ , regardless of the reactant gas ratio, the nitrogen content is higher than the carbon content in the case of precursor I, whereas it increases when the ratio of  $H_2$  gas is increased regarding precursor E. In terms of the reaction conducted under  $H_2/Ar$  3:1 using precursor I, the nitrogen and carbon contents were comparable whereas for precursor E there is much more carbon than nitrogen. However, in the reaction conducted under a nitrogen atmosphere, both precursors show similar XRD patterns, with additional reflections corresponding to the presence of molybdenum carbide and molybdenum dioxide in the case of precursor E, which were difficult to observe in the case of precursor I. It is surprising that the nitrogen value obtained from precursor E is greater than that in precursor I.

The surface area measurements of the results obtained from both precursors under all reactant gases have indicated that the products generated via precursor I show low surface area except under  $N_2$  atmosphere, whilst samples derived from precursor E shows a reasonable surface area. Figure 4.12 summarises the resultant materials obtained from thermal decomposition of ethylenediammonium molybdate under different atmospheres.

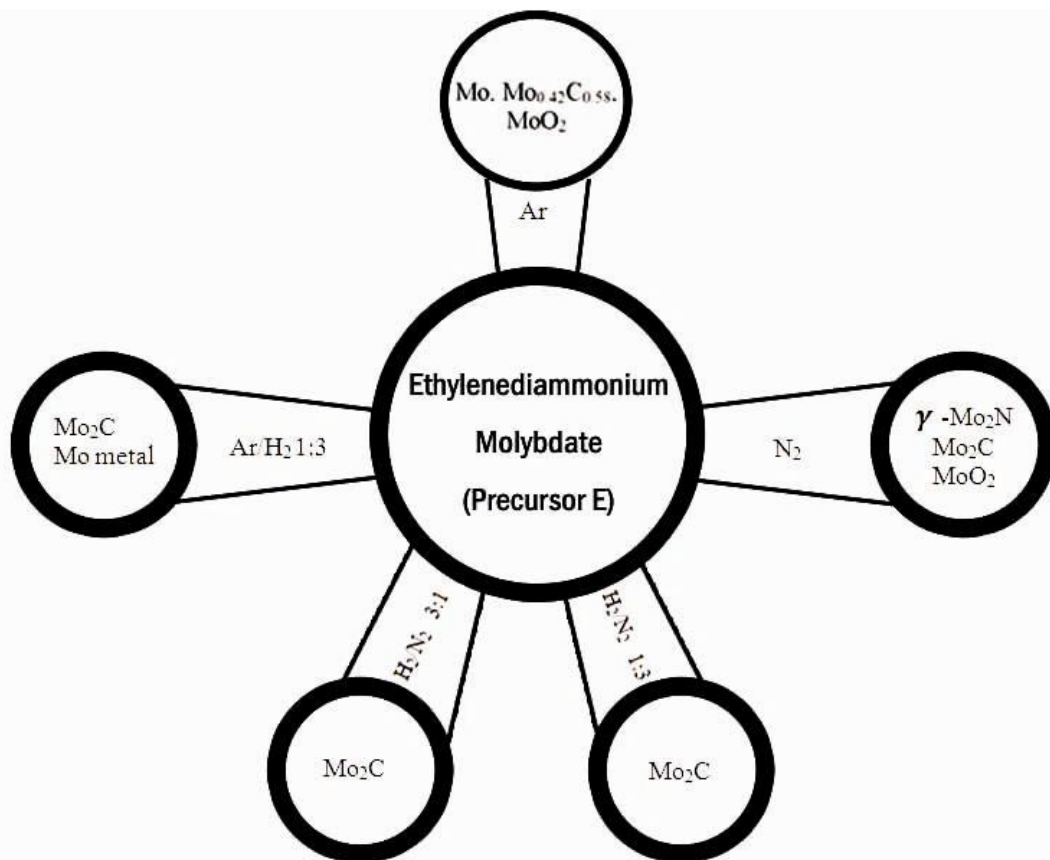


**Figure 4.12 Schematic diagram showing the resultant materials from thermal decomposition of ethylenediammonium molybdate under different atmospheres**

## 4.2 Conclusion

Thermal decomposition of ethylenediammonium molybdate (precursor E) tends to produce phase impure products. However, it can be concluded that decomposition of precursor E under a N<sub>2</sub> atmosphere leads to the production of a phase mixture of gamma molybdenum nitride, molybdenum oxide and molybdenum carbide with a higher nitrogen value compared to that observed in the decomposition of precursor I. In contrast, molybdenum carbide, molybdenum dioxide and molybdenum metal were obtained from the reactions involving all the other reacting gases. Applying different flow rates was found to have a small effect on the nitrogen and carbon content.

## **Chapter 5: Lattice Nitrogen Reactivity and Stability Studies**

In this chapter, the work conducted to determine the reactivity and stability of the lattice species of some of the materials obtained is described. As described earlier, different materials were obtained using two different precursors under various gas atmospheres. These materials were identified as various molybdenum containing carbide, carbonitride or nitride phases. These materials could potentially be of interest as nitrogen and/or carbon transfer materials, in which the molybdenum carbonitrides and nitrides may act as “reservoirs” of activated nitrogen or carbon, as described in the introduction chapter. Various techniques were used in order to assess the reactivity of lattice carbon and nitrogen. These techniques were temperature programmed reduction (TPR), thermal stability studies, thermal volatilisation analysis (TVA) and thermogravimetric analysis (TGA). As mentioned, the aim of this study was to investigate the potential of the materials for the possible production of important nitrogen containing organic products (e.g. amines) by the controlled reduction of carbonitride and nitride phases.

### **5.1 TPR Studies of Lattice Nitrogen Reactivity**

Lattice nitrogen reactivity was studied by evaluation of the  $\text{NH}_3$  generated from the denitridation of the materials by  $\text{H}_2$  reactant. Three different materials, which have been identified in Chapters 3 and 4, were investigated under  $\text{H}_2/\text{Ar}$  3:1 at temperatures between 400 °C to 700 °C, and the temperature profile which was applied is shown in Figure 2.3.

### 5.1.1 Reaction Data

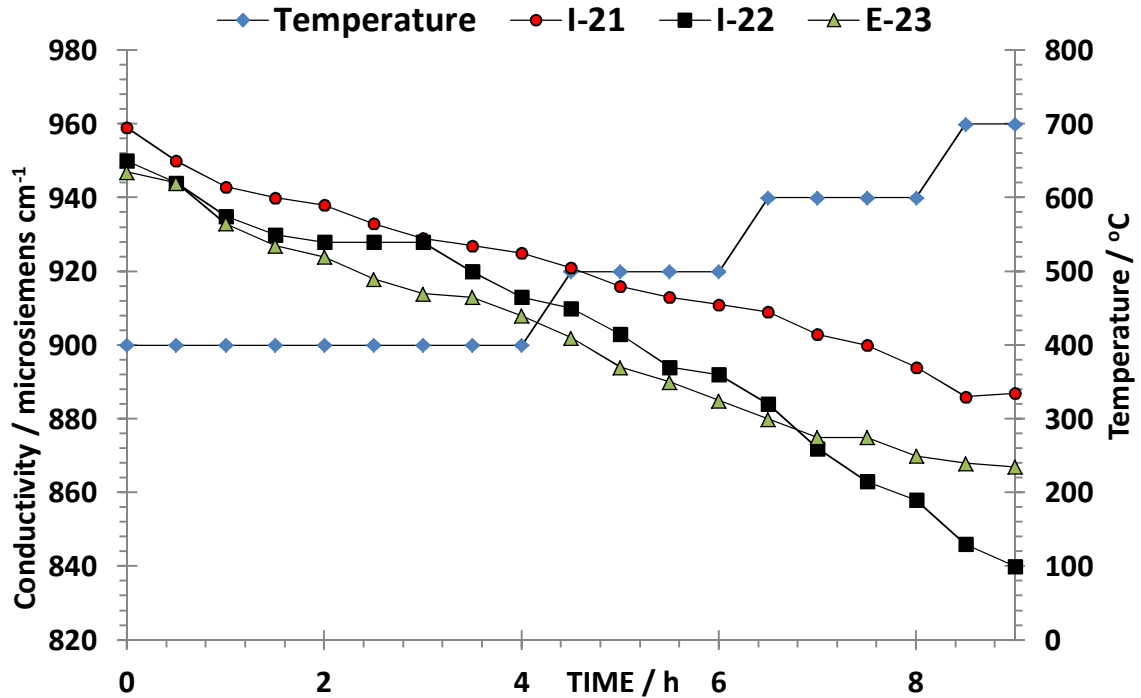


**Figure 5.1 Conductivity versus time plots for temperature programmed reactions of samples I-21, I-22 and E-23 under Ar/H<sub>2</sub> 1:3**

Figure 5.1 presents conductivity data of samples I-21, I-22 and E-23 under a 60 ml/min flow of Ar/H<sub>2</sub> 1:3. These data supply information on the temperature dependence of ammonia production via hydrogenation of the nitride based materials. Although the hydrogen is important factor to remove nitrogen from the lattice at high temperature as NH<sub>3</sub>, the majority of nitrogen is generally lost as N<sub>2</sub> gas under these reaction regimes [26]. However, it can be seen from the profile that the conductivity of all samples, at 400 °C, decreases in the first 2 hours then the samples behave differently in the second 2 hours. After further increment of temperature to 500 °C the conductivity decreased in the case of all samples. Upon increasing the temperature to 600 °C and then to 700 °C, the conductivity showed a slowly declining rate regarding samples I-21 and E-23, whereas sample I-22 exhibited a higher rate of decrease. In terms of the conductivity profiles, consideration should be given to the possible contribution of adsorbed NH<sub>x</sub> species

resulting from preparation or pretreatment meaning that the conversion of  $\text{NH}_3$  by direct hydrogenation of lattice N may be lower than implied in Figure 5.4 [50].

### 5.1.2 XRD patterns

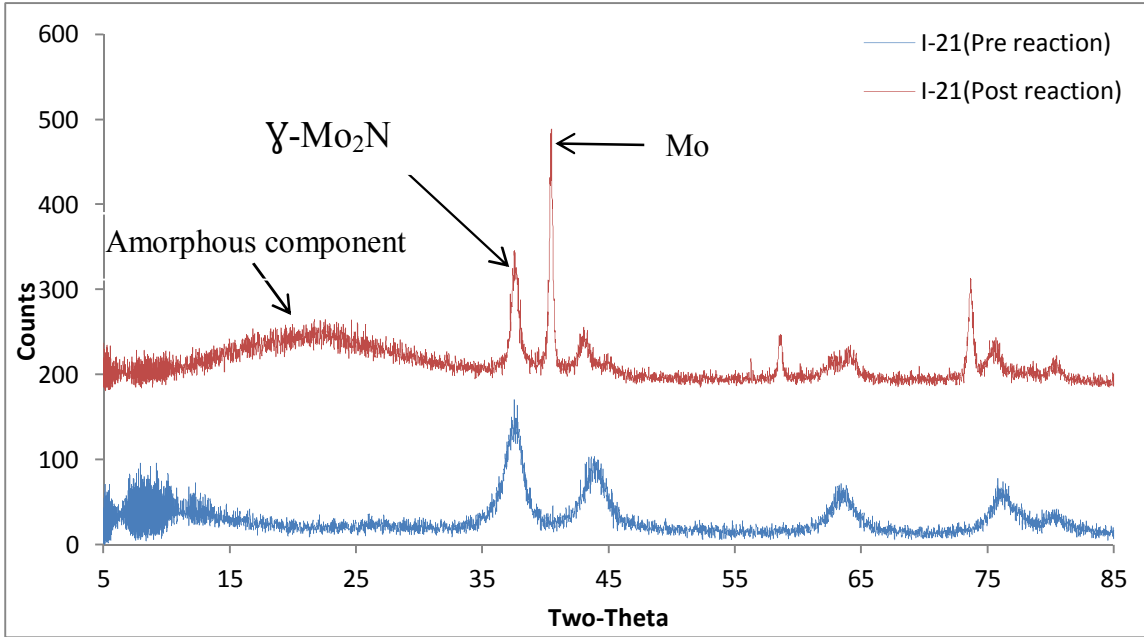


Figure 5.2 XRD patterns showing the differences before and after reaction for sample I- 21

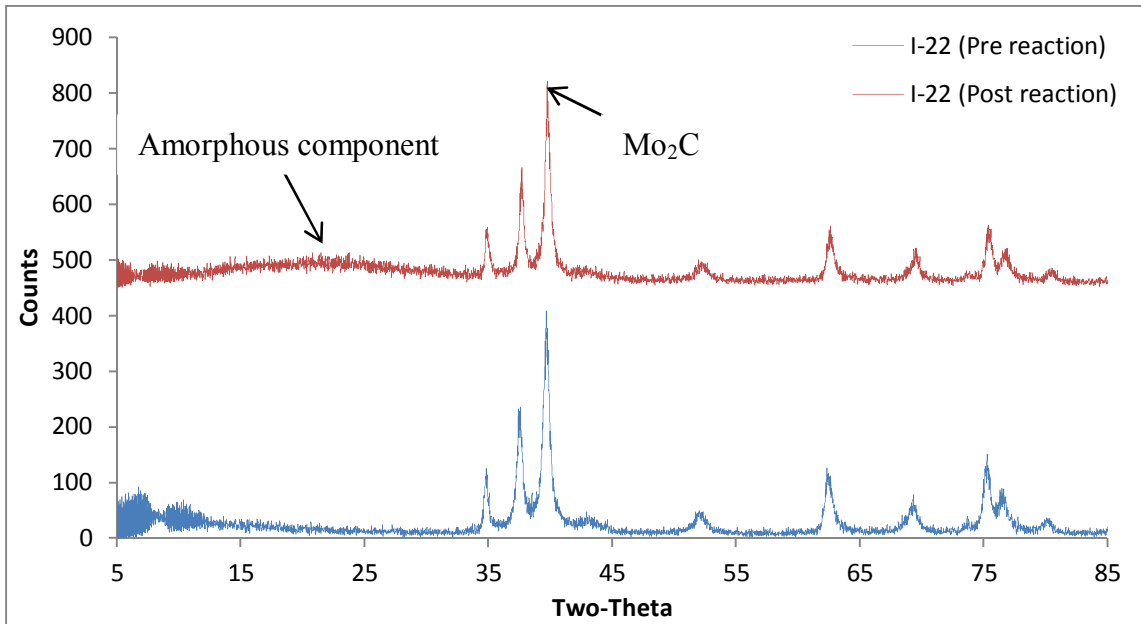
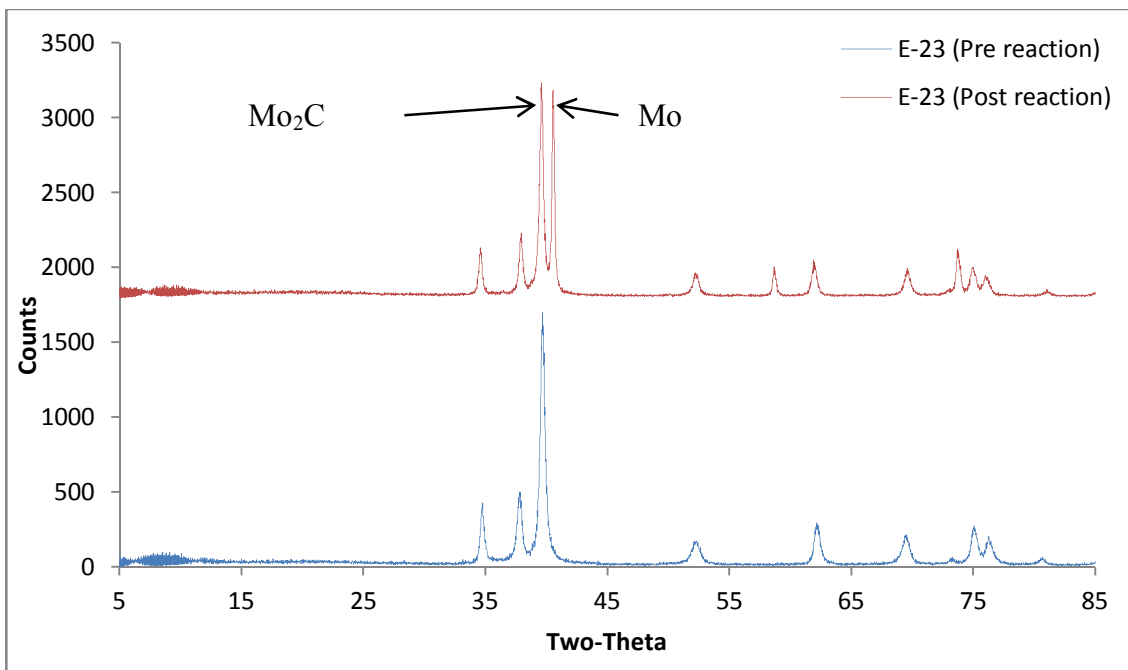


Figure 5.3 XRD patterns showing the differences before and after reaction for sample I- 22



**Figure 5.4 XRD patterns showing differences before and after reaction for sample E- 23**

Figures 5.2, 5.3 and 5.4 present XRD patterns showing differences pre- and post- reaction for samples I-21, I-22 and E-23. As discussed in the previous chapters, the patterns for I-22 and E-23 match to the Mo<sub>2</sub>C phase with a small shift in the positions of their diffraction peaks compared with the standard pattern. When employing Ar/H<sub>2</sub> 1:3 in the reaction between 400 °C to 700 °C for 9 hours, as described in temperature profile shown in Figure 5.1, the molybdenum carbide diffraction peaks became identical to the standard pattern. There is an additional reflection in the XRD pattern at 40.5° 2θ which became apparent after reaction in the case of sample E-23 and which corresponds to the presence of molybdenum metal. In the case of sample I-21 which possesses a diffraction pattern which matches to the γ-Mo<sub>2</sub>N phase, as discussed previously; metallic Mo is also evident post-reaction.

### 5.1.3 C H N analysis

Table 5.1 presents the carbon and nitrogen content pre - and post- reaction. Stoichiometries corresponding to these data have been determined assuming single phases and these are also presented. It can be seen from these results that nitrogen content decreased in all samples upon reaction. The nitrogen content of samples I-21 and I-22 has been slightly reduced, by 15% in sample I-21 and 13% in sample I-22. By contrast, two thirds of the original nitrogen content of sample E-23 has been removed by reaction. It should be noted that in calculating the stoichiometry of all samples, it has been assumed that no oxygen is present. It should be also noted that there is an increase of carbon content after reaction in both carbon-containing systems. This is most likely a consequence of the preferential removal of N, the more reactive lattice species.

**Table 5.1 Carbon and nitrogen content pre- and post- reaction and assumed stoichiometry of samples I-21, I-22 and E-23 in lattice reactivity study**

sample code	Pre-reaction		Post-reaction		Assumed stoichiometry	
	C (wt. %)	N (wt. %)	C (wt. %)	N (wt. %)	Pre-reaction	Post-reaction
I-21	0	4.60	0	3.90	Mo N <sub>0.33</sub>	Mo N <sub>0.27</sub>
I-22	1.55	4.45	1.78	3.86	Mo C <sub>0.13</sub> N <sub>0.33</sub>	Mo C <sub>0.15</sub> N <sub>0.29</sub>
E-23	2.35	2.53	3.01	0.87	Mo C <sub>0.20</sub> N <sub>0.18</sub>	Mo C <sub>0.25</sub> N <sub>0.06</sub>

### 5.1.4 Summary

There is a significant difference between the behaviour of samples derived from precursor I and precursor E in the lattice reactivity experiments. Despite apparently comprising a single phase (molybdenum nitride) or a mixed phase (molybdenum carbonitride as implied by XRD data and CHN results), the percentage of nitrogen lost in the samples derived from precursor I are much lower than that derived from the precursor E. In terms of carbon content, it was difficult to verify the loss of carbon from the materials by elemental analysis considering the accompanying loss of N, but carbon seemed to be more stable than the nitrogen, as confirmed by XRD results and C H N

analysis. Consistent with this, in a study of phase transformations of molybdenum carbide and nitride, Yao and co-workers observed the carbide to be more stable than the nitride [60].

## 5.2 Thermal stability studies

In this study, precursor I-22 and precursor E-23 were prepared as previously described and then each batch of both precursors was sub-divided further into two batches in order to minimise potential influences of differences in their morphology/composition. These batches were studied under two different conditions. The first condition was analogous with that applied in lattice nitrogen reactivity study. The second was carried out under an Ar only atmosphere at a range of temperatures between 400 °C to 900 °C; the temperature profile is presented in Figure 2.4.

### 5.2.1 Ar/H<sub>2</sub> 1:3 feed gas reactions

#### 5.2.1.1 XRD patterns

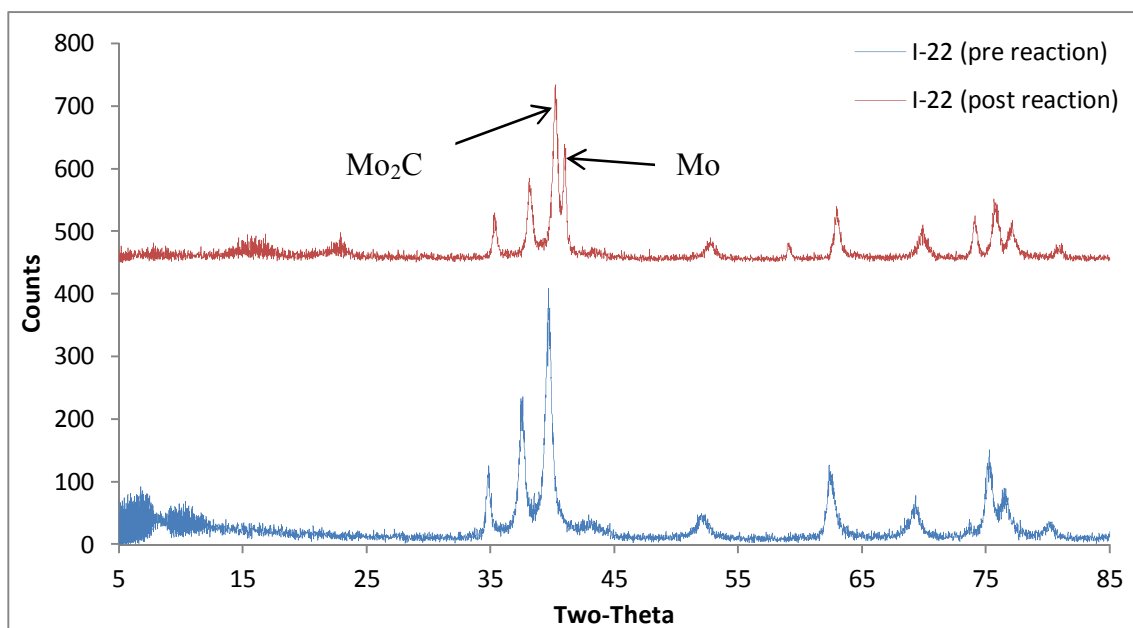


**Figure 5.5 XRD patterns showing differences before and after reaction for sample I-22 under Ar/H<sub>2</sub> 1:3**

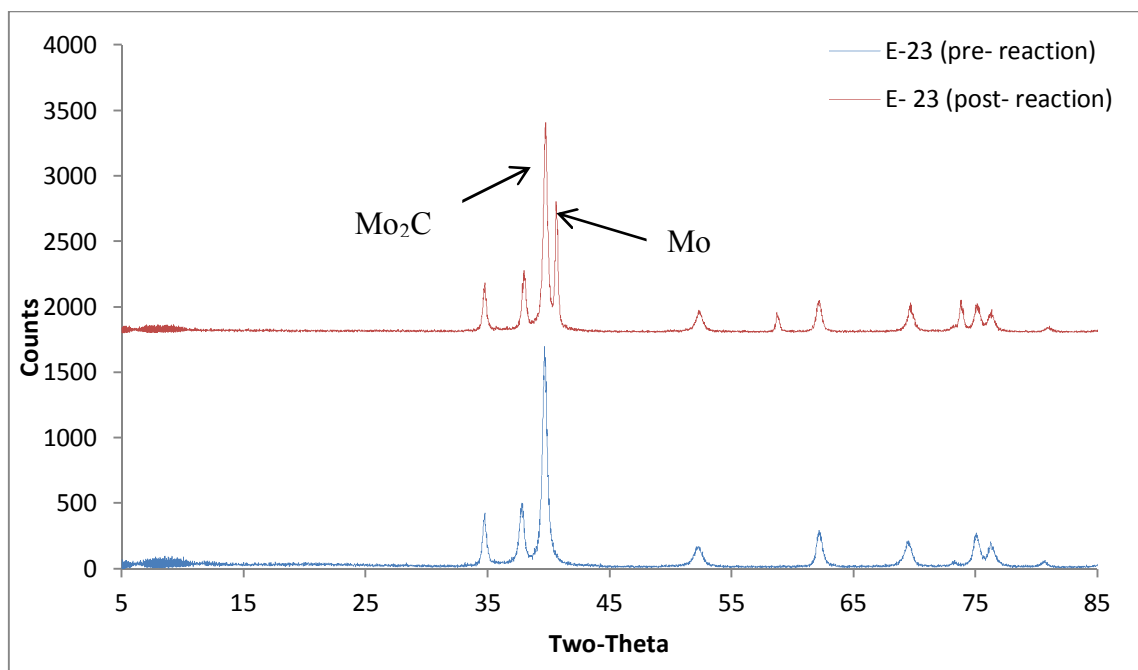


**Figure 5.6 XRD patterns showing the differences between before and after reaction for sample E-23 under Ar/H<sub>2</sub> 1:3.**

The pre-reaction and post-reaction X-ray diffraction patterns of samples I-22 and E-23 are shown in Figures 5.5 and 5.6. As mentioned above, the conditions of those reactions were similar to those reactions conducted in lattice reactivity section except for the amount of sample used in both reactions, which was approximately 0.40g in the case of lattice reactivity reactions and approximately 0.15g in these experiments. In addition, the maximum temperature applied to the samples was 200 °C higher (900°C rather than 700°C regarding lattice reactivity reaction). However, the XRD results in this experiment are comparable to those in lattice reactivity study. Besides this, there are additional diffraction peaks which appear after reaction in the case of sample I-22. These diffraction peaks correspond to the presence of molybdenum metal.

### 5.2.1.2 C H N analysis

Table 5.2 presents the carbon and nitrogen content in pre-reaction and post-reaction samples and the assumed stoichiometry of the samples. As can be observed from the table, the proportion of nitrogen lost in sample E-23, which is 56%, is much greater than I-22, which is 30%. However, in comparison between the data obtained from this reaction, which used 0.15g of precursor, and the data obtained from the lattice reactivity reaction, which used 0.40g of precursor there may well be an influence of space velocity on the nitrogen loss of the sample I-22 in addition to reaction temperature. In terms of carbon content, there is a small difference in post-reaction analysis of sample E-23 in this reaction compared to that in the reactivity study which could be also attributed to the effect of the different space velocity/ reaction temperature.

**Table 5.2 Carbon and nitrogen content pre-and post -reaction and assumed stoichiometry of samples I-22 and E-23 in the stability study in Ar/H<sub>2</sub> 1:3**

sample code	Pre-reaction		Post-reaction		Assumed stoichiometry	
	C (wt. %)	N (wt. %)	C (wt. %)	N (wt. %)	Pre-reaction	Post-reaction
I-22	1.71	4.58	1.72	3.20	Mo C <sub>0.14</sub> N <sub>0.33</sub>	Mo C <sub>0.14</sub> N <sub>0.23</sub>
E-23	3.24	3.14	3.03	1.38	Mo C <sub>0.28</sub> N <sub>0.22</sub>	Mo C <sub>0.25</sub> N <sub>0.10</sub>

## 5.2.2 Ar-only feed gas reactions

### 5.2.2.1 XRD patterns

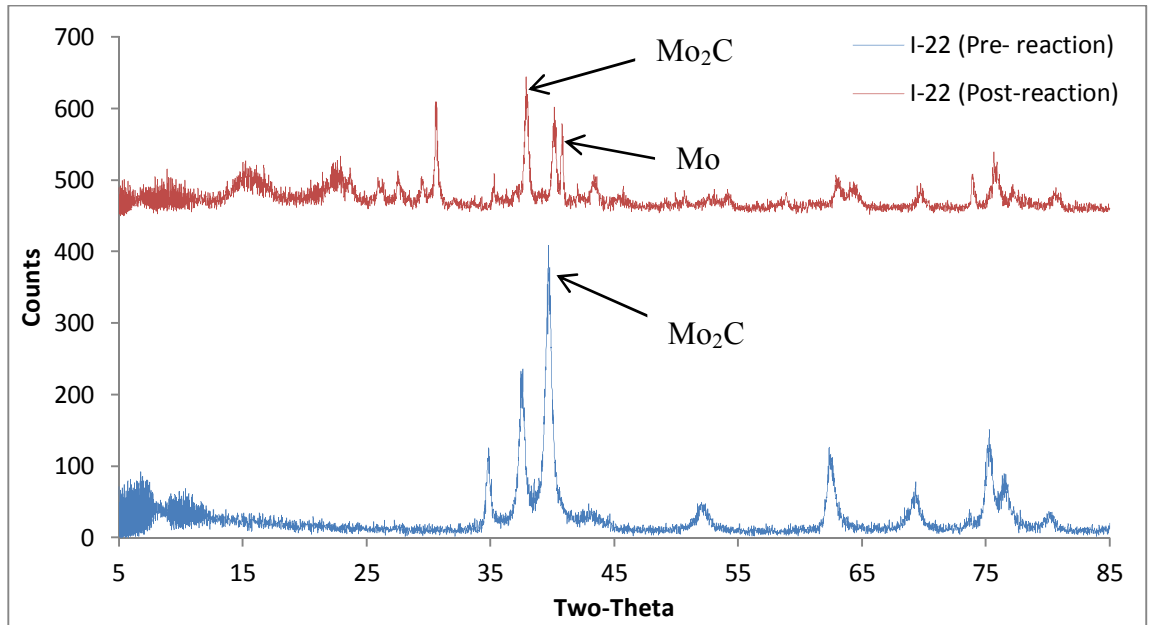


**Figure 5.7 XRD patterns showing the differences before and after reaction for sample I-22 under an Ar-only atmosphere**

The pre-reaction and post-reaction X-ray diffraction patterns of sample I-22 run under Ar-only are shown in Figure 5.7. The pre-reaction pattern of sample I-22 shows a Mo<sub>2</sub>C phase, as described in Chapter 3. However, it is clear from the diffraction pattern that at least two different phases are evident post-reaction. The signature reflection of molybdenum carbide can be clearly seen (e.g. at 39.51° 2θ). Diffraction peaks of molybdenum metal (e.g. at 40.50° 2θ) are also apparent. It should be noted that there is a shift of the diffraction peak to higher angles for the molybdenum carbide phase in particular.

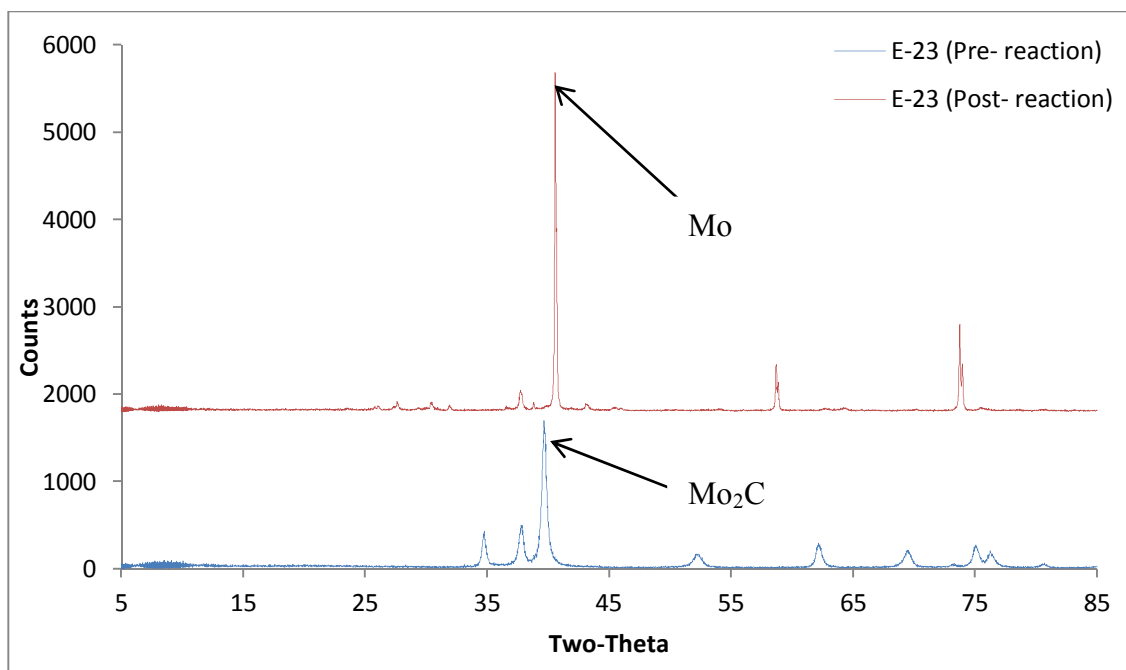


**Figure 5.8 XRD patterns showing the differences between before and after reaction for sample E-23 under an Ar atmosphere**

The pre-reaction and post-reaction X-ray diffraction patterns of sample E-23 are shown in Figure 5.8. The pre-reaction pattern of sample E-23 matches to molybdenum carbide, as described in Chapter 4. In the post-reaction pattern Mo metal is the predominant phase evident, although there are much weaker reflections corresponding to other phases, e.g. molybdenum nitride, evident.

### 5.2.2.2 C H N analysis

Table 5.3 presents the carbon and nitrogen content in pre-reaction and post-reaction samples and their calculated stoichiometry. The decomposition of both precursors under the Ar atmosphere in the range of temperature between 400 °C and 900 °C was totally different from that in Ar/H<sub>2</sub> 1:3 in temperature range between 400 °C to 700 °C. A 74% loss of carbon can be observed upon treatment in the case of sample I-22, whilst there is no evidence of any carbide, as confirmed by the C H N analysis and XRD pattern, after reaction regarding sample E-23. In terms of the nitrogen content of both samples, the nitrogen lost post-reaction in sample E-23 is much greater than that in sample I-22. It is interesting to note that the nitrogen loss of sample I-22 in both types of reaction (Ar only and Ar/H<sub>2</sub>) is similar.

**Table 5.3 Carbon and nitrogen content pre- and post-reaction and assumed stoichiometry of samples I-22 and E-23 in the stability study in Ar-only**

sample code	Pre-reaction		Post-reaction		Assumed stoichiometry	
	C (wt.%)	N (wt.%)	C (wt.%)	N (wt. %)	Pre-reaction	Post-reaction
I-22	1.71	4.58	0.45	3.21	Mo C <sub>0.14</sub> N <sub>0.33</sub>	Mo C <sub>0.04</sub> N <sub>0.23</sub>
E-23	3.24	3.14	0	0.75	Mo C <sub>0.28</sub> N <sub>0.22</sub>	Mo N <sub>0.05</sub>

### 5.2.3 Summary

The studies described in this section have demonstrated that, whilst being more stable than lattice nitrogen upon reduction with H<sub>2</sub>, lattice carbon is lost upon reaction under an Ar-only atmosphere when treated up to 900 °C. The resultant phase compositions are very different from those obtained when samples from the same batches are treated under Ar/H<sub>2</sub> 1:3.

In the case of Ar-only, whilst the loss of lattice N species can be envisaged as occurring via N<sub>2</sub> elimination, the loss of C is more difficult to visualise, unless there is an influence of oxygen species/ additional phase not observable by XRD. It may also be the case that elimination occurs via a carbon containing volatile product such as cyanogen ((CN)<sub>2</sub>). In order to investigate this possibility thermal volatilisation analysis (TVA) was undertaken as described in the next section.

### **5.3 Thermal Volatilisation Analysis (TVA)**

The thermal volatilisation analysis technique (TVA) has been applied to determine the range of species evolved when the materials were heated to high temperature in a vacuum. The interest in applying this method was outlined in the summary of the previous section as being to characterise the range of species evolved by simple thermal treatment of the materials. Three different materials were investigated under vacuum from room temperature to 850°C. A schematic of the system used for thermal volatilisation (TVA) and sub-ambient differential distillation analysis is shown in Figure 2.6. The samples for investigation were carefully selected. Samples I-26 and E-23 are possibly carbonitrides of similar composition prepared from the two different precursors, whereas I-21 corresponded to a nitride. It was anticipated that comparison of the behaviour of these three samples would provide the greatest insight into the processes involved.

#### **5.3.1 TVA of sample I-21**

The sample was heated to 850°C at 10°C /min under vacuum with cryogenic-trapping of condensable products and real-time mass spectrometry of non-condensable products, as described in the experimental chapter. However, a significant level of volatile off-gassing was observed under vacuum over the temperature range of study. These volatiles were sequestered in a liquid N<sub>2</sub> trap for subsequent characterisation. A significant fraction of the total evolved volatiles were, however, non-condensable products.

### 5.3.1.1 Non-condensable products analysis

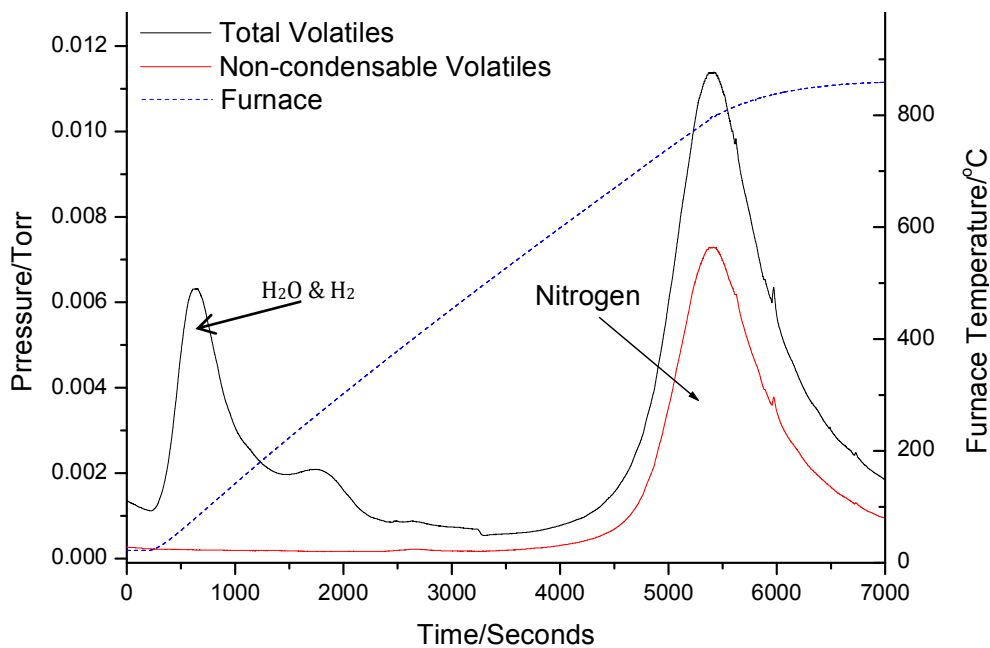


**Figure 5.9 TVA plot of the degradation of sample I-21 showing non-condensable volatile product in the liquid N<sub>2</sub> trap**

It can be seen from Figure 5.9 that the sample I-21 evolves significant quantities of volatile material, which start being evolved at around 650°C in addition to the evolution of H<sub>2</sub> and H<sub>2</sub>O observed at lower temperature. A significant fraction of the total volatile evolution was determined to be nitrogen by online mass spectrometry (as characterised by a peak with m/z 28) along with H<sub>2</sub> and H<sub>2</sub>O. Figure 5.10 presents the mass spectrum of the evolved nitrogen from the sample.

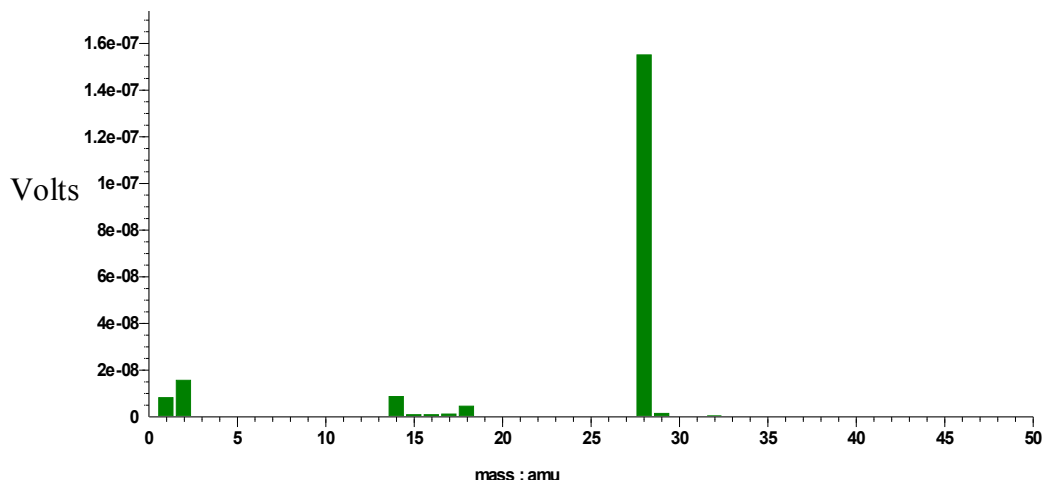


**Figure 5.10 the mass spectrum for the N<sub>2</sub>, H<sub>2</sub> and H<sub>2</sub>O evolved from sample I-21 in TVA**

### 5.3.1.2 Condensable products analysis

As mentioned in experimental chapter, sub-ambient differential distillation of collected volatiles was performed by increasing the temperature of primary cold trap from -196 °C to 30 °C. The volatiles were separated into four secondary cold traps and transferred to IR and GC-MS sample cells. A combination of GC-MS, FTIR spectroscopy and MS was used to analyse the separated volatiles. Figure 5.11 presents the sub-ambient thermal volatilisation analysis of volatiles and components evolved by heating the liquid N<sub>2</sub> trap.

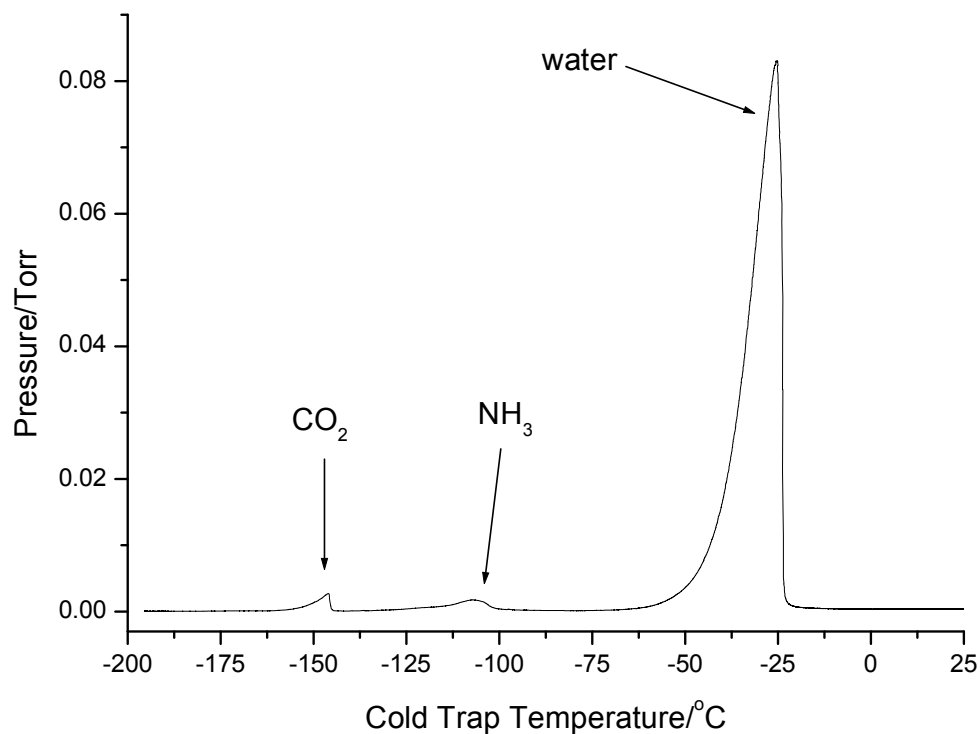


**Figure 5.11 Sub-ambient thermal volatilisation analysis of volatiles and components evolved by heating the liquid N<sub>2</sub> trap**

It can be seen that the collected volatiles consist primarily of water with a small quantity of CO<sub>2</sub> and NH<sub>3</sub>. The CO<sub>2</sub> may be background level. It can be also observed that no higher boiling species were apparent on the sub-ambient thermal volatilisation analysis trace. However, the fraction from -75 °C to room temperature (containing the water fraction) was collected and analysed by GC-MS to confirm if there were any higher boiling species which were masked by the water.

The GC-MS results showed a spectrum resembling the chloroform blank which confirms that the only volatiles evolved from sample I-21 were CO<sub>2</sub>, NH<sub>3</sub> and H<sub>2</sub>O. The mass spectrum for the evolved CO<sub>2</sub>, NH<sub>3</sub> and water from sample I-21 are shown in Figures 5.12, 5.13 and 5.14.

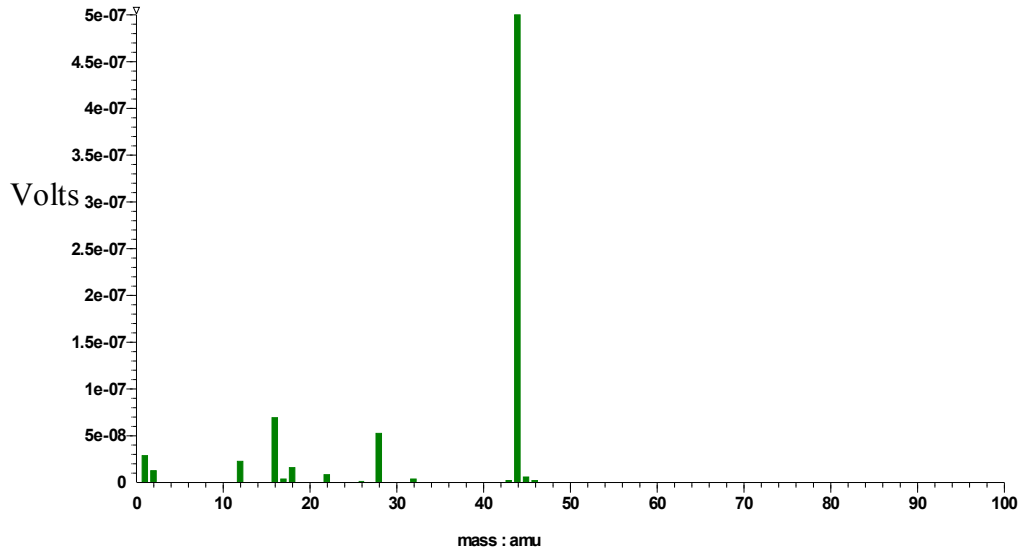


**Figure 5.12** The mass spectrum for the CO<sub>2</sub> evolved from sample I-21 in TVA

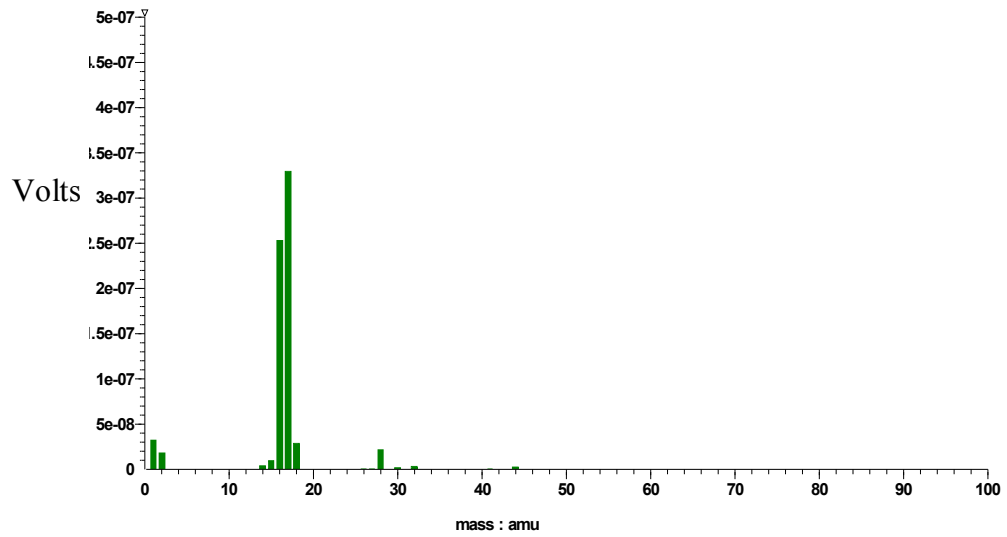


**Figure 5.13** The mass spectrum for the NH<sub>3</sub> evolved from sample I-21 in TVA

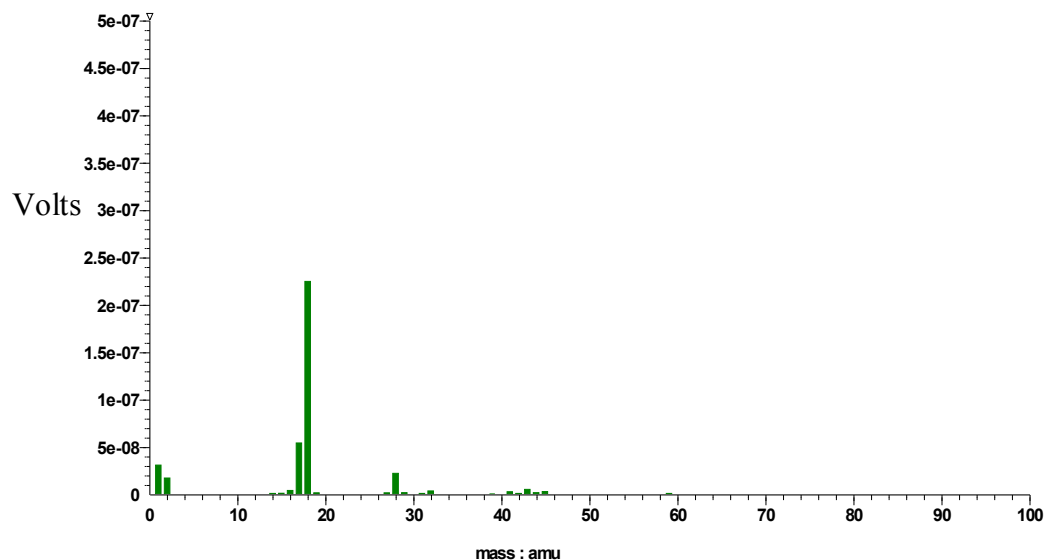


**Figure 5.14 the mass spectrum for water evolved from sample I-21 in TVA**

It should be noted that there was no visible cold-ring fraction in the tube. However, the area was swabbed with chloroform and analysed using FTIR spectroscopy in order to confirm the absence of a cold-ring fraction. The FTIR spectrum showed no peaks of interest which confirms that no higher molar mass species were evolved from this sample.

### 5.3.1.3 Summary

It can be observed from the TVA results of sample I-21 that a significant fraction of the total volatiles evolved were non-condensable products which are identified as  $N_2$ . However, the results obtained from the volatiles and liquid nitrogen-condensable fractions have indicated that there is a significant amount of water with a small quantity of  $CO_2$  and  $NH_3$ . The observation of carbon dioxide and water may possibly be attributed to background species. However, the onset of volatile evolution commences at around  $650^\circ C$ .

### 5.3.2 TVA of sample I-26

The TVA of sample I-26 was conducted according to the general procedure that described in section 5.3.1. However, a significant level of volatile off-gassing was observed under vacuum over the temperature range of the study. These volatiles were sequestered in a liquid N<sub>2</sub> trap for subsequent characterisation. A significant fraction of the total evolved volatiles were, however, non-condensable products.

#### 5.3.2.1 Non-condensable product analysis

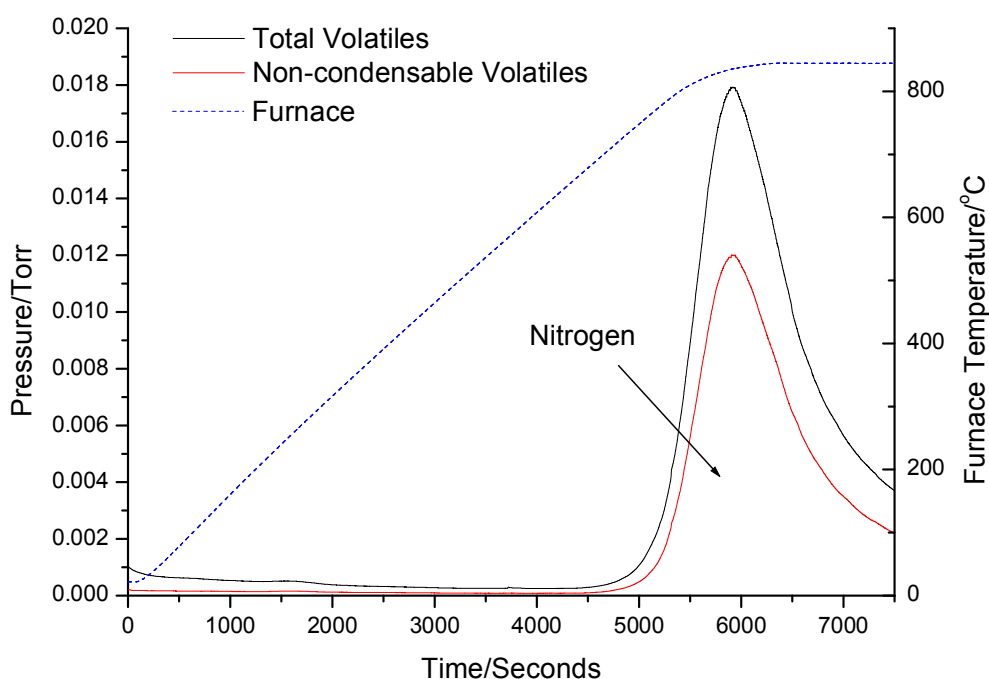


**Figure 5.15 TVA plot of the degradation of sample I-26 showing non-condensable volatile product in the liquid N<sub>2</sub> trap**

It can be seen from Figure 5.15 that the sample I-26 evolves significant quantities of volatile material, which start to be eliminated at around 700°C. It is also clear that a large proportion of the total volatile evolution has been determined to be nitrogen by online mass spectrometry (peak with mass of 28). It is worth noting that the low temperature evolution of H<sub>2</sub>O and H<sub>2</sub> which was apparent in sample I-21 is absent in this sample. Figure 5.16 presents the mass spectrum of the evolved nitrogen from the sample.

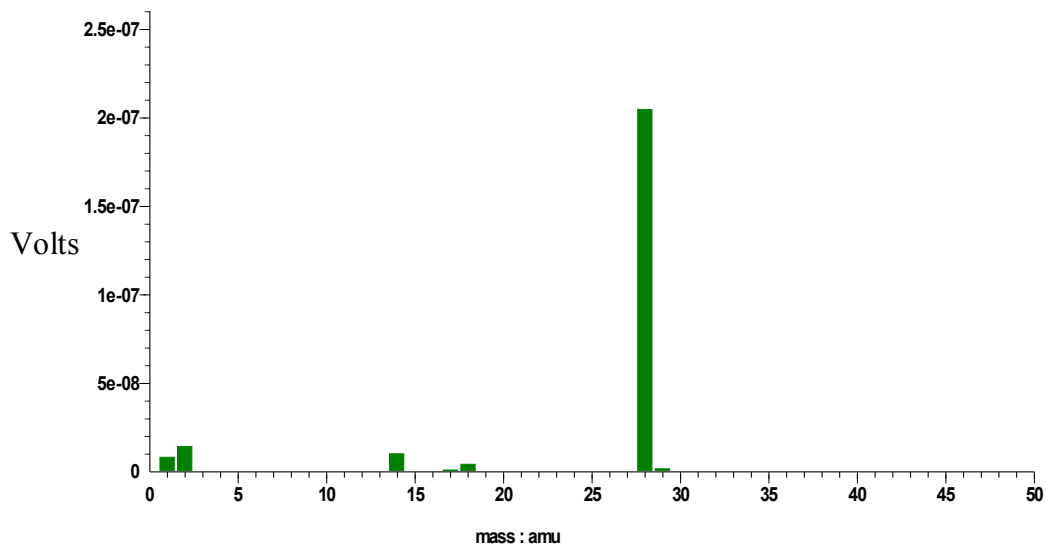


**Figure 5.16** the mass spectrum for the nitrogen evolved from sample I-26 in TVA

### 5.3.2.2 Condensable products analysis

Condensable products of sample I-26 were collected and characterised similarly as described in section 5.3.1.2. Figure 5.17 presents the sub-ambient thermal volatilisation analysis of volatiles and components evolved by heating the liquid N<sub>2</sub> trap.

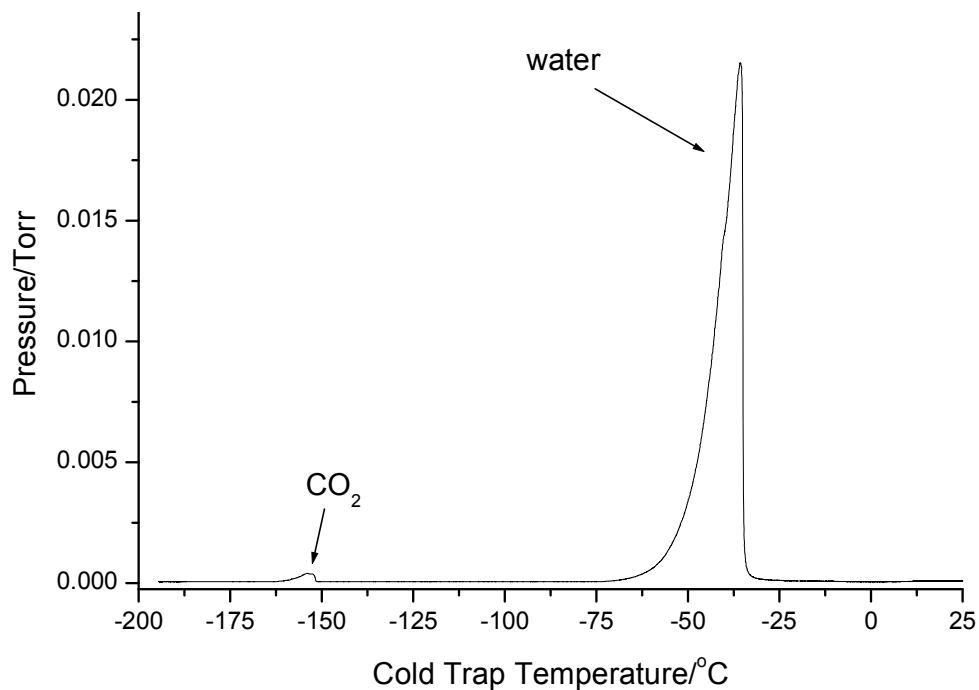


**Figure 5.17** Sub-ambient thermal volatilisation analysis of volatiles and components evolved by heating the liquid N<sub>2</sub> trap

Unlike sample I-22, no  $\text{NH}_3$  formation was observed for sample I-22. GCMS analysis conducted on the water fraction confirmed the absence of higher components. Mass spectra of the  $\text{CO}_2$  and  $\text{H}_2\text{O}$  components are presented in Figures 5.18 and 5.19.

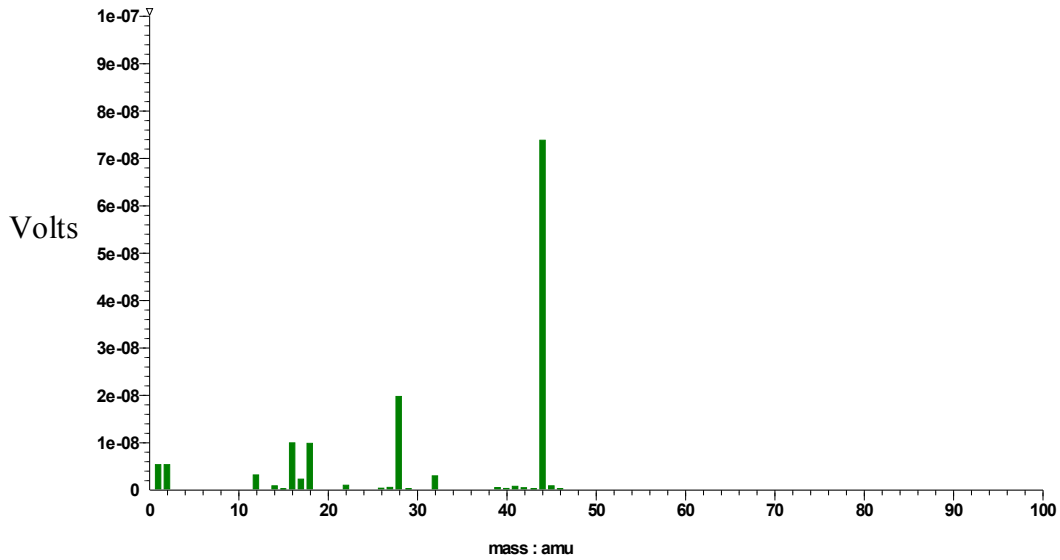


**Figure 5.18** The mass spectrum for the carbon dioxide evolved from sample I-26 in TVA

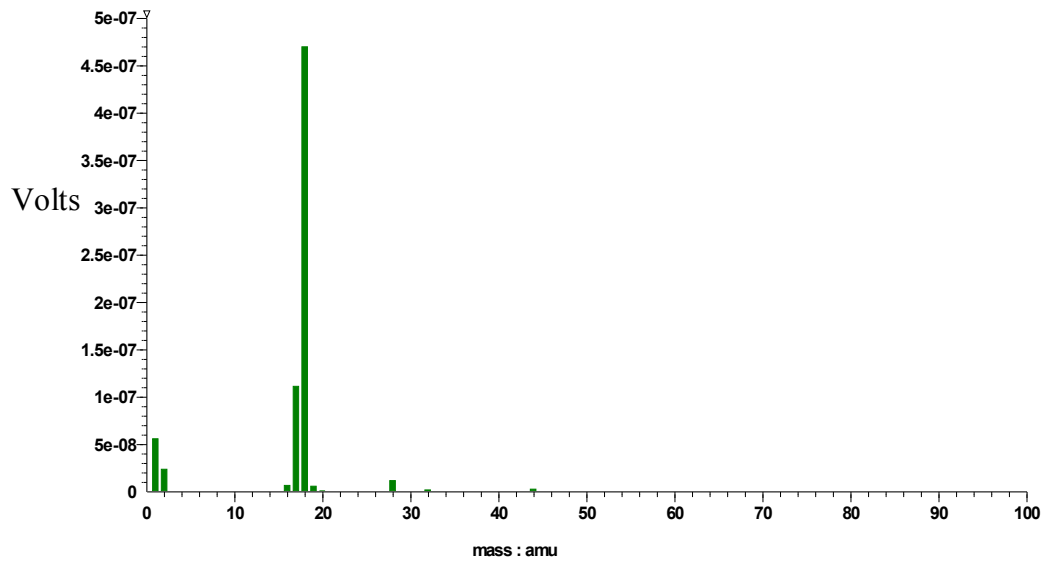


**Figure 5.19** The mass spectrum for the water evolved from sample I-26 in TVA

It should be noted that there was no visible cold-ring fraction in the tube. The area of cold-ring fraction was swabbed with chloroform and analysed using FTIR spectroscopy as described in previous sample. The results obtained from FTIR spectrum showed no peaks of interest which confirms that no higher molar mass species were evolved from this sample.

### **5.3.2.3 Summary**

It can be observed from the TVA results a significant fraction of the total volatiles evolved were non-condensable products which are identified as N<sub>2</sub>. However, the results obtained from the volatiles and liquid nitrogen-condensable fractions have indicated that there is a significant amount of water with a small quantity of CO<sub>2</sub>. The observation of carbon dioxide and water may possibly be attributed to background species. However, the onset of volatile evolution commences at around 700°C.

### **5.3.3 TVA of sample E-23**

The TVA of sample E-23 was conducted according to the general procedure that was described in section 5.3.1. Again, a significant level of volatile off-gassing was observed under vacuum over the temperature range of study. These volatiles were sequestered in a liquid N<sub>2</sub> trap for subsequent characterisation. A significant fraction of the total evolved volatiles were however, non-condensable products.

### 5.3.3.1 Non-condensable product analysis

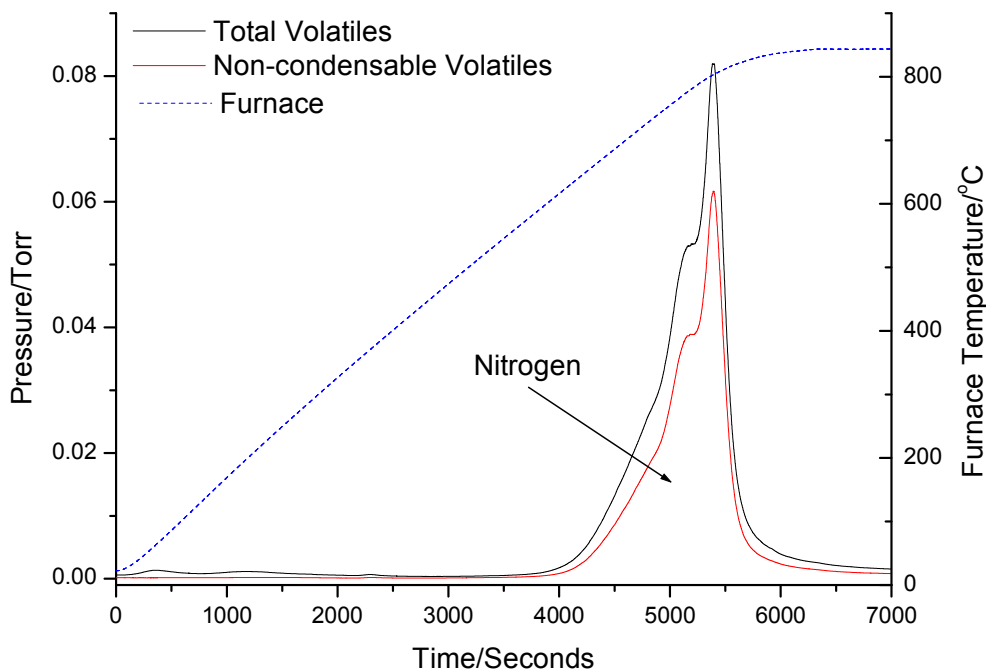


**Figure 5.20 TVA plot of the degradation of sample E-23 showing non-condensable volatile product in the liquid N<sub>2</sub> trap**

It can be seen from Figure 5.20 that the sample E-23 evolves significant quantities of volatile material, which start to be lost at around 610°C. The large proportion of the total volatile evolution which was determined to be nitrogen by online mass spectrometry. Again, the lower temperature peaks observed for sample I-21, and described earlier, were absent for this sample. Figure 5.21 presents the mass spectrum of the evolved nitrogen from the sample. It is also worth noting that the observed curve shape for this sample is different from that for samples I-21 and I-26, exhibiting shoulders on the main peak. This may indicate that different processes of volatile evolution are occurring in this sample. It can be also observed that the evolved volatiles appear over a narrower temperature/time range with the peak max occurring at a lower temperature for the E-23 sample. Figure 5.21 presents the mass spectrum of evolved nitrogen from the sample.

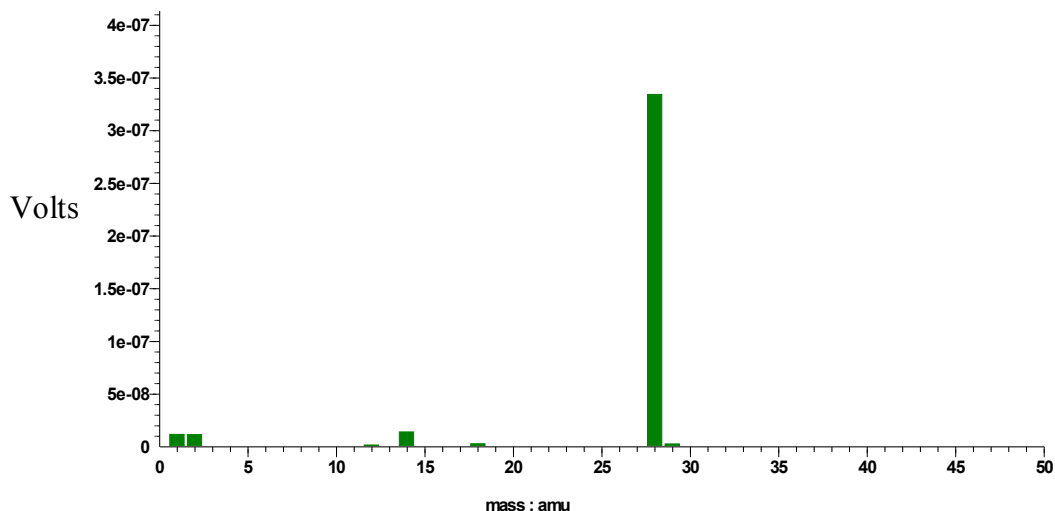


**Figure 5.21** The mass spectrum for the nitrogen evolved from sample E-23 in TVA

### 5.3.3.2 Condensable products analysis

Condensable products of sample E-23 were collected and characterised similarly as described in section 5.3.1.2. Figure 5.22 presents the sub-ambient thermal volatilisation analysis of volatiles and components evolved by heating the liquid N<sub>2</sub> trap.

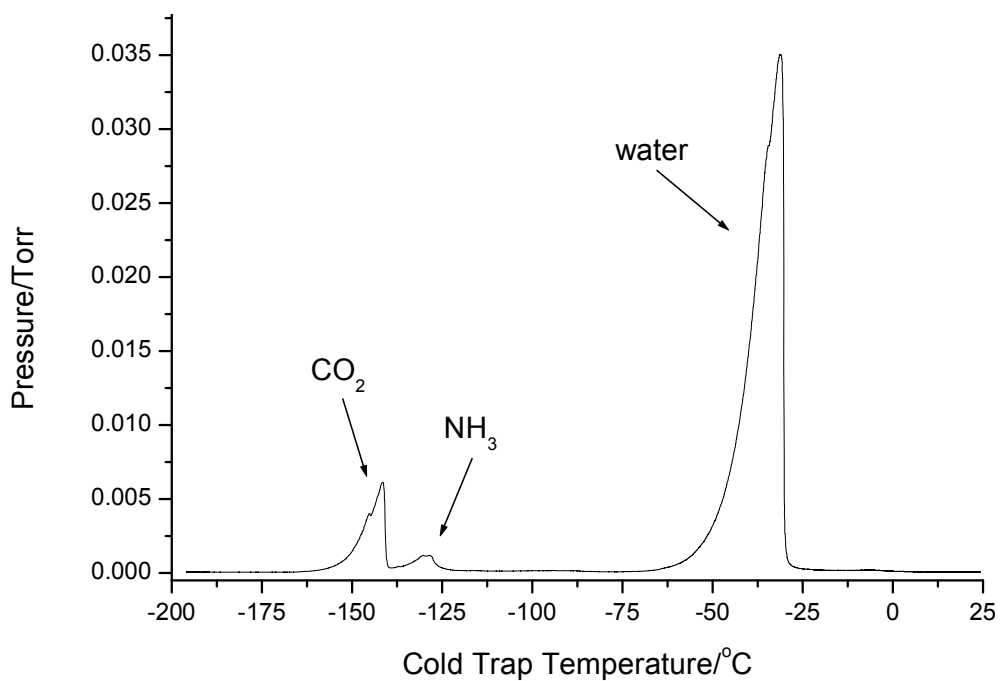


**Figure 5.22** Sub-ambient thermal volatilisation analysis of volatiles and components evolved by heating the liquid N<sub>2</sub> trap

It can be seen from Figure 5.22 that the collected volatiles consist primarily of water with small quantities of CO<sub>2</sub> and NH<sub>3</sub> also being present. The CO<sub>2</sub> may be background level. It can be also observed that no higher boiling species were apparent on the sub-ambient thermal volatilisation analysis trace. However, the fraction from -75°C to room temperature (containing the water fraction) was collected and analysed by GC-MS to confirm if there were any additional species masked by the water. The GC-MS results showed a spectrum resembling the chloroform blank which confirms that the only volatiles evolved from sample E-23 were CO<sub>2</sub>, NH<sub>3</sub> and water. The mass spectrum for the evolved CO<sub>2</sub>, NH<sub>3</sub> and water from sample E-23 are shown in Figures 5.23, 5.24 and 5.25.

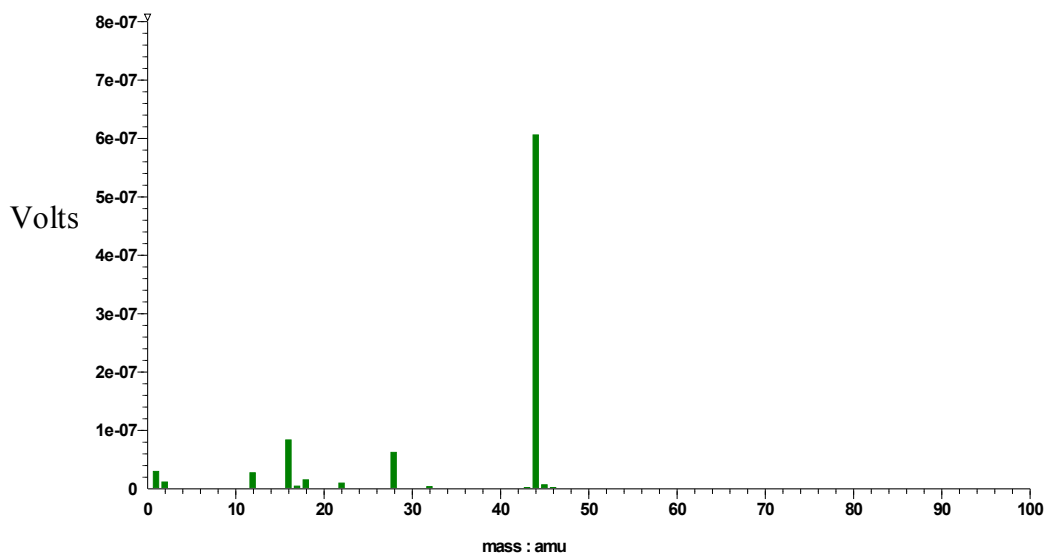


**Figure 5.23 The mass spectrum for the CO<sub>2</sub> evolved from sample E-23 in TVA**

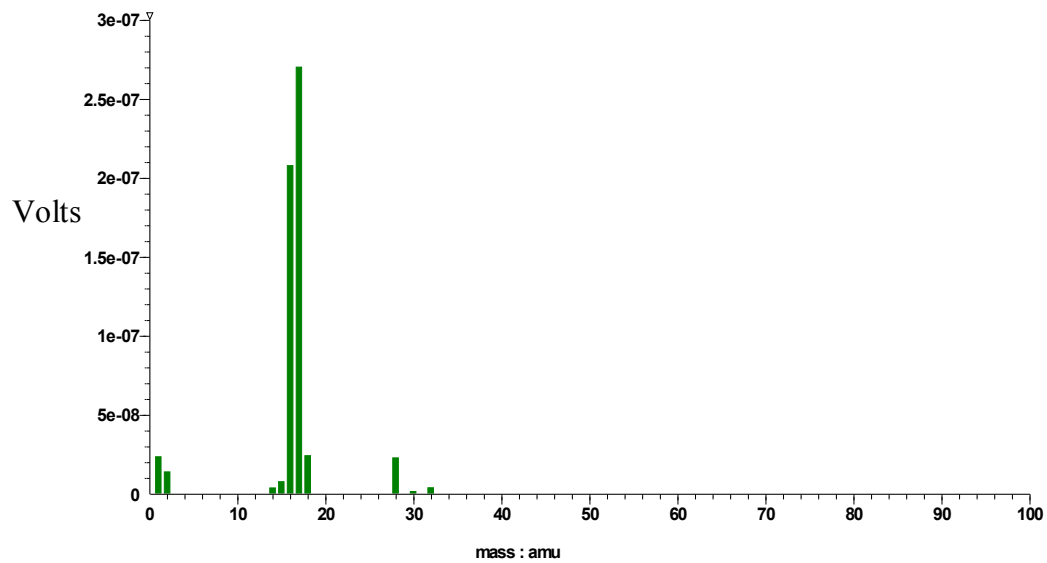


**Figure 5.24** The mass spectrum for the NH<sub>3</sub> evolved from sample E-23 in TVA

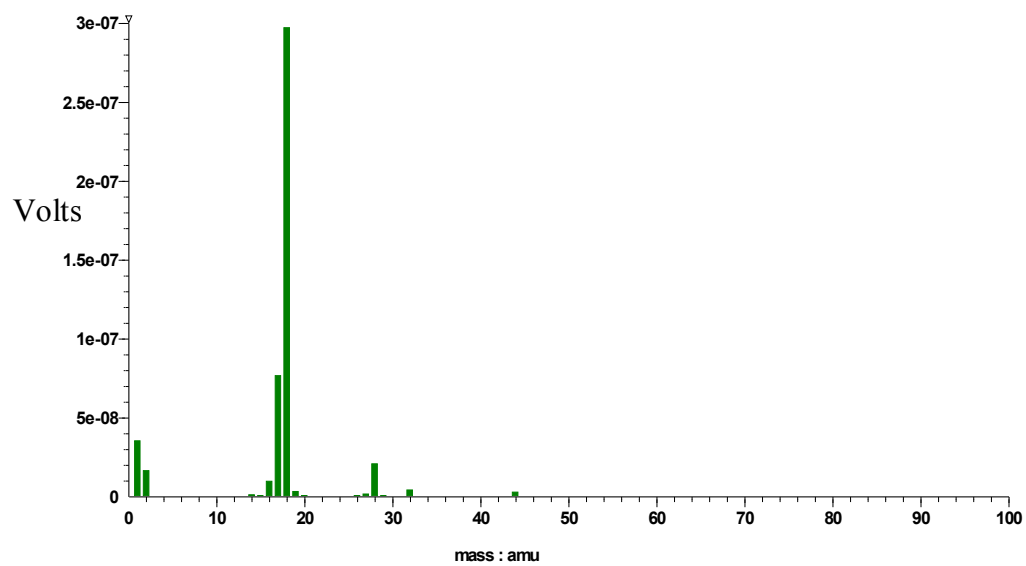


**Figure 5.25** The mass spectrum for the water evolved from sample E-23 in TVA

### 5.3.3.3 Summary

It can be observed from the TVA results of the samples that a significant fraction of the total volatiles evolved were non-condensable products which were identified as N<sub>2</sub>. However, the results obtained from the volatiles and liquid nitrogen-condensable fractions have indicated that there is a significant amount of water with a small quantity of CO<sub>2</sub> and NH<sub>3</sub> in some case. The observation of carbon dioxide and water may possibly be ascribed to background species. The nature of the elimination of N<sub>2</sub> seems to be sample dependent, with that from sample E-23 occurring over a narrower temperature range and possibly in more stages when compared to other samples.

### 5.3.4 C H N analysis

Table 5.4 presents the carbon and nitrogen content pre-TVA and post- TVA and assumed stoichiometry of samples I-21, I-26 and E-23. It can be observed from this table that sample I-21, which appeared to be a pure  $\gamma$ -Mo<sub>2</sub>N phase as discussed in Chapter 3, lost around 30% of its nitrogen content in the TVA procedure. It can be also observed that the nitrogen content of samples I-26 and E-23, which possibly comprised carbonitride as discussed in Chapters 3 and 4, completely lost their nitrogen. It is worth noting that the carbon content of sample I-26 seems to be stable, whereas only 55% of the original carbon content remained after TVA in the case of sample E-23.

**Table 5.4 Carbon and nitrogen content of samples I-21, I-26 and E-23 in pre-reaction and post- reaction in TVA and assumed stoichiometry**

sample code	Pre-reaction		Post-reaction		Assumed stoichiometry	
	C (wt. %)	N (wt. %)	C (wt. %)	N (wt. %)	Pre-reaction	Post-reaction
I-21	0	4.60	0	3.19	Mo N <sub>0.33</sub>	Mo N <sub>0.23</sub>
I-26	2.37	2.39	2.46	0	Mo C <sub>0.20</sub> N <sub>0.17</sub>	Mo C <sub>0.21</sub>
E-23	2.62	2.62	1.44	0	Mo C <sub>0.22</sub> N <sub>0.19</sub>	Mo C <sub>0.12</sub>

### 5.3.5 Summary

In this section investigation of various materials, which corresponded to molybdenum nitride and molybdenum carbonitride systems, by TVA was described. TVA involves heating the samples from room temperature to 850°C under vacuum, and involves detailed analysis of the evolved species from the sample which are collected as various fractions. This technique is more generally used in polymer degradation studies [61].

The TVA results indicated that all samples evolved similar products which consist of a high level of nitrogen along with small quantities of water and carbon dioxide. The only notable difference in the products evolved was ammonia which was evolved from samples I-22 and E-23. The evolved NH<sub>3</sub> most probably original from NH<sub>x</sub> species deposited on the sample surfaces during their preparation. The observation of ammonia in this study seems to be consistent with the temperature programmed studies of lattice nitrogen reactivity. It can be also observed that there is a significant difference between the onset temperatures for N<sub>2</sub> elimination of all samples, where they were around 650°C and 700°C respectively for samples I-22 and I-26, and around 610°C in the case of sample E-23. In this respect, the order of the structural stability of these samples, derived from this study was as follows: I-26 > I-22 > E-23.

The significant loss of carbon from sample E-23, as also observed in the Ar only treatment experiment, is worthy of note. It does not immediately appear that there is an enhanced evolution of CO<sub>2</sub> for this sample and no other C-containing products were observed. Further investigation of this aspect is warranted.

## 5.4 Thermogravimetric Analysis (TGA)

In this study, different batches of precursor E-23 (designated E-23-A and E-23-B) were investigated using TGA equipped with mass spectrometric evolved gas analysis under Ar/H<sub>2</sub> 1:3, as previously described in the experimental chapter. It should be noted that only approximately 0.025g of both precursors were studied due to the small size of pan used in the apparatus. This technique was applied in order to detect and characterise the products evolved from heated materials, and also to give an overview of the possibility for producing carbon/nitrogen containing products from the investigated material.

### 5.4.1 TGA profile

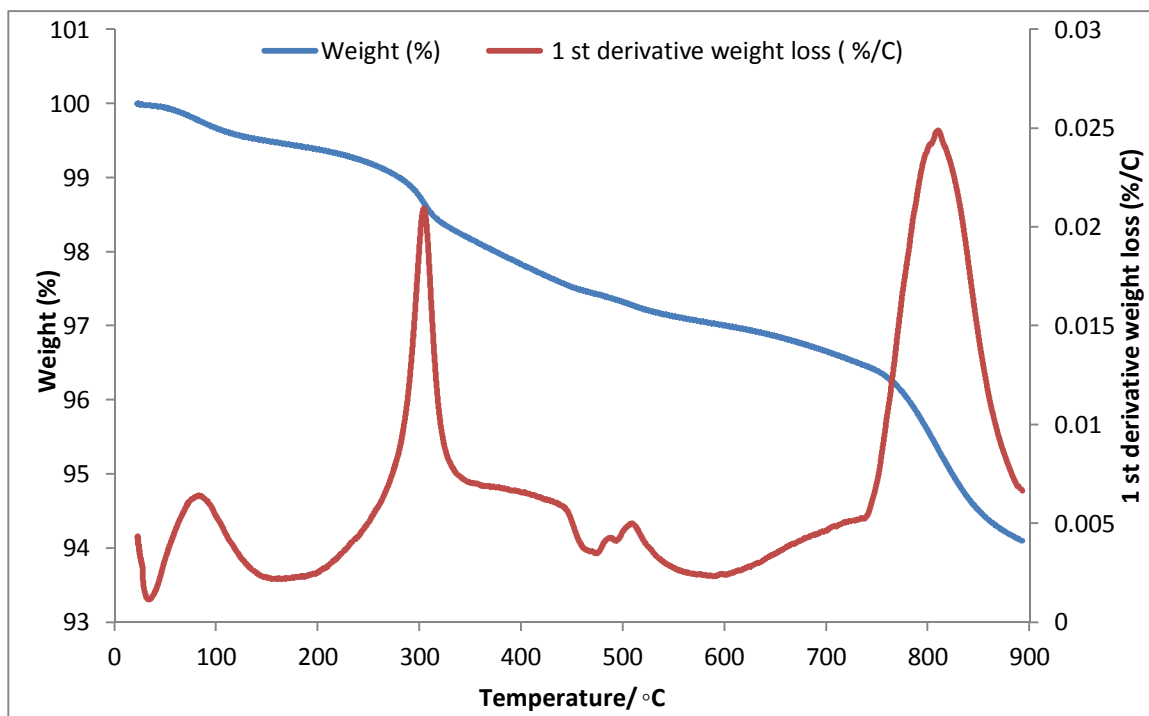


Figure 5.26 TGA profile of sample E-23-A under Ar/H<sub>2</sub> 1:3

Figure 5.26 presents the TGA profile of sample E-23-A. It can be observed from this profile that the total weight loss of this sample is around 6% under the conditions of the experiment. It should be noted that around 2.5% weight loss occurred between 730°C and the final temperature (900°C). It can be also observed that there are five clear weight loss

events at 70°C, 300°C, 480°C, 516°C and 805°C. Since, sample E-23-B showed a similar TGA profile and mass spectrometry results, only TGA profiles corresponding to sample E-23-A are reported.

#### 5.4.2 Mass spectrometry results

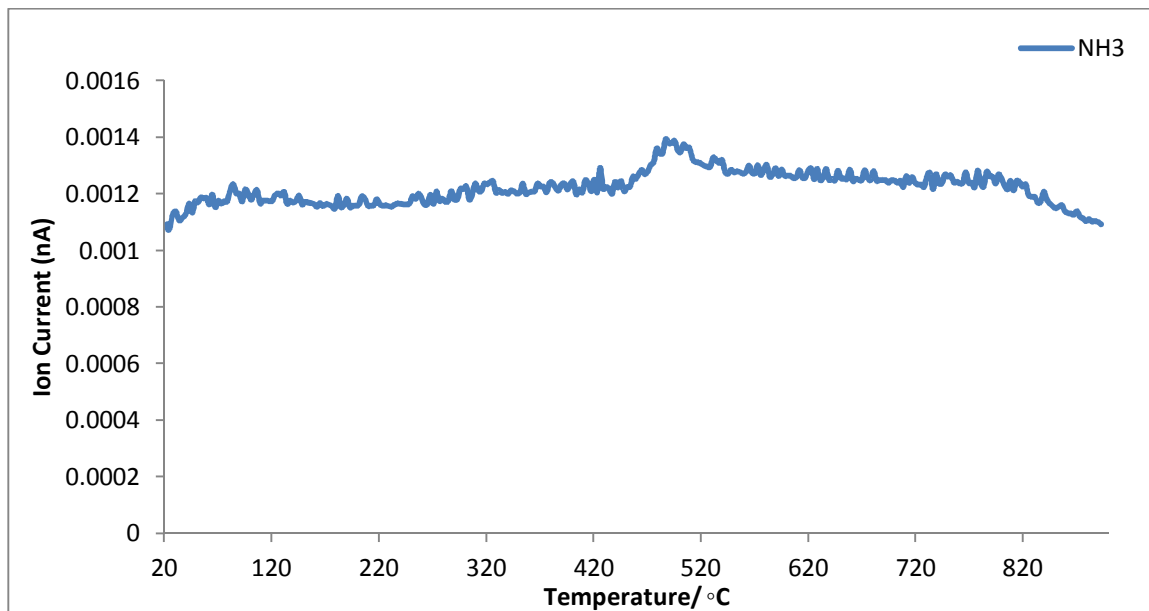


Figure 5.27 the mass spectrum for NH<sub>3</sub> evolved from sample E-23-A in TGA

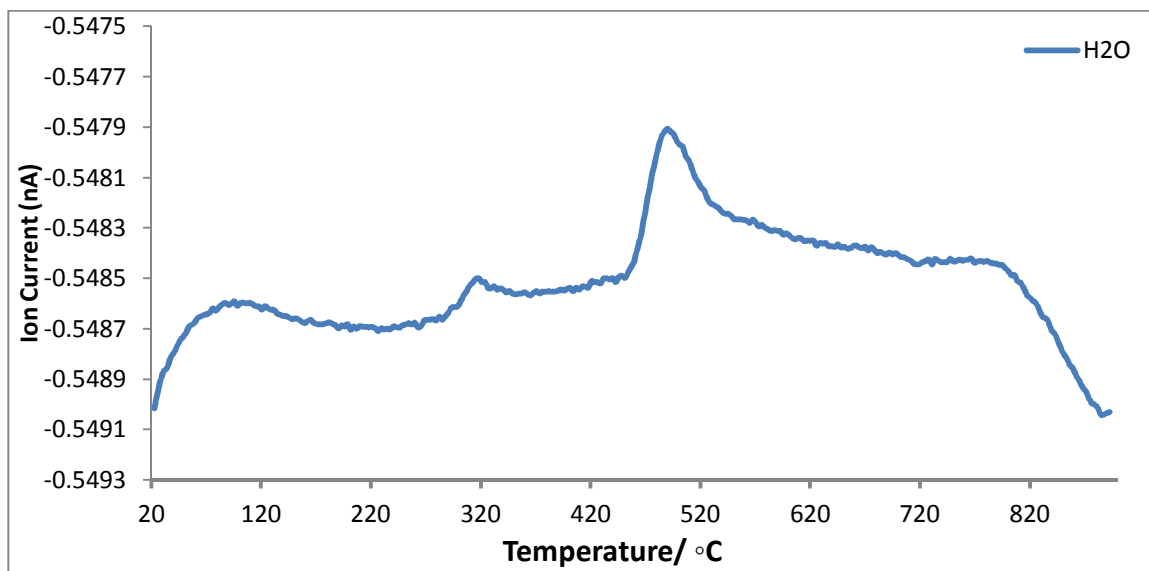
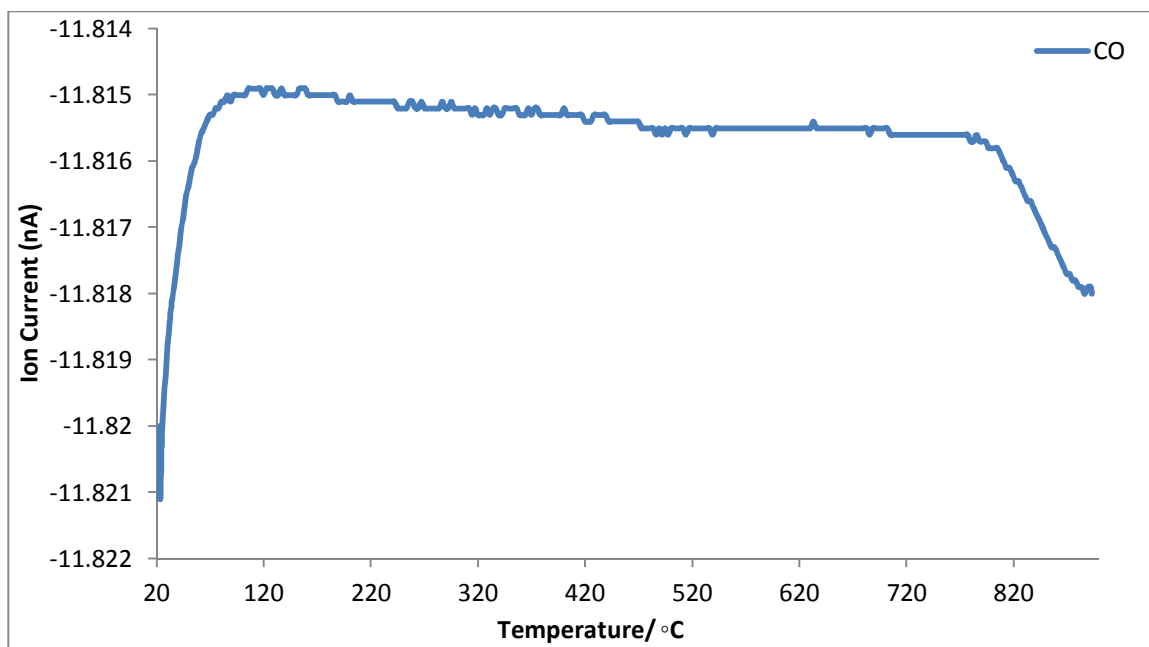


Figure 5.28 the mass spectrum for H<sub>2</sub>O evolved from sample E-23-A in TGA



**Figure 5.29 the mass spectrum for CO evolved from sample E-23-A in TGA**

The above figures show mass spectrometry data of products evolved. The results obtained from the weight loss are in relatively good agreement with the evolution of  $\text{NH}_3$  and water shown in the mass spectrometry data. It can be concluded that the weight loss events occurring at  $70^\circ\text{C}$ ,  $300^\circ\text{C}$  and  $480^\circ\text{C}$  corresponded to the evolution of water which is confirmed by mass spectrometry data.  $\text{NH}_3$  was apparently evolved at a similar temperature to water at around  $480^\circ\text{C}$  and may indicate that hydrolytic processes are important in its generation.

### 5.4.3 C H N results

Table 5.5 presents the carbon and nitrogen content pre-TGA and post- TGA and assumed stoichiometry of the samples. This table indicates that the nitrogen content of both samples is totally lost whereas the carbon content is seemed to be relatively stable. This provides independent confirmation of the higher reactivity of lattice N compared to lattice C, as observed elsewhere in this chapter.

**Table 5.5 Carbon and nitrogen content of samples E-23-A and E-23-B in pre-reaction and post- reaction in TGA and assumed stoichiometry**

sample code	Pre-TGA		Post-TGA		Assumed stoichiometry	
	C (wt. %)	N (wt. %)	C (wt. %)	N (wt. %)	Pre-reaction	Post-reaction
E- 23-A	3.27	2.81	3.26	0	Mo C <sub>0.28</sub> N <sub>0.20</sub>	Mo C <sub>0.27</sub>
E- 23-B	2.62	2.62	3.26	0	Mo C <sub>0.22</sub> N <sub>0.19</sub>	Mo C <sub>0.27</sub>

### 5.4.4 Summary

In this study, sample E-23 was selected for further investigation by TGA due to the higher reducibility of the nitride observed in the previous techniques compared with that observed in the other samples. The results indicated that a small quantity of ammonia was generated at ca. 480°C. However, although there is no evidence of nitrogen or ammonia evolution in the final stage of heating, 2.5% mass loss occurred beyond 750°C which could not be attributed to specific products.

## 5.5 Conclusion

Various techniques were applied to investigate the reactivity and stability of lattice nitrogen and carbon in various different materials derived from single-source routes. It is well known that the nitrogen can be removed from the materials at high temperature under a H<sub>2</sub> atmosphere. In this study, there is an effect of using different precursors on the percentage of nitrogen lost, where the samples derived from precursor E is lost a much higher proportion of nitrogen than those generated from precursor I. It was also found that the lattice carbon seemed to be more stable than the nitrogen. Although the lattice carbon is more stable than nitrogen, it is lost upon reaction under an Ar atmosphere when treated up to 900 °C, where the elimination of carbon from system occurs via an unknown form.

TVA results have demonstrated that all samples evolved similar species which consist of high levels of nitrogen with small quantities of H<sub>2</sub>O. It is interesting to note that the carbon content was stable in all samples except sample E-23 where the route to its loss still needs to be identified.

In terms of the TGA technique which was applied for studying the decomposition of sample E-23 under a H<sub>2</sub>/Ar 3:1 atmosphere, the results indicated that the sample lost all nitrogen content during the procedure whereas the carbon content exhibited good stability.

## Chapter 6: Conclusion

In this thesis, various materials have been investigated to synthesise molybdenum nitride, carbide and oxycarbonitride by single source routes under various gas atmospheres. The main precursors used for this study were hexamethylenetetramine molybdate and ethylenediammonium molybdate. Thermal decomposition of both precursors produces different materials. However, the obtained results suggest that gas atmosphere, final temperature and flow rate are important parameters. The decomposition of both precursors under  $H_2/N_2$  in a ratio of 3:1 or 1:3 leads to production of molybdenum carbide-like products, and molybdenum metal and molybdenum carbide-like products can also be obtained from the thermal decomposition of both precursors under Ar/ $H_2$  1:3. In contrast, the decomposition of hexamethylenetetramine molybdate under  $N_2$  or Ar leads to production of  $\gamma$ - $Mo_2N$ , whereas impure phases were obtained from the decomposition of ethylenediammonium molybdate where molybdenum carbide-like compounds, molybdenum metal and molybdenum dioxide were obtained under an Ar atmosphere while gamma molybdenum nitride, molybdenum carbide like compounds and molybdenum dioxide were obtained under an  $N_2$  atmosphere. The results from this study have confirmed that a precursor rich in carbon and nitrogen is very important to generate molybdenum carbide or nitride by applying different reaction atmospheres.

The reactivity and stability of lattice nitrogen and carbon of some selected materials that obtained from both precursors have been investigated using various techniques. The results suggest that the elimination of carbon and nitrogen from the lattice was strongly dependent on the gas atmosphere and temperature applied. The results have confirmed the lattice N to be the more reactive species, and also the reactivity of N species in molybdenum carbonitrides is higher than that in molybdenum nitride. It can be concluded that generation of nitrogen containing organic products such as amines upon direct hydrogenation using these materials would be a significant challenge due to the apparent differences in reactivity of the C and N species. Furthermore, it was found that the reactivity of N and C species is a function of phase composition and single-source precursor.

## **Future work**

Future work should involve the preparation of  $\text{MoC}_x\text{NyO}_z$  using different nitrogen and carbon containing compounds and be directed towards understanding the mechanism of formation different compositions of molybdenum (oxy) carbonitrides, so that designed synthesis of desired compositions with specific catalytic properties could be achieved.

## References

- [1] E. Furimsky, *Applied Catalysis A: General*, 240 (2003) 1-28.
- [2] C. Kral, W. Lengauer, D. Rafaja, P. Ettmayer, *Journal of Alloys and Compounds*, 265 (1998) 215-233.
- [3] A.-M. Alexander, J.S.J. Hargreaves, *Chemical Society Reviews*, 39 (2010) 4388-4401.
- [4] G. Vitale, M.L. Frauwallner, E. Hernandez, C.E. Scott, P. Pereira-Almao, *Applied Catalysis A: General*, (2011).
- [5] C.C. Yu, S. Ramanathan, S.T. Oyama, *Journal of Catalysis*, 173 (1998) 1-9.
- [6] S. Wang, X. Wang, Z. Zhang, Y. Qian, *Journal of Materials Science*, 38 (2003) 3473-3478.
- [7] P. Liu, J.A. Rodriguez, *The Journal of Chemical Physics*, 120 (2004) 5414.
- [8] J.C. Grossman, A. Mizel, M. Côté, M.L. Cohen, S.G. Louie, *Physical Review B*, 60 (1999) 6343-6347.
- [9] J.S. Lee, *Metal Carbides*, in: *Encyclopedia of Catalysis*, John Wiley & Sons, Inc., 2002.
- [10] J.S. Lee, D.J. Ham, *Metal Nitrides*, in: *Encyclopedia of Catalysis*, John Wiley & Sons, Inc., 2002.
- [11] L.I. Johansson, *Surface Science Reports*, 21 (1995) 177-250.
- [12] S.T. Oyama, *The chemistry of Transition Metal Carbides and Nitrides*, First ed., Blackie Academic & Professional, Glasgow, 1996.
- [13] J.G. Chen, *Chemical Reviews*, 96 (1996) 1477-1498.
- [14] S.T. Oyama, *Journal of Solid State Chemistry*, 96 (1992) 442-445.
- [15] P. Ettmayer, *Annual Review of Materials Science*, 19 (1989) 145-164.
- [16] L. Volpe, M. Boudart, *Journal of Solid State Chemistry*, 59 (1985) 332-347.
- [17] S.T. Oyama, J.C. Schlatter, J.E. Metcalfe III, J.M. Lambert Jr, *Industrial & Engineering Chemistry Research*, 27 (1988) 1639-1648.
- [18] R. Marchand, F. Tessier, F. J. DiSalvo, *Journal of Materials Chemistry*, 9 (1999) 297-304.
- [19] A.G. Cairns, J.G. Gallagher, J.S.J. Hargreaves, D. McKay, E. Morrison, J.L. Rico, K. Wilson, *Journal of Alloys and Compounds*, 479 (2009) 851-854.
- [20] S.T. Oyama, *Catalysis Today*, 15 (1992) 179-200.
- [21] R. Levy, M. Boudart, *Science*, 181 (1973) 547-549.
- [22] J.S. Lee, S.T. Oyama, M. Boudart, *Journal of Catalysis*, 106 (1987) 125-133.
- [23] H. He, H. Dai, K. Ngan, C. Au, *Catalysis Letters*, 71 (2001) 147-153.
- [24] S. Li, W.B. Kim, J.S. Lee, *Chemistry of Materials*, 10 (1998) 1853-1862.
- [25] J.S.J. Hargreaves, D. McKay, *Catalysis*, 19 (2006) 84-108.
- [26] D. McKay, J.S.J. Hargreaves, J.L. Rico, J.L. Rivera, X.L. Sun, *Journal of Solid State Chemistry*, 181 (2008) 325-333.
- [27] L. Volpe, M. Boudart, *Journal of Solid State Chemistry*, 59 (1985) 348-356.
- [28] J.C. Schlatter, S.T. Oyama, J.E. Metcalfe III, J.M. Lambert Jr, *Industrial & Engineering Chemistry Research*, 27 (1988) 1648-1653.
- [29] S. Ramanathan, S. Oyama, *The Journal of Physical Chemistry*, 99 (1995) 16365-16372.
- [30] E. Markel, J. van Zee, *Journal of Catalysis*, 126 (1990) 643-657.

- [31] H.M. Wang, X.H. Wang, M.H. Zhang, X.Y. Du, W. Li, K.Y. Tao, *Chemistry of Materials*, 19 (2007) 1801-1807.
- [32] Z.-Q. Wang, Z.-B. Zhang, M.-H. Zhang, *Dalton Transactions*, 40 (2011) 1098.
- [33] E. Furimsky, *Applied Catalysis A: General*, 199 (2000) 147-190.
- [34] K.-I. Aika, A. Ozaki, *J. Catal.*, 14 (1969) 311-321.
- [35] S.T. Oyama, *Transition Metal Carbides, Nitrides, and Phosphides. Handbook of Heterogeneous Catalysis.*, 2008.
- [36] L. Leclercq, K. Imura, S. Yoshida, T. Barbee, M. Boudart, *Synthesis of New Catalytic Materials: Metal Carbides of the Group VI B Elements*, in: P.G.P.J. B. Delmon, G. Poncelet (Eds.) *Studies in Surface Science and Catalysis*, Elsevier, 1979, pp. 627-639.
- [37] A. Griboval-Constant, J.M. Giraudon, G. Leclercq, L. Leclercq, *Applied Catalysis A: General*, 260 (2004) 35-45.
- [38] I. Kojima, E. Miyazaki, *Journal of Catalysis*, 89 (1984) 168-171.
- [39] J.G. Chen, B. Frühberger, *Surface Science*, 367 (1996) L102-L110.
- [40] Y. Li, Y. Fan, J. He, B. Xu, H. Yang, J. Miao, Y. Chen, *Chemical Engineering Journal*, 99 (2004) 213-218.
- [41] D. McKay, "Catalysis over Molybdenum Containing Nitride Materials" PhD, University of Glasgow, 2008
- [42] M. Olea, M. Florea, I. Sack, R. Prada Silvy, E.M. Gaigneaux, G.B. Marin, P. Grange, *Journal of Catalysis*, 232 (2005) 152-160.
- [43] T. Koerts, M.J.A.G. Deelen, R.A. van Santen, *Journal of Catalysis*, 138 (1992) 101-114.
- [44] S. Decker, A. Löfberg, J.M. Bastin, A. Frennet, *Catalysis Letters*, 44 (1997) 229-239.
- [45] S. Montéverdi, M.M. Bettahar, D. Bégin, F. Maréché, *Fuel Processing Technology*, 77-78 (2002) 119-124.
- [46] W. Lengauer, *Journal of Crystal Growth*, 87 (1988) 295-298.
- [47] F. Cardenas-Lizana, S. Gomez-Quero, N. Perret, L. Kiwi-Minsker, M.A. Keane, *Catalysis Science & Technology*, 1 (2011) 118-125.
- [48] A. Gomathi, A. Sundaresan, C.N.R. Rao, *Journal of Solid State Chemistry*, 180 (2007) 291-295.
- [49] J.-G. Choi, R.L. Curl, L.T. Thompson, *Journal of Catalysis*, 146 (1994) 218-227.
- [50] A.G. Cairns, J.G. Gallagher, J.S.J. Hargreaves, D. McKay, J.L. Rico, K. Wilson, *Journal of Solid State Chemistry*, 183 (2010) 613-619.
- [51] K.T. Jung, W.B. Kim, C.H. Rhee, J.S. Lee, *Chemistry of Materials*, 16 (2004) 307-314.
- [52] P. Afanasiev, *Inorganic Chemistry*, 41 (2002) 5317-5319.
- [53] L.E. McCandlish, L.W. Turaew, *Molybdenum Oxycarbonitride Compositions*, US Patent 4,426,366, 17th January 1984
- [54] D.J. Shaw, *Introduction to Colloid & Surface Chemistry*, Redwood Books, Trowbridge, Wiltshire in, 1992, pp. 131.
- [55] S. Chouzier, T. Czeri, M. Roi, C. Pichon, C. Geantet, M. Vrinat, P. Afanasiev, *Journal of Solid State Chemistry*, 184 (2011) 2668-2677.
- [56] C. Thomazeau, V. Martin, P. Afanasiev, *Applied Catalysis A: General*, 199 (2000) 61-72.
- [57] R. Kojima, K.-i. Aika, *Applied Catalysis A: General*, 219 (2001) 141-147.

- [58] Z. Wei, Q. Xin, P. Grange, B. Delmon, *Journal of Catalysis*, 168 (1997) 176-182.
- [59] P. Hugh O, *Handbook of Refractory Carbides and Nitrides*, William Andrew Publishing, Westwood, NJ, 1996, pp. 11-12
- [60] Z. Yao, Z. Lai, X. Zhang, F. Peng, H. Yu, H. Wang, *Materials Research Bulletin*, 46 (2011) 1938-1941.
- [61] L.J. France, D.C. Apperley, E.J. Ditzel, J.S.J. Hargreaves, J.P. Lewicki, J.J. Liggat, D. Todd, *Catalysis Science & Technology*, (2011) 932-939.
- [62] Z.B. Zhaobin Wei, P. Grange and B. Delmon, *Applied Surface Science*, 135 (1998) p.107.
- [63] M. Nagai, Y. Goto, A. Irisawa, S. Omi, *Journal of Catalysis*, 191 (2000) 128-137.
- [64] D. McKay, J. Hargreaves, R. Howe, *Catalysis Letters*, 112 (2006) 109-113.
- [65] S.M.L. Jenny Lee, S. M. Lee, *Handbook of Composite Reinforcements*, Paperback ed., Wiley-VCH Verlag GmbH, 1992.

## Appendix

### Appendix 1

#### Calculation of TGA analysis of precursor I



$$\frac{3.5 \text{ Mo}_2\text{N}}{\text{C}_{12}\text{H}_{44} \text{ O}_{26} \text{ N}_{12} \text{ Mo}_7} = \frac{720.44}{1443.50} = 49.90 \text{ w.t \%}$$

$$\text{Mo}_2\text{N} = 49.90 \text{ w.t \%}$$

## Appendix 2

### Calculation of TGA analysis of precursor E

Assuming that final product phase is  $\text{MoO}_{0.43}\text{C}_{0.31}\text{N}_{0.33}$  as reported by McCandlish and Co-workers [53], the mass change in for the decomposition process can be calculated for comparison with the TGA data as follows :

$$\frac{\text{MoO}_{0.43} \text{C}_{0.31} \text{N}_{0.31}}{\text{Mo N}_2 \text{O}_4 \text{H}_{10} \text{C}_2} = \frac{107.55}{220.95} = 48.68 \text{ wt. \%}$$

## Appendix 3

### XPS data for selected samples

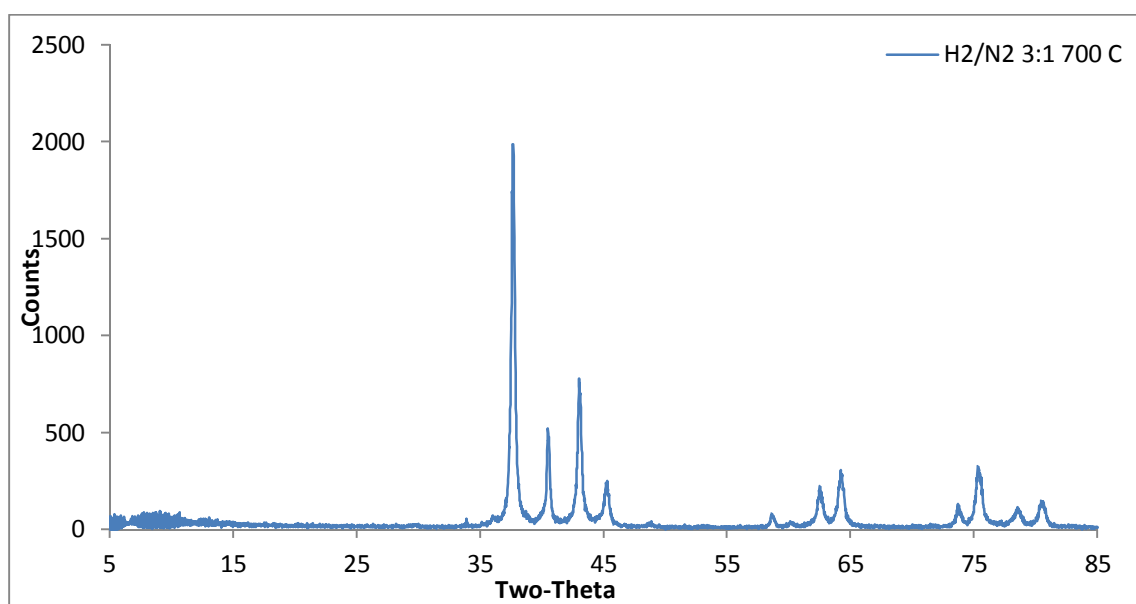
Preliminary XPS analysis has been undertaken in conjunction with the EPSRC service at Cardiff University. The aim of this was to determine whether it is possible to distinguish between nitrides, carbides, carbonitrides and oxycarbonitrides by XPS analysis. The data obtained is preliminary and further measurements and fuller analysis is necessary. Consequently, it is presented in terms of an Appendix. The XPS data for all samples was analysed using the Casa program. The curve fitting of the Mo 3d peaks was performed using linked doublets of the same full half-maximum (FWHM). The Mo 3d<sub>5/2</sub> and Mo 3d<sub>3/2</sub> peaks were separated by 3.2 eV with intensity peak ratio 3/2. For example in sample M-4, Mo 3d<sub>3/2</sub> = 231.9 eV and Mo 3d<sub>5/2</sub> = 228.7 eV, the difference between them is 3.2 eV, the intensity peak ratio 49.3/32.9 = 1.5 (3/2). The binding energy was obtained by using the C 1s binding energy as internal reference which is set at 285 eV in order to account for possible charging effects.

### Sample M-4

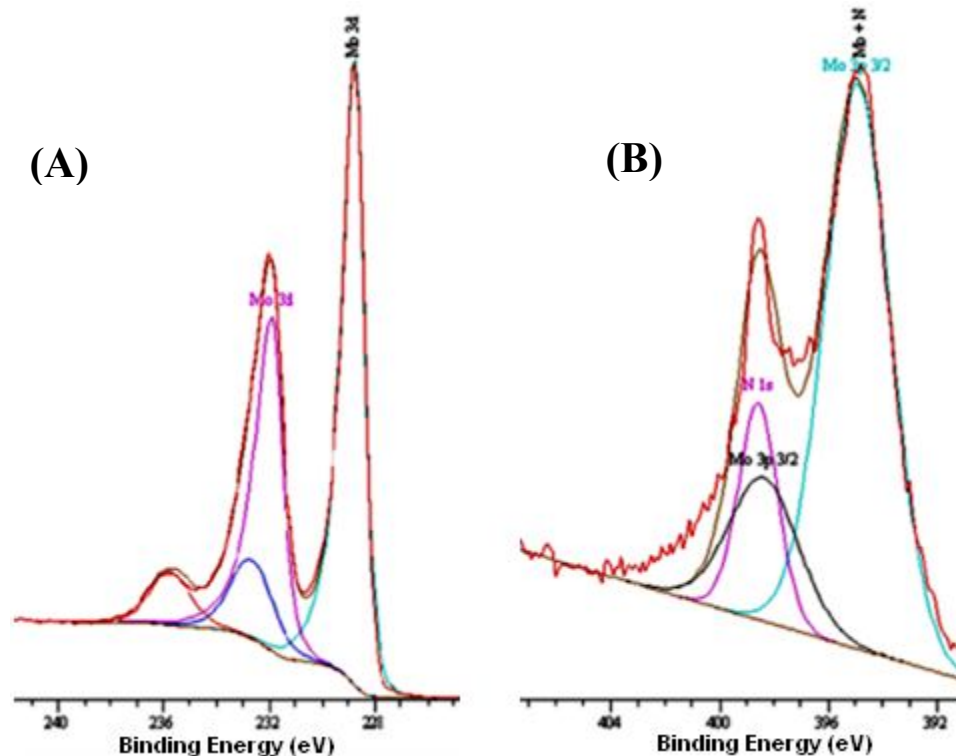
The sample M-4 was prepared by using 0.4g of MoO<sub>3</sub> under H<sub>2</sub>/N<sub>2</sub> 3:1 at 700°C, as described in the experimental chapter and in Chapter 3. The XRD pattern indicates the presence of β-Mo<sub>2</sub>N<sub>0.78</sub> and molybdenum metal phases (as shown in Figure 1). The C H N results indicated the sample contained 5.00 wt. % nitrogen and no carbon.

**Table 1: The distribution of Mo binding energies as measured by XPS for sample M-4 before and after argon ion etching**

	Posit eV	Conc. %	Posit eV	Conc. %	Posit eV	Conc. %	Posit eV	Conc. %
<b>Original</b>	231.9	32.9	228.7	49.3	235.9	7.2	232.8	10.7
<b>Sputtering 1</b>	231.9	32.5	228.5	48.8	230.1	7.5	227.1	11.2
<b>Sputtering 2</b>	231.9	40.0	228.5	60.0	0	0	0	0

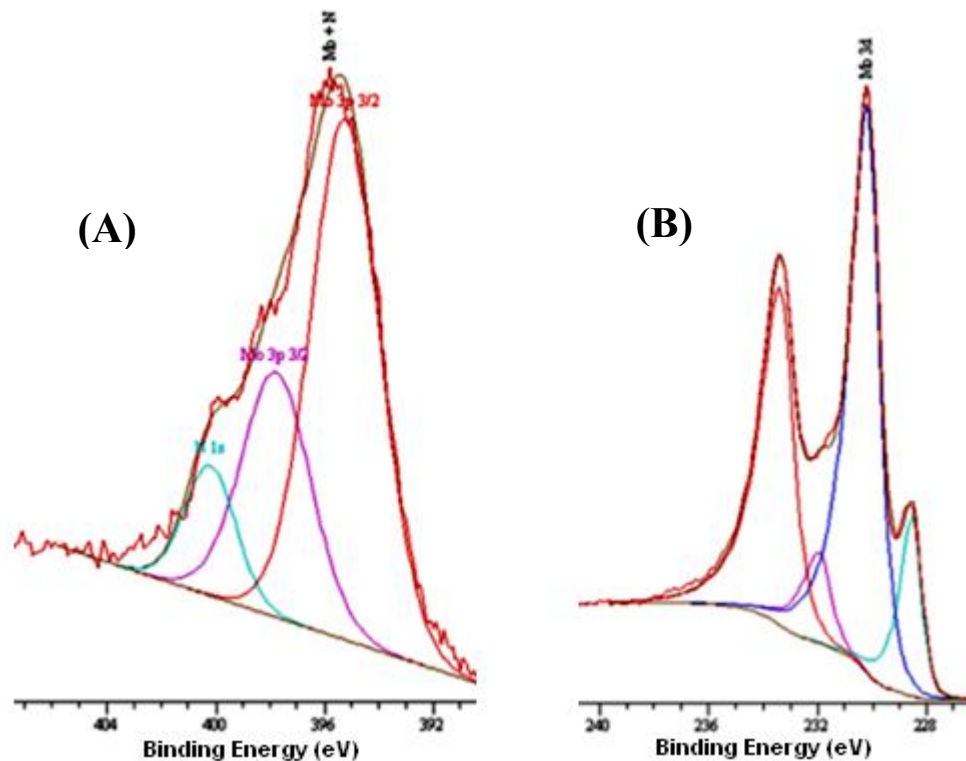


**Figure 1 XRD pattern of sample M-4**



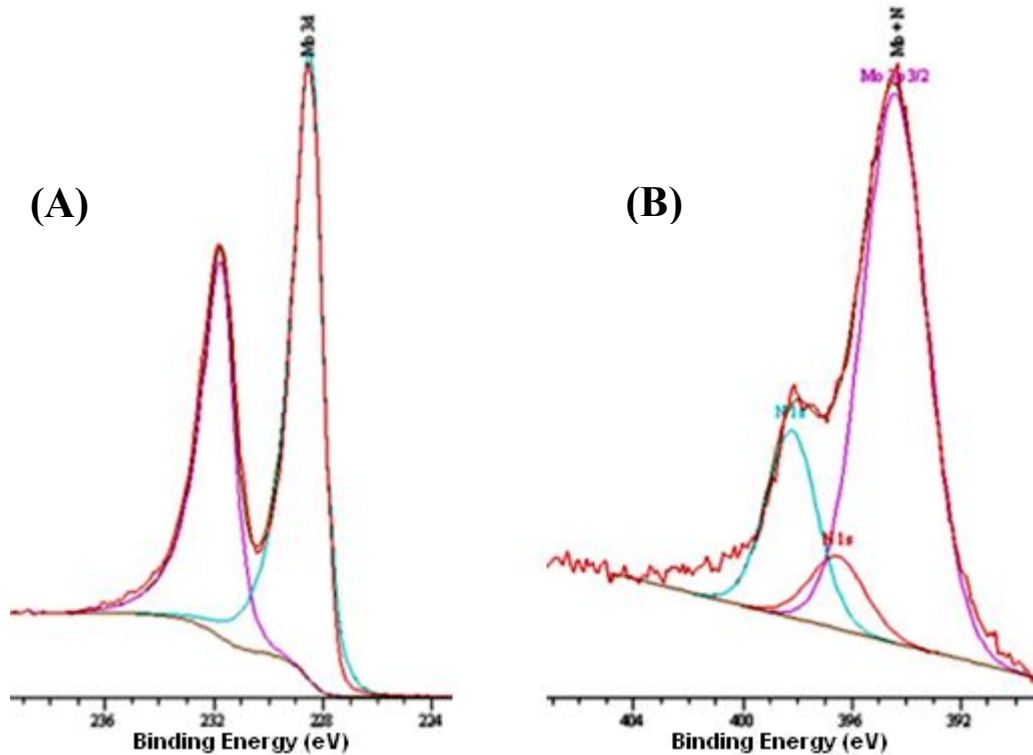
**Figure 2. XPS spectra in the (A) Mo 3d and (B) Mo 3p and N 1s regions of sample M-4 as prepared.**

Table 1 presents the Mo  $3d_{5/2}$  and Mo  $3d_{3/2}$  binding energy and the proportions of species before and after sputtering which was performed twice, (sputtering 1 & 2). Figure 2 (A) shows the XPS spectrum in the Mo 3d region of the as-prepared molybdenum nitride. The results indicate that two types of Mo were observed with Mo  $3d_{5/2}$  binding energy 228.7 eV and 232.8 eV. The Mo  $3d_{5/2}$  peak position at  $228.7 \pm 0.2$  eV is assigned to  $\text{Mo}^{+\delta}$  with  $\delta < 4$ , corresponding to  $\gamma\text{-Mo}_2\text{N}$  [55, 62, 63]. The binding energy of Mo  $3d_{5/2}$  at 232.8 eV corresponds to  $\text{Mo}^{\text{VI}}$  in  $\text{MoO}_3$  which is ascribed to the passivating oxide layer [62-64]. Figure 2 (B) presents the XPS spectrum of the Mo 3p region. It should be noted that the N1s peak is overlapped with the Mo  $3p_{3/2}$  peak and appeared as shoulder at 398.8 eV. The binding energy of N1s is reported to be  $399.0 \pm 0.2$  for  $\text{Mo}_2\text{N}$  which is apparently consistent with this study [64].



**Figure 3. XPS spectra in the (A) Mo 3p and N 1s and (B) Mo 3d regions of sample M-4 after the initial argon ion etch.**

Figure 3 (B) shows the XPS spectra of the Mo 3d region of the sample after the initial argon ion etch. It can be observed from the figure that there is a lower binding energy (Mo 3d<sub>5/2</sub> ~ 227.8 ± 0.3 eV) component which is close to that reported for molybdenum metal [63]. It can be also seen that the binding energy (Mo 3d<sub>5/2</sub> ~ 228.5 eV) matches well with that observed elsewhere for molybdenum nitride [55, 62, 63], suggesting that the oxide layer is readily removed from the surface by brief argon ion etch. However, the XPS spectrum in the N 1s region of the sample after argon ion etch is shown in Figure 3 (A). As discussed previously, the Mo 3p<sub>3/2</sub> spectra overlap with N 1s spectra, and thus the determination of the binding energy of N 1s is very difficult. The binding energy of N 1s at ~ 398.2 eV is assigned to N 1s from molybdenum nitride [64].



**Figure 4. XPS spectra in the (A) Mo 3d and (B) N 1s and Mo 3p regions of sample M-4 after the second argon ion etch.**

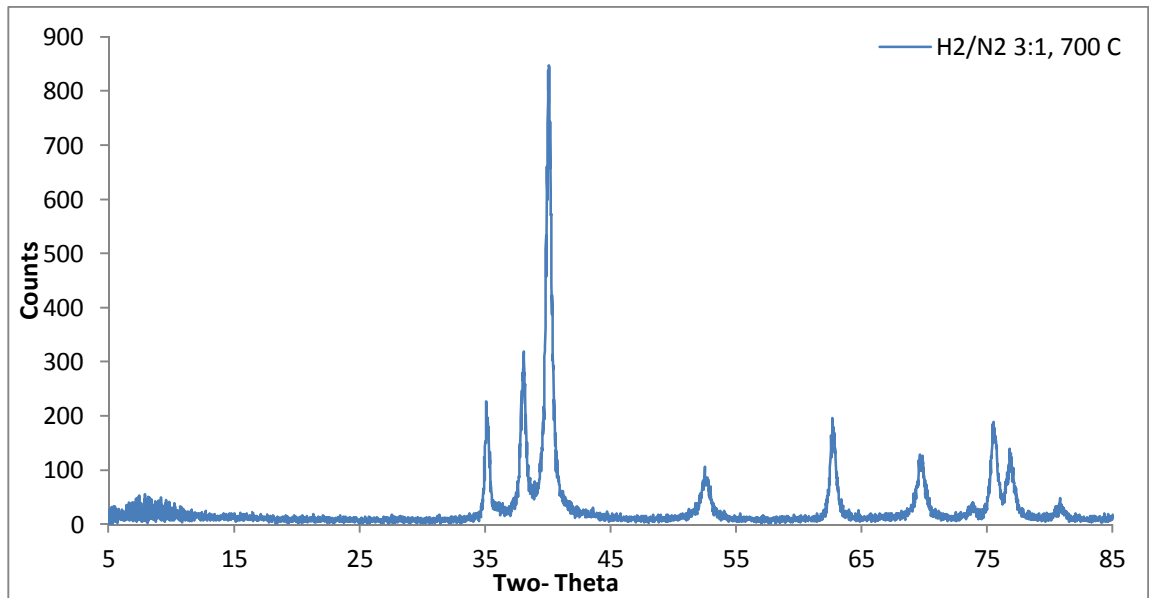
Figure 4 (A) shows the XPS spectrum in the Mo 3d region of the sample after the second argon ion etching. The figure indicates that a large amount of molybdenum nitride with a binding energy (Mo  $3d_{5/2}$  ~ 228.5 eV) was present when the sample was subjected to the second argon ion etch. Furthermore, the binding energy of N 1s, as shown in Figure 4 (B), is confirmed the presence of nitride which gives a binding energy at ~398.2 eV.

### **Sample I-24**

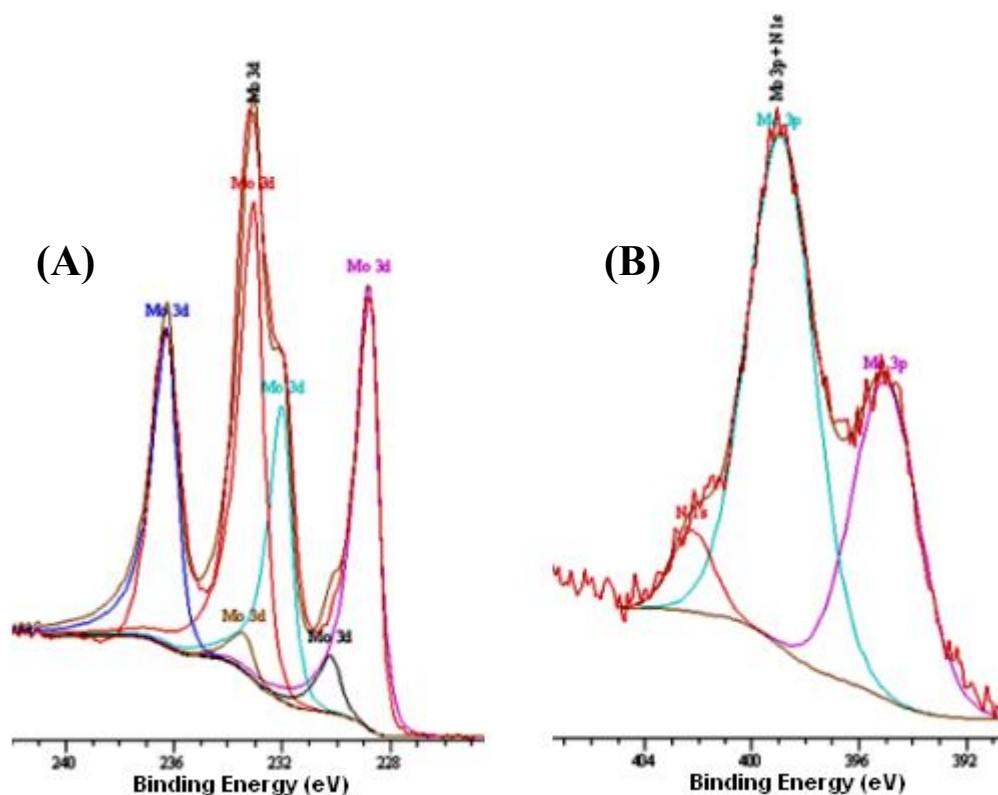
The sample I-24 was prepared by using 1g of hexamethylenetetramine molybdate under H<sub>2</sub>/N<sub>2</sub> 3:1 at 700°C, as described in the experimental chapter and in Chapter 3. The XRD pattern shows Mo<sub>2</sub>C (as shown in Figure 5). Elemental analysis showed that the sample contained 3.43 wt. % N and 2.45 wt. % C.

**Table 2: The distribution of Mo binding energies as measured by XPS for sample I-24 before and after argon ion etching.**

	Posit eV	Conc. %	Posit eV	Conc. %	Posit eV	Conc. %	Posit eV	Conc. %
<b>Original</b>	228.8	44.3	230.2	5.8	233.0	50.1	—	—
<b>Sputtering 1</b>	226.1	15.0	229.3	10.0	229.6	45.0	232.8	30.0
<b>Sputtering 2</b>	229.8	60.0	233.0	40.0	—	—	—	—

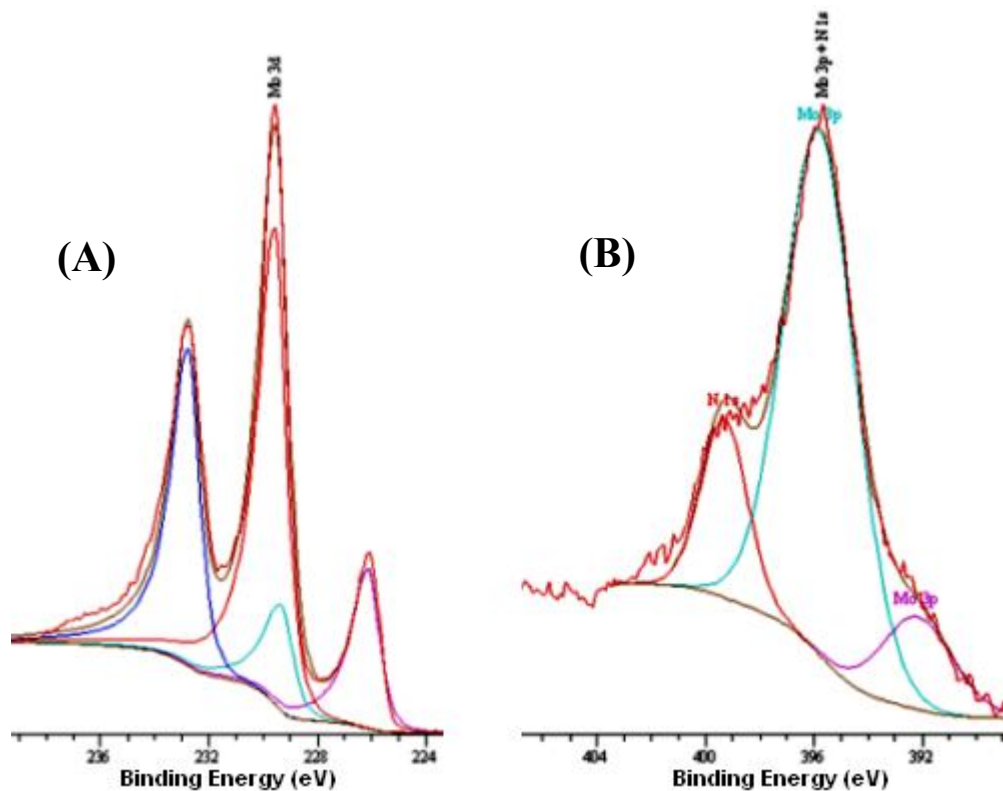


**Figure 5. XRD pattern of sample I-24**



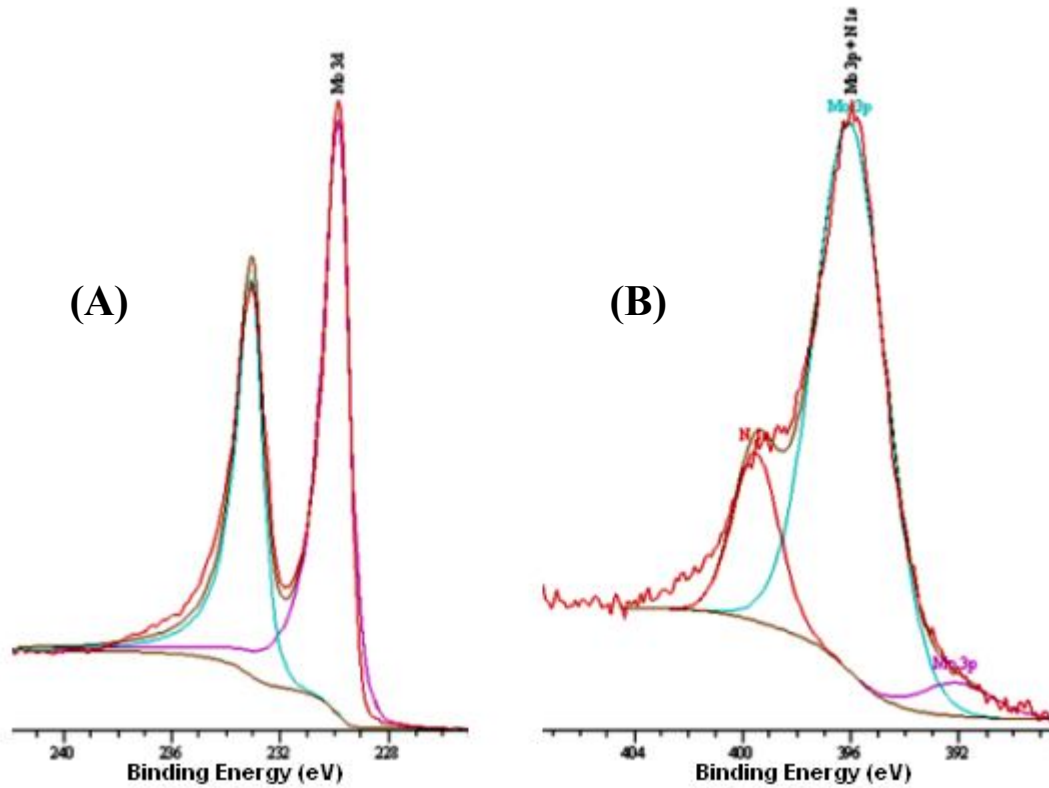
**Figure 6. XPS spectra in the (A) Mo 3d and (B) N 1s and Mo 3p regions of sample I-24 as prepared.**

Figure 6 (A) shows the XPS spectrum in the Mo 3d region of the as synthesised sample. The result indicates that three different molybdenum oxidation states are evident. The figure shows the presence of components at 228.8eV, 230.2 eV and 233.0 eV. According to the literature [62, 63], these values match well with the Mo 3d<sub>5/2</sub> lines for Mo<sup>δ+</sup>, Mo<sup>IV</sup> and Mo<sup>VI</sup> respectively. The N 1s spectrum, as shown in Figure 6 (B), indicates that the N 1s binding energy at 402.3 eV may be ascribed to the presence of oxynitride or carbonitride species. However, the XPS spectrum in the O 1s region indicates that there are two kinds of oxygen species are present on the surface. The oxygen peak at 531.0 eV is due to oxide (O<sup>2-</sup>) such as that which could be expected in MoO<sub>3</sub> and MoO<sub>2</sub>. It should be noted that the operator (Dr. David Morgan), who analysed this sample, does not perform the curve fitting of peak of O 1s region.



**Figure 7. XPS spectra in the (A) Mo 3d and (B) N 1s and Mo 3p regions of sample I-24 after the initial argon ion etch.**

Figure 7 (A) shows the XPS spectrum of the Mo 3d region of the sample after the initial argon ion etch. It can be seen from the figure that there is a binding energy Mo 3d<sub>5/2</sub> at ~226.1 eV. This does not correspond to any oxidation states that are known for molybdenum and also is lower than that reported for Mo<sup>0</sup>. It can be also observed that a high amount of molybdenum dioxide with a Mo 3d<sub>5/2</sub> binding energy of 229.4 eV may be present. The binding energy of N 1s, as shown in Figure 7 (B) is ~399.2 eV, which could be assigned to the molybdenum nitride [64].

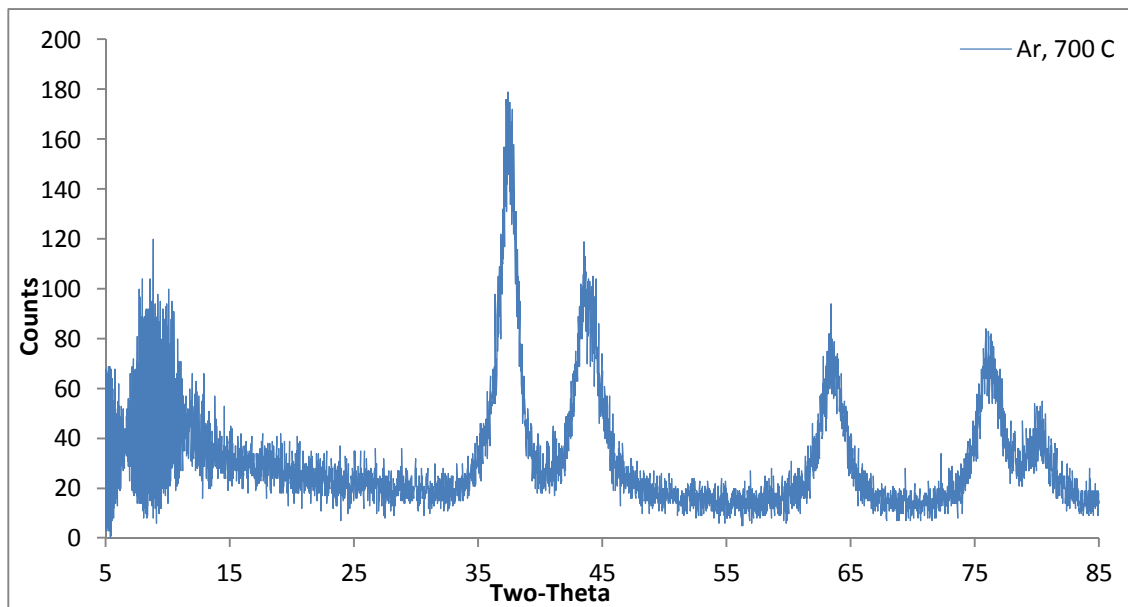


**Figure 8. XPS spectra in the (A) Mo 3d and (B) Mo 3p and N 1s regions of sample I-24 after the second argon ion etch.**

Figure 8 (A) shows the XPS spectra of the Mo 3d region of the sample after the second argon ion etch. The figure indicates that ( $\text{Mo}^{\text{IV}}$ ) with a binding energy of 229.8eV is apparent. The binding energy of N 1s at ~399.6 eV, as shown in Figure 8 (B), is slightly higher than that reported for nitride from molybdenum nitride [64].

### **Sample I-14**

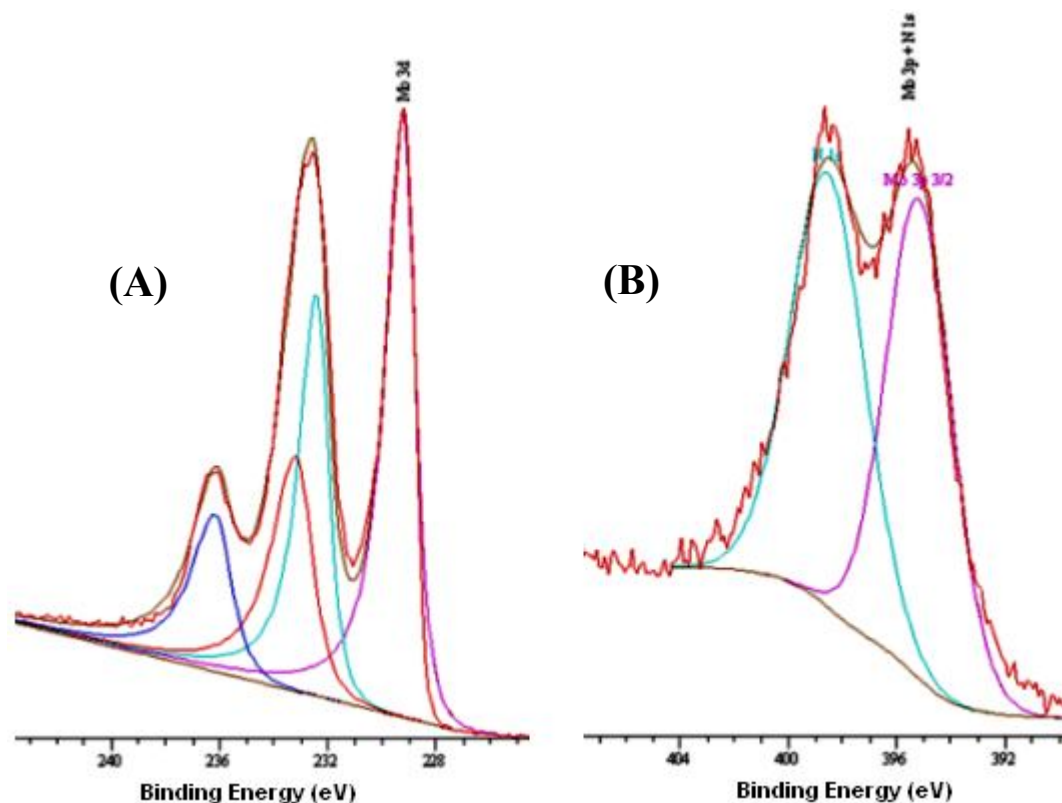
The sample I-14 was prepared by heating 1g of hexamethylenetetramine molybdate under an argon atmosphere at 700°C. The XRD pattern shows the presence of  $\gamma$ -Mo<sub>2</sub>N phase (as shown in Figure 9). Elemental analysis demonstrated that the sample contained 4.60 wt. % N and no carbon.



**Figure 9. XRD pattern of sample I-24**

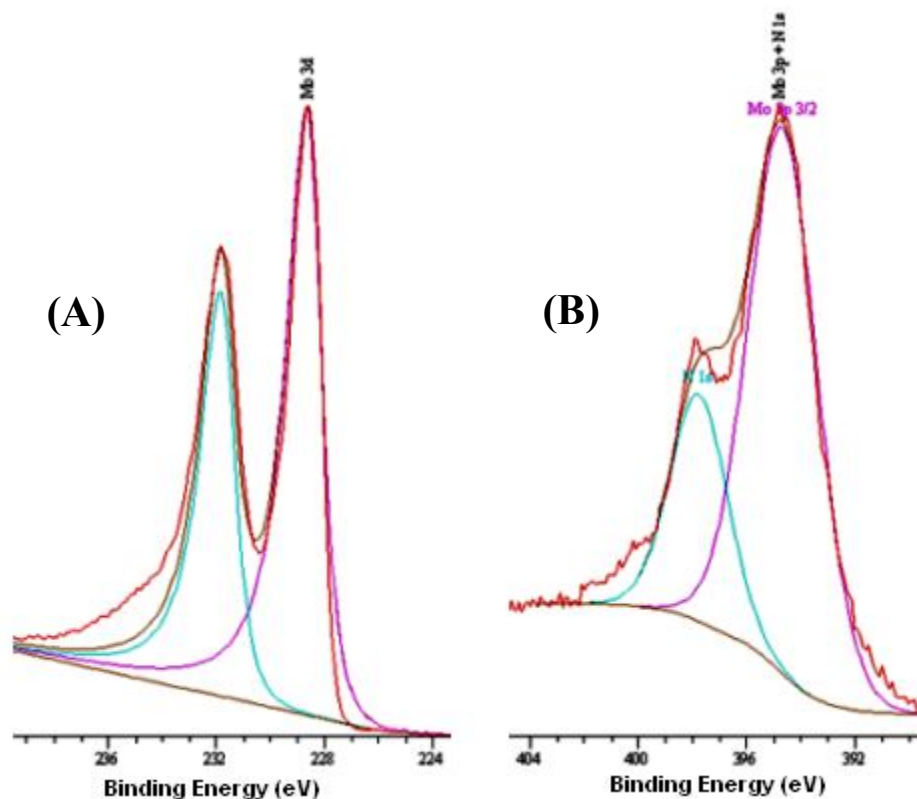
**Table 3: The distribution of Mo binding energies as measured by XPS for sample I-14 before and after argon ion etching**

	Posit eV	Conc. %	Posit eV	Conc. %	Posit eV	Conc. %	Posit eV	Conc. %
<b>Original</b>	229.2	39	232.4	26	232.6	21	236.2	14
<b>Sputtering 1</b>	228.6	60	231.8	40	—	—	—	—
<b>Sputtering 2</b>	228.8	60	232.0	40	—	—	—	—



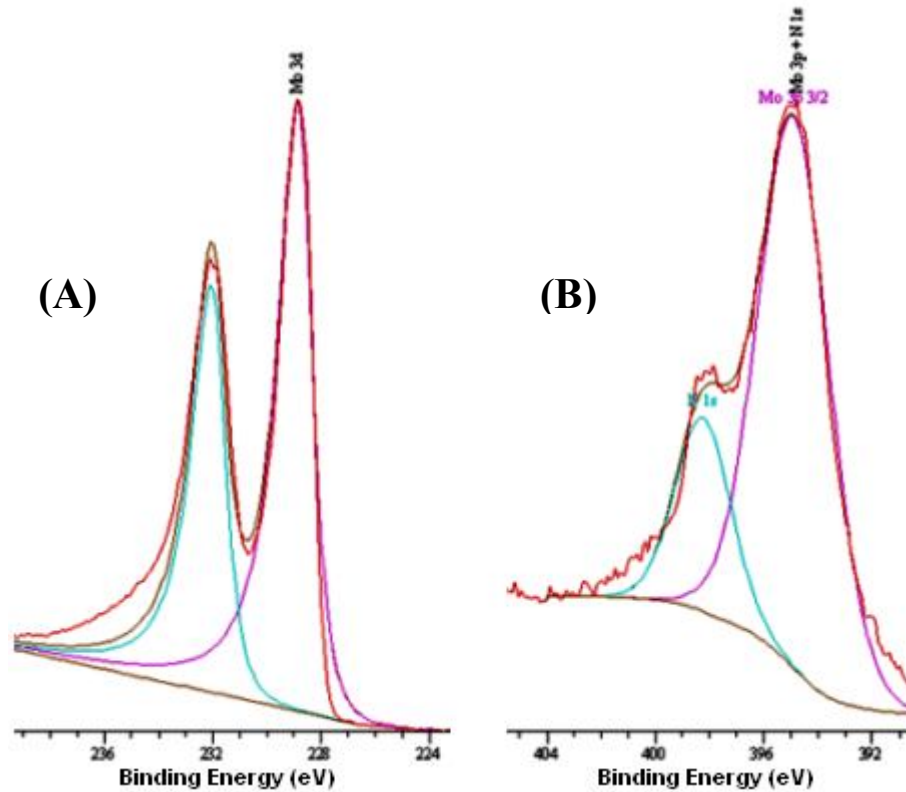
**Figure 10. XPS spectra in the (A) Mo 3d and (B) Mo 3p and N 1s regions of sample I-14 as prepared.**

Figure 10 (A) shows the XPS spectrum in the Mo 3d region of the as-prepared molybdenum nitride. The results indicate that two types of Mo were observed with Mo 3d<sub>5/2</sub> binding energies of 229.2 eV and 232.6 eV. The Mo 3d<sub>5/2</sub> peak position at 229.2 eV could be assigned to Mo<sup>IV</sup> possibly relating to (MoO<sub>2</sub>) which is expected to occur at 229.6 eV, 229.7 eV [63], 229.9 eV [64] or 230 eV[55]. The binding energy of Mo 3d<sub>5/2</sub> at 232.6 eV corresponds to Mo<sup>VI</sup> in MoO<sub>3</sub>. Figure 10 (B) presents the XPS spectrum of Mo 3p region. The N1s peak is overlapped in the Mo 3p<sub>3/2</sub> spectra and appeared as a shoulder at 398.7 eV which could be assigned to that reported for molybdenum nitride.



**Figure 11. XPS spectra in the (A) Mo 3d and (B) Mo 3p and N 1s regions of sample I-14 after the initial argon ion etch**

Figure 11 (A) shows the XPS spectra of the Mo 3d region of the sample after the initial argon ion etch. It can be observed from the figure that there is a lower binding energy component (Mo 3d<sub>5/2</sub> ~ 228.6 eV). This matches well with that observed elsewhere for molybdenum nitride [55, 63], suggesting that the oxide layer is readily removed from the surface by a brief argon ion etch. However, the XPS spectrum in the Mo 3p region of the sample after the argon ion etch is shown in Figure 11 (B). As discussed previously, the Mo 3p<sub>3/2</sub> spectra overlapped with N 1s spectra, thus the determination of the binding energy of N 1s is very difficult. The binding energy of N 1s at ~ 397.8 eV is assigned to N 1s from molybdenum nitride [64].



**Figure 12. XPS spectra in the (A) Mo 3d and (B) Mo 3p and N 1s regions of sample I-14 after the second argon ion etch**

Figure 12 (A) shows the XPS spectrum in the Mo 3d region of the sample after the second argon ion etch. The figure indicates the possible contribution of a relatively large amount of molybdenum nitride with a binding energy (Mo  $3d_{5/2}$  ~ 228.8 eV). Furthermore, the binding energy of N 1s, as shown in Figure 12 (B), is also consistent with the presence of molybdenum nitride which gives a binding energy at ~398.2 eV [63].

### **Sample E-23**

The sample E-23 was prepared by heating 1g of ethylenediamine molybdate under H<sub>2</sub>/N<sub>2</sub> 1:3 at 700°C. The XRD pattern shows molybdenum carbide as the product phase (as shown in Figure 13). The product contained 2.45 wt. % N and 3.43 wt. % C.

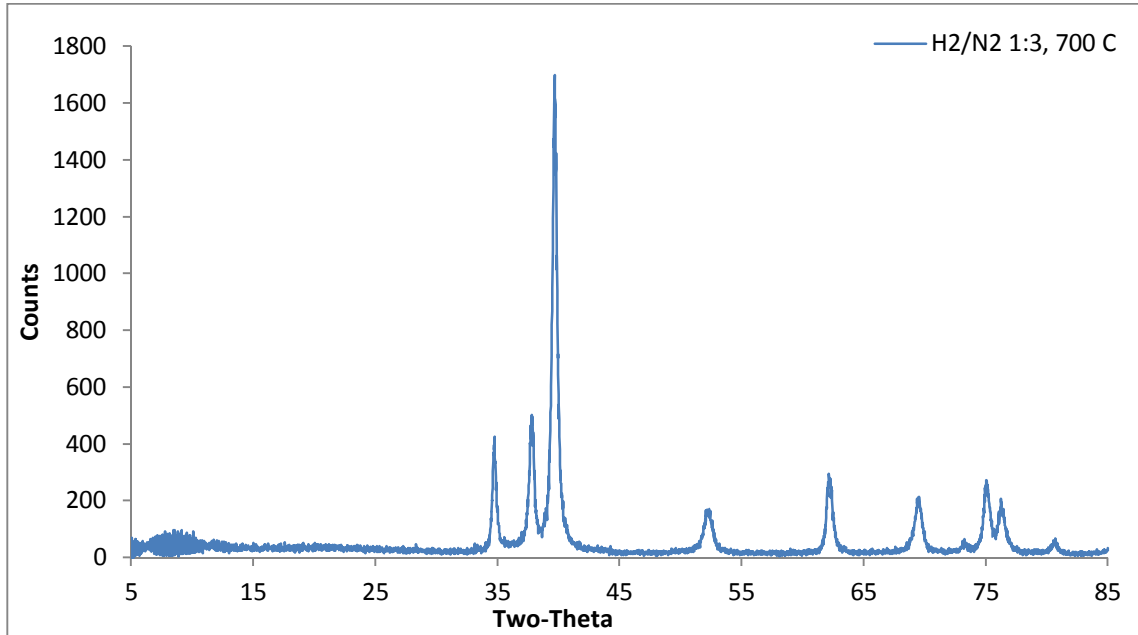


**Figure 13. XRD pattern of sample E-23**

**Table 4: The distribution of Mo binding energies as measured by XPS for sample E-23 before and after argon ion etching**

	Posit eV	Conc. %	Posit eV	Conc. %	Posit eV	Conc. %	Posit eV	Conc. %
<b>Original</b>	229.3	38.0	232.4	25.0	233.2	21.0	236.4	14.0
<b>Sputtering 1</b>	227.1	4.2	230.3	2.8	228.8	55.8	232.1	37.1
<b>Sputtering 2</b>	226.9	4.0	230.0	2.7	228.5	56.0	231.8	37.4

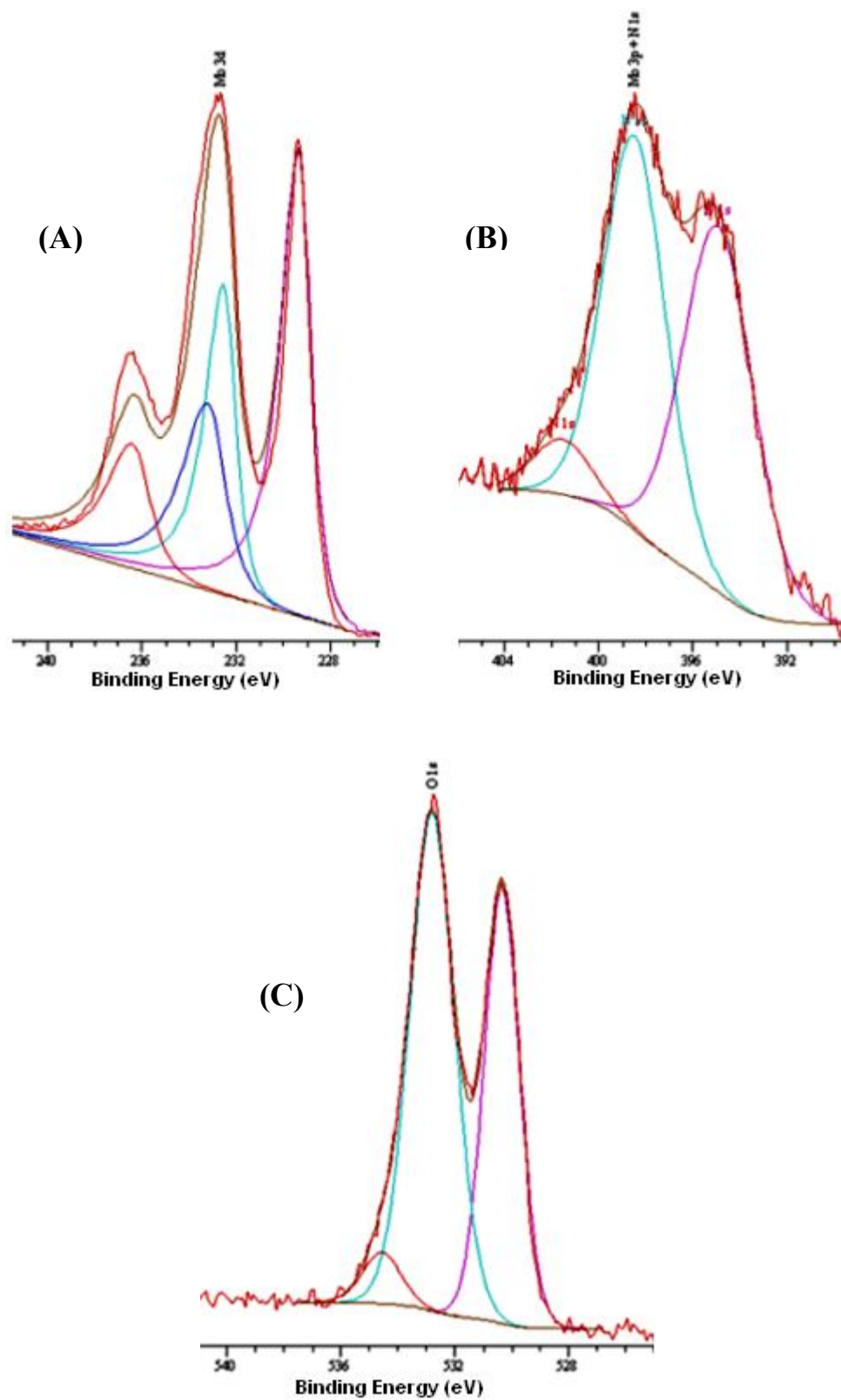
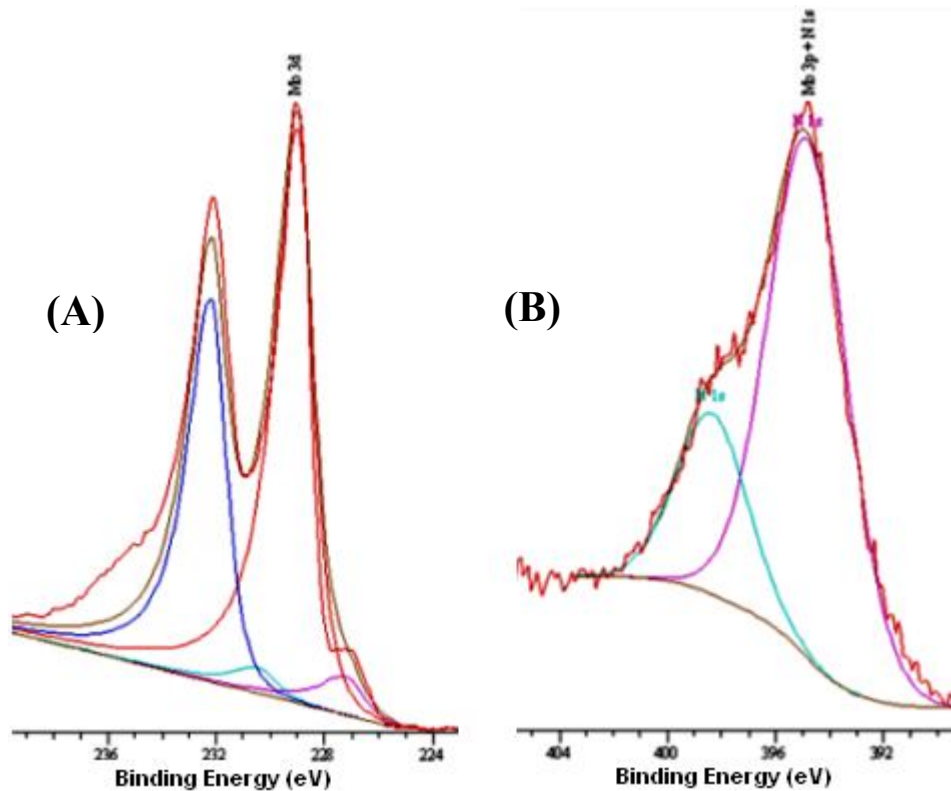
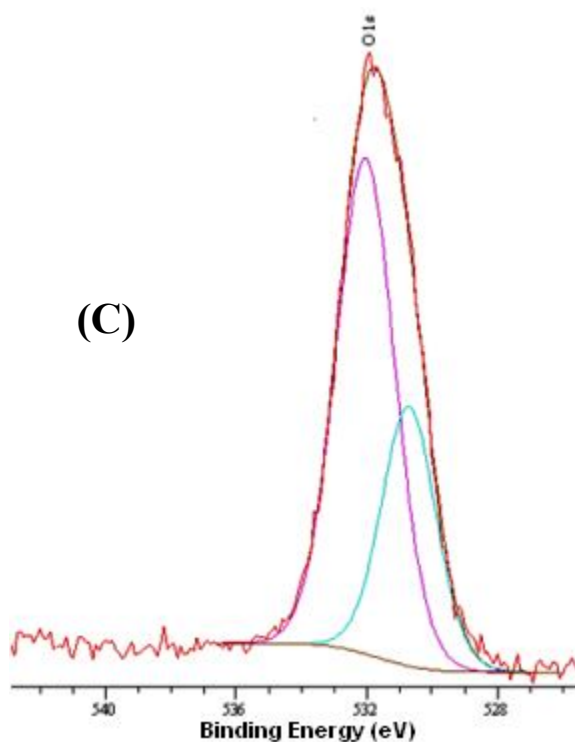


Figure 14. XPS spectra in the (A) Mo 3d, (B) Mo 3p and N 1s and (C) O 1s regions of sample E-23 as prepared

Figure 14 (A) shows the XPS spectrum in the Mo 3d region of the as synthesised sample. The result indicates that high amounts of MoO<sub>2</sub> and MoO<sub>3</sub> (65% and 35% respectively) are present in the near surface region. The Mo3d<sub>5/2</sub> peak position located at 229.3 eV is assigned to Mo<sup>IV</sup>, MoO<sub>2</sub>. It can be observed that the Mo3d<sub>5/2</sub> binding energy of MoO<sub>2</sub> shifts to a lower energy level than that reported elsewhere [62, 63] which could be due to the contribution of oxycarbide, oxynitride or oxycarbonitride species. The binding energy of Mo3d<sub>5/2</sub> at 233.2 eV is attributed to Mo<sup>VI</sup>, MoO<sub>3</sub>. The N 1s spectrum, as shown in Figure 14 (B), indicates that the N 1s binding energy at 401.5 eV which could be ascribed to the presence of oxynitride or carbonitride species [65]. However, the XPS spectrum in the O 1s region, as shown in Figure 14 (C), indicates that there are two kinds of oxides present in the surface. The oxygen peak at 530.7 eV (38 %) is due to oxide (O<sup>2-</sup>) such as MoO<sub>3</sub> and MoO<sub>2</sub> and the one at 532.0 eV (56 %) is attributed to strongly adsorbed oxygen species such as O<sup>-</sup>, OH<sup>-</sup> or H<sub>2</sub>O, or due to the contribution of oxycarbide, oxynitride or oxycarbonitride species [62].





(C)

**Figure 15. XPS spectra in the (A) Mo 3d, (B) Mo 3p and N 1s and (C) O 1s regions of sample E-23 after the initial argon ion etch**

Figure 15 (A) shows the XPS spectra of the Mo 3d region of the sample after the initial argon ion etch. It can be observed from the figure that there is at Mo 3d<sub>5/2</sub> binding energy (at ~ 228.8 eV). This can be assigned to molybdenum nitride with a small shift to higher energy level which could be due to oxidation of molybdenum nitride [62]. It can be also observed that there is a small peak (Mo 3d<sub>5/2</sub>~ 227.1eV) which corresponds to molybdenum metal, which seems to be at a slightly lower energy than that reported in the literature (Mo 3d<sub>5/2</sub>~ 227.6 eV, 227.8 eV) [63]. The binding energy of N 1s at ~ 398.3 eV, as shown in Figure 15 (B), confirmed the presence of molybdenum nitride. However, corresponding spectra in the O 1s region are presented in Figure 15 (C). It is apparent that the oxygen peak at 530.8 eV which is attributed to O<sup>2-</sup> species shows lower relative intensity (32%) than that observed before ion etching, whilst the one at 532.2eV which is ascribed to other forms of oxygen species exhibits higher relative intensity (67 %).

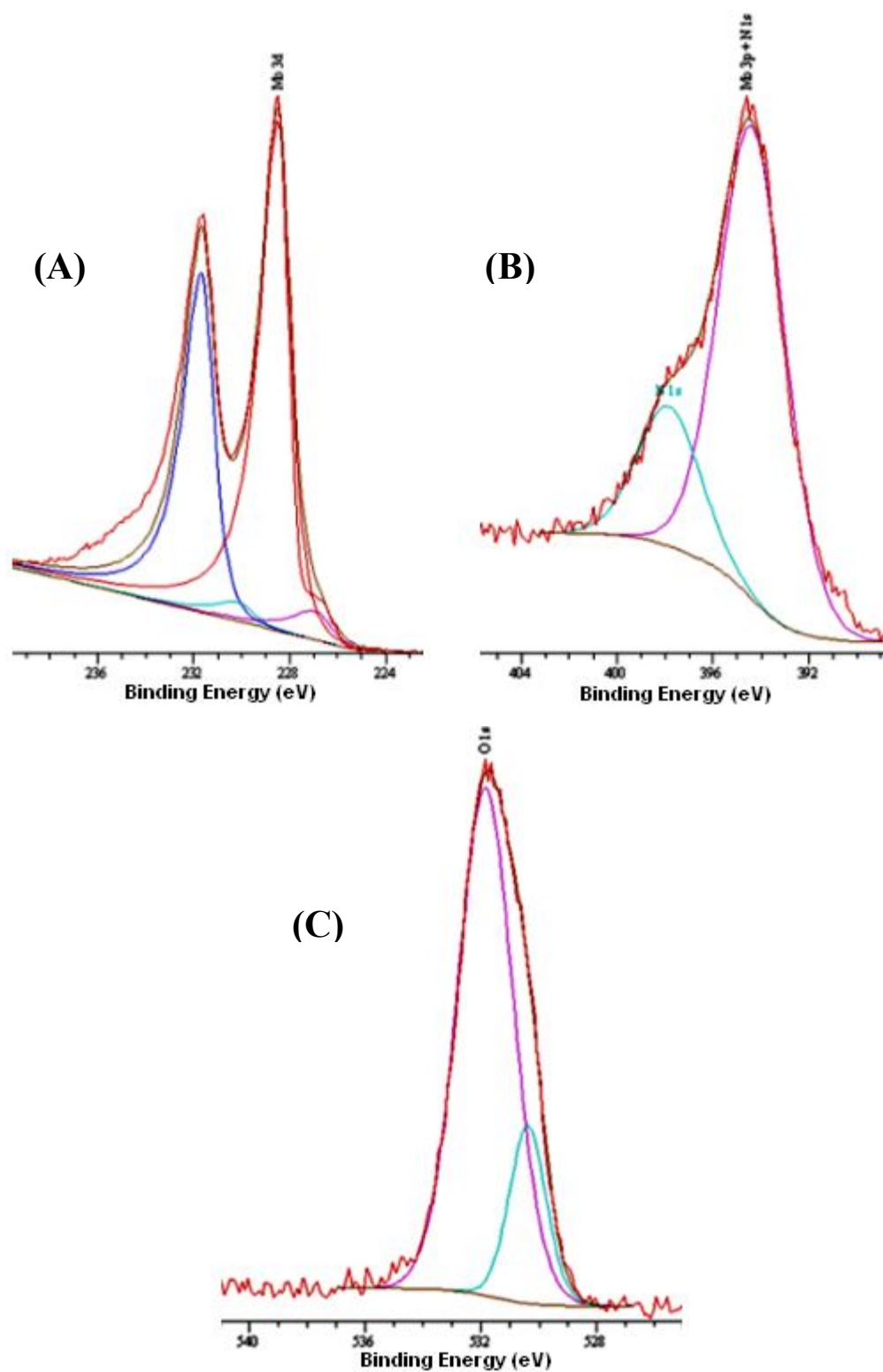


Figure 16. XPS spectra in the (A) Mo 3d, (B) Mo 3p and N 1s and (C) O 1s regions of sample E-23 after the second argon ion etch

Figure 16 (A) shows the XPS spectra of the Mo 3d region of the sample after the second argon ion etch. The figure indicates that a relatively large amount of molybdenum nitride with a binding energy Mo 3d<sub>5/2</sub> ~ 228.5 eV may be present and also the possible presence of a small amount of metallic Mo (6%) with a binding energy ~ 227 eV. Furthermore, the binding energy of N 1s, as shown in Figure 16 (B), confirmed the presence of molybdenum nitride which is consistent with a binding energy of ~397.8 eV. However, Figure 16 (C) shows the XPS spectrum in the O1s region of the sample. It can be observed that a higher relative level of the non-O<sup>2-</sup> species (81%) is observed, suggesting that the sample contains molybdenum oxycarbide or oxynitride or even oxycarbonitride components.